DEPARTMENT OF PHYSICS
UNIVERSITY OF JYVÄSKYLÄ
RESEARCH REPORT No. 3/2011

DEVELOPMENT OF MEV ION BEAM LITHOGRAPHY TECHNIQUE FOR MICROFLUIDIC APPLICATIONS

BY
NITIPON PUTTARAKSA

Academic Dissertation
for the Degree of
Doctor of Philosophy

To be presented, by permission of the
Faculty of Mathematics and Natural Sciences
of the University of Jyväskylä,
for public examination in Auditorium FYS–1 of the
University of Jyväskylä on May 20, 2011
at 12 o'clock noon

Jyväskylä, Finland
May 2011

Preface

First of all, I would like to express sincere gratitude to my supervisors, Assoc. Prof. Dr. Somsorn Singkarat and Prof. Harry J. Whitlow DSc, DPhil for their kindness guidance, encouragement, wisdom and support. I would like to thank Assoc. Prof. Somsorn Singkarat for his efforts in arranging the financial support from the Royal Golden Jubilee (RGJ) Scholarship of the Thailand Research Fund (TRF) throughout my graduate study at Chiang Mai University (CMU). His inspiration and vision made a deep impression and his helpfulness will be important in my future career. I would also like to thank Prof. Harry J. Whitlow who persuaded me to work in the field of MeV ion beam lithography (MeV–IBL). He is an enthusiastic and dynamic supervisor. His ideas, suggestions and advice were excellent. Together, they instigated the Dual Doctorate Agreement between the Faculty of Mathematics and Natural Science in Jyväskylä and the Faculty of Science, Chiang Mai University under which this thesis work is carried out.

I would also like to thank Assoc. Prof. Dr. Yu Liengdeng and Docent Dr. Timo Sajavaara, who are my co–supervisors. Their suggestions and discussions were very helpful in completing this thesis.

I am very grateful to thank Prof. Emeritus Dr. Thiraphat Vilaithong for his suggestions and recommendations for my research career.

I would also like to express special thanks researcher colleagues: Dr. Sergey Gorelick, Mikko Laitinen, Ananda Sagari A.R., Dr. Teerasak Kamwanna, Asst. Prof. Kanda Singkarat, Dr. Nirut Pussadee, Somrit Unai, Rattachai Pinchaiphat, Assoc. Prof. Dr. Orapin Chienthavorn, University lecturer Dr. Leona Gilbert, Mari Napari, Rattanaporn Norarat and Peerapong Yotprayoonsak for their cooperation and help.

It is my pleasure to many thanks to all the technical staff of the Plasma and Beam Physics Research Facility (PBP) at Chiang Mai University (CMU) and at the Accelerator Laboratory (JYFL), University of Jyväskylä (JYU) for their support in mechanical and electronic construction work for this project.

I am thankful to Mr. Chome Thongleum for keeping the Tandertron accelerator running very well. Mr. Michael W. Rhodes and Mr. Vitoon Ginamoon are also acknowledged for their special support. It is also my pleasure to thank Mr. Rachen Charoennugul for his shared discussions and beautiful images.

I would also like to thank Mrs. Thanita Decthammrong, Mr. Pollakit Padungchat, Soili Leskinen, Ann–Liisa Blå, Marjut Hilska and all the secretaries from the Department of Physics and Materials Science at CMU for their help with the administration.

I gratefully acknowledge the financial support from the Royal Golden Jubilee (RGJ) Scholarship of Thailand Research Fund (TRF). The financial support from the Development and Promotion of Science and Technology Talents Project (DPST) scholarship is also acknowledged for supporting my first semester in the first year of my studies.

I would also like to thank the Thailand Center of Excellence in Physics (ThEP Center) and the Academy of Finland Centre of Excellence in Nuclear and Accelerator–Based Physics (Ref. 213503) for the financial support of this project.

I am also grateful to the pre–examiners Prof. Dr. Jyrki Räisänen and Docent Dr. Jens Jensen for their helpful suggestions on how to improve this thesis.

Finally, I would like to thank my family for their help, understanding and support. In particular, my mother (Jidaporn Wongviboonchai) who has supported me a great deal in many ways on my road to becoming a researcher.

Abstract

In this study, a novel MeV ion beam lithographic (MeV–IBL) technique, called a programmable proximity aperture lithography (PPAL) technique, was developed at the Accelerator Laboratory, University of Jyväskylä (JYU) in Finland and at the Plasma and Beam Physics Research Facility (PBP), Chiang Mai University (CMU) in Thailand. The PPAL technique utilizes a pair of computerized L–shaped aperture blades to define an irradiated rectangular or square area of 0.2–500 μm size. In combination with sample movement in X and Y directions, a complex exposure pattern can be built–up from rectangular exposed regions using this method. The structures produced by the PPAL method have special characteristics such as a high aspect ratio with vertical side walls. The PPAL approach was used for fabricating prototype microfluidic circuits, where the pattern usually consists of large reservoirs that are connected together with small micro–channel and other structures.

The PPAL technique has been shown to be suitable for fabricating 3D microstructure and the dose distributions for straight edge and internal and external corners were studied. It was found that beam fluence measurement was important for repeatable results and two methods to measure this based on backscattering from a rotating vane and measurement of intercepted ion beam charge on aperture were developed. The main part of the work was directed towards study of the fluence dependence of poly(methyl methacrylate) (PMMA) resist exposure. The fluences for clearing, the onset of cross linking and complete cross linking were measured for 2 MeV protons, 3 MeV ^{4}He and 6 MeV ^{12}C ions. It was found that by selection of the ion fluence the PMMA could be used as a positive tone or negative tone resist. A pattern written in negative tone was used as a master mold for fabricating microfluidic circuits by soft–lithography in poly(dimethylsiloxane) (PDMS). This was sealed using PDMS spin coated on a glass substrate. The microfluidic device was used to generate water droplets in an oil carrier phase. Direct writing of silica was also demonstrated and the exposure characteristic for 6.8 MeV ^{16}O ions was characterised.

บทสรุปวิทยานิพนธ์

กว่า 20 ปีที่ผ่านมา วิทยาการสมัยใหม่ที่รวมศาสตร์หลายแขนง เช่น ฟิสิกส์ เคมี ชีววิทยา และ วิศวกรรมศาสตร์ ฯ ได้ถือกำเนิดและมีการพัฒนาอย่างรวดเร็วมีชื่อเรียกว่า วิทยาการของไหลระดับไมครอน (microfluidics) วิทยาการนี้เกี่ยวข้องกับการควบคุมของไหลเช่นของเหลวหรือแก๊สในปริมาณน้อยๆ ระดับนาโนลิตรถึงอัตโตลิตร (attolitre) หรือ 10^{-18} ลิตร ให้ไหลไปตามท่อที่มีขนาดเล็กระดับไมครอน จุดประสงค์การพัฒนาวิทยาการของไหลระดับไมครอนโดยทั่วไปเพื่อย่อขนาดเครื่องมือและการปฏิบัติการที่สลับซับซ้อนเช่น การเตรียมสารตัวอย่าง การเพิ่มความเข้มข้นของสารก่อนการวิเคราะห์ และการตรวจวัดปริมาณสารต่างๆ ให้อยู่ในอุปกรณ์เพียงชิ้นเดียว หรือที่รู้จักกันในนาม Lab-on-a-chip หรือ Micro-total-analysis-system (μ-TAS) การย่อขนาดให้เล็กลงนี้ทำให้อุปกรณ์ของไหลระดับไมครอน (microfluidic device) ใช้ปริมาณสารตัวอย่างและสารเคมีในการวิเคราะห์น้อยลง ทำให้ประหยัดค่าใช้จ่ายในการวิเคราะห์ อีกทั้งยังรวดเร็วและมีสภาพไวสูง

วิทยานิพนธ์นี้ มีวัตถุประสงค์ในการพัฒนานวัตกรรมเทคนิคลิโทกราฟี (lithography) ที่ใช้ลำไอออนพลังงานระดับเมกะอิเล็กตรอนโวลท์ (megaelectronvolt, MeV) ที่มีชื่อเรียกว่า programmable proximity aperture lithography (PPAL) ขึ้นที่กลุ่มวิจัยฟิสิกส์เครื่องเร่งอนุภาค ณ มหาวิทยาลัยยูวาสคูลา (University of Jyväskylä) ประเทศสาธารณรัฐฟินแลนด์ และ ศูนย์วิจัยฟิสิกส์ของพลาสมาและลำอนุภาค ณ มหาวิทยาลัยเชียงใหม่ ประเทศไทย เพื่อใช้ในการสร้างลวดลาย 3 มิติ บนชั้นพอลิเมอร์ชนิด polymethylmethacrylate (PMMA) และ วัสดุซิลิกา สำหรับการประยุกต์ใช้งานด้านของไหลระดับไมครอน

เทคนิคลิโทกราฟีโดยทั่วไปจะใช้ รังสีอัลตราไวโอเลต รังสีเอกซ์ ลำอิเล็กตรอน (electron beam) ในการบันทึกลวดลายลงบนชั้นพอลิเมอร์ไวแสง หรือที่เรียกว่า polymer resist ต่อมานำชิ้นงานพอลิเมอร์นี้มาทำปฏิกิริยาด้วยสารเคมีที่เหมาะสมให้เกิดการสึกกร่อน ถ้าบริเวณที่บันทึกลวดลายเกิดปฏิกิริยาสึกกร่อนทำให้มีร่องลึก polymer resist นั้นมีสมบัติที่เรียกว่า positive resist และในกรณีที่การสึกกร่อนไม่ได้เกิดในบริเวณที่บันทึกลวดลายแต่เกิดในส่วนอื่นที่เหลือทำให้ลวดลายเป็นสันนูน polymer resist นั้นมีสมบัติที่เรียกว่า negative resist เทคนิค PPAL เป็นเทคนิคลิโทกราฟีที่ใช้ลำไอออนได้แก่ ลำโปรตอน ลำฮีเลียม (helium) ลำคาร์บอน ลำออกซิเจน ที่มี

พลังงานระดับ MeV วิ่งเข้าไปในวัสดุในแนวตรงและลึกเพื่อบันทึกลวดลาย ทำให้ลวดลายที่สร้างขึ้นด้วยวิธีการนี้มีสมบัติพิเศษเฉพาะตัวคือ อัตราส่วนระหว่างความลึกต่อความกว้างของลวดลายมีค่าสูง และผนังของลวดลายมีความเรียบตรงอีกด้วย ทำให้เทคนิคนี้น่าสนใจกว่าเทคนิคลิโทกราฟีทั่วไป

เทคนิคลิโทกราฟีที่ใช้ลำโปรตอนที่มีพลังงานระดับ MeV แบบทั่วไปมีชื่อเรียกว่า proton beam writing (PBW) ทำโดยการโฟกัสลำอนุภาคโปรตอนให้มีขนาดเส้นผ่าศูนย์กลางเล็กระดับนาโนเมตรในการบันทึกลวดลาย เทคนิค PPAL ที่นำเสนอในงานวิจัยนี้มีความแตกต่างจากเทคนิค PBW ตรงที่เทคนิค PPAL ใช้แผ่นกั้นลักษณะรูปตัว L หนึ่งคู่ซึ่งควบคุมการเคลื่อนที่ด้วย คอมพิวเตอร์สำหรับกำหนดช่องผ่านของลำไอออนให้เป็นรูปทรงสี่เหลี่ยมผืนผ้า หรือสี่เหลี่ยมจัตุรัสขนาด 0.2-500 ไมครอน และเมื่อประกอบกับการเคลื่อนสารตัวอย่างไปตามตำแหน่งต่างๆ ในแนวแกน X และ แกน Y ทำให้สามารถนำมาใช้ในการสร้างลวดลายต่างๆ ที่สลับซับซ้อนได้ เทคนิค PPAL เป็นเทคนิคที่จะใช้เวลาสั้นกว่าเทคนิค PBW แต่นานกว่าเทคนิคที่ใช้การฉายอนุภาคผ่านหน้ากาก (mask) ซึ่งมีราคาแพง จึงทำให้เทคนิค PPAL เหมาะแก่การนำมาประยุกต์ใช้ในการสร้างวงจรของไหลระดับไมครอน (microfluidic circuits) ที่ประกอบไปด้วยโพรงเก็บของไหลหลาย ๆ โพรงเชื่อมต่อถึงกันผ่านท่อเล็กขนาดไมครอน

งานวิจัยนี้ได้ทำการศึกษาการแผ่ออกทางด้านข้าง (lateral spreading) ของลำโปรตอนพลังงาน 2 MeV และไอออนของฮีเลียมพลังงาน 3 MeV หลังจากเคลื่อนทะลุผ่านฟิล์ม PMMA หนา 7.5 ไมครอน โดยใช้โปรแกรมการจำลองและคำนวณการเคลื่อนที่ของไอออนในวัสดุ หรือที่เรียกว่า The Stopping and Range of Ions in Matter (SRIM) รวมทั้งการใช้อินทิกรัลแบบง่ายในการศึกษาการกระจายตัวความเข้มข้นของไอออนสำหรับรูปแบบการยิงไอออนแบบขอบตรง ขอบมุมฉากภายใน และขอบมุมฉากภายนอก โดยที่การกระจายตัวความเข้มข้นของไอออนข้างนอกบริเวณที่ยิงส่งผลต่อความตรงของผนังลวดลาย จากการทดลองพบว่ารูปแบบการกระจายตัวของความเข้มข้นของไอออนคล้ายคลึงกับฟังก์ชันค่าผิดพลาดเติมเต็ม (complimentary error function) และพบว่ากรณีโปรตอนพลังงาน 2 MeV และไอออนของฮีเลียมพลังงาน 3 MeV มีความกว้างของการกระจายตัวมีค่าประมาณ 50 และ 64 นาโนเมตรตามลำดับ และไม่ขึ้นอยู่กับรูปแบบการยิงไอออนไม่ว่าเป็นแบบขอบตรง ขอบมุมฉากภายใน หรือขอบมุมฉากภายนอก

งานวิจัยนี้ยังมีการพัฒนาระบบตรวจวัดความเข้มข้นของไอออน 2 ระบบ ได้แก่ ระบบการสุ่มวัดจำนวนไอออนที่กระเจิงกลับ (backscattering) เนื่องจากกังหันใบคู่ที่เคลือบทองซึ่งหมุนอย่างเป็นจังหวะสม่ำเสมอด้วยอัตราเร็ว 0.98 รอบต่อวินาที และระบบการตรวจวัดจำนวนประจุไอออนที่พุ่งชนแผ่นกั้นรูปตัว L ในการศึกษาความเข้มข้นของโปรตอนพลังงาน 2 MeV ไอออนของฮีเลียมพลังงาน 3 MeV และไอออนของคาร์บอนพลังงาน 6 MeV ที่ทำให้ PMMA เหมาะแก่การทำลิโทกราฟี การเริ่มเกิดการเชื่อมโยงข้ามสายพอลิเมอร์ (cross-linking) และการเชื่อมโยงข้ามสายพอลิเมอร์อย่างเต็มที่ จากการทดลองพบว่าความเข้มข้นของไอออน (ซึ่งเขียนย่อได้คือ Φ) ที่มีค่าน้อยกว่าค่าความเข้มข้นที่เหมาะแก่การทำลิโทกราฟีสามารถนำมาใช้ในการสร้างลวดลายขรุขระขนาดนาโนเมตรในขณะที่ความเข้มข้นของไอออนที่มีค่าอยู่ระหว่างค่าความเข้มข้นที่เหมาะแก่การทำลิโทกราฟีกับค่าความเข้มข้นของไอออนที่เริ่มเกิดการเชื่อมโยงข้ามสายพอลิเมอร์ สามารถนำมาใช้ในการสร้างลวดลายบนชั้น PMMA ในสมบัติแบบ positive resist ส่วนความเข้มข้นของไอออนที่มีค่ามากกว่าค่าความเข้มข้นของไอออนที่ทำให้เกิดการเชื่อมโยงข้ามสายพอลิเมอร์อย่างเต็มที่สา-มารถนำมาใช้ในการสร้างลวดลายบนชั้น PMMA ในสมบัติแบบ negative resist

งานวิจัยนี้ยังได้ใช้เทคนิค PPAL ในการสร้างลวดลาย 3 มิติแบบ positive resist และ negative resist บนชั้น PMMA ที่เคลือบอยู่บนฐานรองซิลิกอน และพัฒนาเทคนิค soft-lithography ซึ่งคือการคัดลอกลวดลายที่สร้างขึ้นจากเทคนิค PPAL ลงบนพอลิเมอร์ชนิด poly(dimethyl-siloxane) (PDMS) เทคนิค soft-lithography เป็นเทคนิคที่ใช้กันอย่างแพร่หลายในการสร้างอุปกรณ์ของไหลระดับไมครอนเนื่องจากเทคนิคนี้เป็นเทคนิคที่ง่ายและยืดหยุ่นต่อการผลิตมีต้นทุนต่ำจึงเหมาะแก่การผลิตจำนวนอุปกรณ์ในปริมาณมากๆ ทำให้สามารถใช้ครั้งเดียวและทิ้งได้

ขั้นตอนในการผลิตอุปกรณ์ของไหลระดับไมครอนด้วยเทคนิค soft-lithography ในงานวิจัยนี้เริ่มจากการสร้างลวดลายแม่พิมพ์ด้วยเทคนิค PPAL จากนั้นทำการผสมสารตั้งต้นที่ใช้ทำ PDMS 2 ชนิดคือสาร silicone elastomer base และสาร silicone elastomer curing agent เข้าด้วยกันในอัตราส่วน 10:1 สารทั้งสองเป็นผลิตภัณฑ์ Sylgard 184 silicon elastomer kit ของบริษัท Dow Corning ประเทศสหรัฐอเมริกา ทำการดูดเอาแก๊สออกจากการผสมด้วยระบบสุญญากาศเป็นเวลา 20 นาที เทการผสมลงบนแม่พิมพ์เพื่อทำการคัดลอกลวดลาย แล้วบ่ม (cure) ชิ้นงานที่อุณหภูมิ 70 องศาเซลเซียส เป็นเวลา 1 ชั่วโมงเพื่อทำให้ PDMS ที่เกิดขึ้นแข็งตัว จากนั้นลอก PDMS ออกจาก

แม่พิมพ์ ปิดผนึกท่อของไหลระดับไมครอนใน PDMS ภายใต้ระบบสุญญากาศเข้ากับฟิล์มบาง PDMS ที่เคลือบบนฐานรองแก้ว ซึ่งฟิล์มบางนี้ได้ทำการบ่มเบื้องต้นที่อุณหภูมิ 70 องศาเซลเซียส เป็นเวลา 6 นาที หลังจากปิดผนึกแล้วจึงนำอุปกรณ์ของไหลระดับไมครอนมาบ่มอีกครั้งที่อุณหภูมิ 70 องศาเซลเซียส เป็นเวลา 45 นาทีเพื่อทำให้ฟิล์ม PDMS แข็งตัวอย่างสมบูรณ์

อุปกรณ์ของไหลระดับไมครอนที่สร้างขึ้นนี้ประกอบด้วยโพรงสำหรับของไหลขาเข้า 2 โพรงเชื่อมต่อกับโพรงของไหลขาออกผ่านท่อลักษณะรูปตัว T (T-junction) คุณภาพอุปกรณ์ของไหลระดับไมครอนนี้สามารถตรวจสอบได้จากการผลิตหยดน้ำในตัวกลางน้ำมันโดยในการทดลองนี้ใช้ปั๊มกระบอกฉีดยาในการฉีดลำน้ำมันผ่านทางโพรงของไหลขาเข้าอันแรกผ่านไปตามท่อหลักขนาด 95 ไมครอนและฉีดสารละลายน้ำสีแดงผ่านทางโพรงของไหลข้าเข้าอันที่สองเข้าไปในท่อรองขนาด 150 ไมครอนซึ่งตั้งฉากกับท่อหลักโดยมีอัตราการไหลที่เท่ากันคือ 0.16 ไมโครลิตรต่อนาที พฤติกรรมการไหลของหยดน้ำในตัวกลางน้ำมันนี้สามารถบันทึกภาพได้ด้วยกล้องวีดีโอบริษัท Sony ที่มีความเร็วในการจับภาพ 30 ภาพต่อวินาทีซึ่งเชื่อมต่อกับกล้องจุลทรรศน์ของบริษัท Zeiss ที่มีกำลังขยายสูงสุด 100 เท่า จากการทดลองพบว่าหยดน้ำมีขนาดความยาว 237.5 ไมครอน โดยขนาดความยาวของหยดน้ำที่ได้จากการคำนวณทางทฤษฎีในการทดลองนี้มีค่า 245 ไมครอน ซึ่งจะเห็นได้ว่าขนาดของหยดน้ำที่ได้จากการทดลองแตกต่างจากขนาดของหยดน้ำจากการคำนวณ ประมาณร้อยละ 3

งานวิจัยนี้ยังแสดงให้เห็นว่าเทคนิค PPAL สามารถนำมาใช้ในการสร้างลวดลายลงบนวัสดุซิลิกาอสัณฐาน โดยบริเวณที่มีการยิงด้วยไอออนนั้นพันธะระหว่างซิลิกากับออกซิเจนในเครือข่ายซิลิกาเกิดการแตกออก และเมื่อนำชิ้นงานซิลิกานี้มาใส่ในกรดไฮโดรฟลูออริก (hydrofluoric acid) ความเข้มข้นร้อยละ 4 โดยปริมาตรจะเกิดปฏิกิริยาการสึกกร่อนในบริเวณที่มีการยิงด้วยไอออนในอัตราที่เร็วกว่าบริเวณที่ไม่ถูกยิง ถ้าให้ค่า effective etched depth หรือ z คือค่าผลต่างความลึกจากการกัดกร่อนด้วยกรดไฮโดรฟลูออริกของบริเวณที่มีการยิงด้วยไอออนกับบริเวณที่ไม่ได้ถูกยิง และเมื่อศึกษาความสัมพันธ์ระหว่างค่าความเข้มข้นของไอออน (Φ) ของออกซิเจนพลังงาน 6.8 MeV กับค่า effective etched depth ของซิลิกาอสัณฐานภายหลังจากการกัดกร่อนด้วยกรดไฮโดรฟลูออริกดังกล่าวเป็นเวลา 60 นาที พบว่าค่า effective etched depth ขึ้นอยู่กับค่าความเข้มข้นของไอออนโดยมีสมการความสัมพันธ์คือ $z = 2.9[1-\exp(-1.5\Phi)]$ โดยที่ค่า z อยู่ในหน่วยไมครอน

และ Φ อยู่ในหน่วย 10^{14} ไอออนต่อตารางเซนติเมตร และเมื่อพิจารณาด้วยฟังก์ชันเชิงเส้นกำกับ (asymptotic function) พบว่าค่า effective etched depth มีค่าเข้าใกล้ค่าคงที่แอมพลิจูดเมื่อความเข้มข้นของไอออนมีค่ามากกว่า 1.6×10^{14} ไอออนต่อตารางเซนติเมตร ข้อมูลเบื้องต้นนี้สามารถนำมาใช้ในการสร้างลวดลายต้นแบบของไหลระดับไมครอน โดยที่ความลึกของลวดลายมีค่าคงที่ประมาณ 2.5 ไมครอน ลวดลายต้นแบบนี้ประกอบด้วยโพรงของไหลขาเข้า 3 โพรงที่มีความกว้างและยาวอย่างละ 200 ไมครอนเชื่อมต่อกับโพรงขาออกขนาดเท่ากันผ่านทางท่อขนาดประมาณ 20 ไมครอน

จากการศึกษาวิจัยนี้สามารถสรุปได้ว่า เทคนิค PPAL ที่พัฒนาขึ้นที่มหาวิทยาลัยยูวาสคูลลาและมหาวิทยาลัยเชียงใหม่เหมาะสำหรับใช้ในการสร้างลวดลาย 3 มิติ บนพอลิเมอร์ PMMA ในสมบัติแบบ positive resist และแบบ negative resist ลวดลายที่สร้างจากพอลิเมอร์ PMMA สามารถนำมาใช้เป็นแม่พิมพ์ในการคัดลอกลวดลายลงบนพอลิเมอร์ PDMS อุปกรณ์ของไหลระดับไม-ครอนที่สร้างจากการศึกษาวิจัยนี้ได้มีการทดสอบคุณภาพโดยการนำมาใช้ในการผลิตหยดน้ำในตัวกลางน้ำมัน นอกจากนี้เทคนิค PPAL ยังสามารถนำมาใช้ในการสร้างลวดลายลงบนวัสดุซิลิกาอสัณฐานซึ่งสามารถทำเป็นอุปกรณ์ของไหลระดับไมครอนได้ในอีกรูปแบบหนึ่ง จะเห็นได้ว่าเทคนิค PPAL ที่ได้พัฒนาขึ้นมานี้สามารถสร้างอุปกรณ์ที่ใช้กับงานได้หลากหลายและสมควรได้รับการพัฒนาเพื่อใช้ในอุตสาหกรรมต่อไปในอนาคต

Publications included in the thesis

This thesis is based on the following publications (my contributions are in parentheses).

Development of MeV ion beam lithography

I. *Programmable proximity aperture lithography with MeV ion beams.* **N. Puttaraksa**, S. Gorelick, T. Sajavaara, M. Laitinen, S. Singkarat, and H.J. Whitlow, J. Vac. Sci. Tech. B 26 (2008) 1732. (Led the testing of development system at JYU, the calibration procedures, investigation of multiple scattering, participated in SEM characterization of the samples, principal author.)

II. *Resolution Performance of Programmable Proximity Aperture MeV Ion Beam Lithography System.* S. Gorelick, T. Sajavaara, M. Laitinen, **N. Puttaraksa**, and H.J. Whitlow, Mater. Res. Soc. Symp. Proc. Vol. 1020–GG03–04 (2007). (Testing the resolution performance of the PPAL system at JYU, contributed to writing the paper.)

III. *In–situ Beam Fluence Monitoring System for MeV Ion Beam Lithography at CMU.* **N. Puttaraksa**, M.W. Rhodes, T. Kamwanna, U. Tippawan, C. Thongleurm, W. Ginamoon, H.J. Whitlow, and S. Singkarat, Thai Journal of Physics, Series 5, 163 (2010). (Let the development of PPAL system at CMU, the development of fluence monitoring, SEM characterization of the samples, principal author.)

IV. *Lithography exposure characteristics of poly(methyl methacrylate) (PMMA) for carbon, helium and hydrogen ions.* **N. Puttaraksa**, R. Norarat, M. Laitinen, T. Sajavaara, S. Singkarat, and H.J. Whitlow, Nucl. Instr. and Meth. B (2011), doi:10.1016/j.nimb.2011.01.056. (Took part in the sample preparation, the exposure characteristics, SEM characterization of the samples, principal author.)

Application of MeV ion beam lithography on Microfluidics

V. *3D Micro–channel fabrication in PMMA based on MeV ion beam lithography.* **N. Puttaraksa**, S. Gorelick, T. Sajavaara, S. Singkarat and H.J. Whitlow, Thai Journal of Physics, Series 4, 89 (2009). (Took part in the sample preparation, SEM characterization

of the sample, principal author).

VI. *Fabrication of microfluidic devices using MeV ion beam Programmable Proximity Aperture Lithography (PPAL).* S. Gorelick, **N. Puttaraksa**, T. Sajavaara, M. Laitinen, S. Singkarat, and H.J. Whitlow, Nucl. Instr. and Meth. B 266 (2008) 2461. (Took part in the sample preparation, participate in SEM characterization of the sample, contributed to writing the paper.)

VII. *Fabrication of a negative PMMA master mold for soft–lithography by MeV ion beam lithography.* **N. Puttaraksa**, S Unai, M.W. Rhodes, K. Singkarat, H.J. Whitlow, and S. Singkarat, Nucl. Instr. and Meth. B (2011), doi:10.1016/j.nimb.2011.01.053. (Led the development of the negative PMMA master mold and microfludic device fabrication, charaterization of microfluidic chip, principal author.)

VIII. *Direct writing of channels for microfluidics in silica by MeV ion beam lithography.* **N. Puttaraksa**, M. Napari, O. Chienthavorn, R. Norarat, T. Sajavaara, M. Laitinen, S. Singkarat, and H.J. Whitlow, Submitted to Advanced Materials Research. (Took part in the sample preparation and measuring the exposure characteristics of silica, SEM characterization of the samples, principal author.)

Contents

1 Introduction **1**

2 Microfluidic devices **5**

2.1 Fundamentals of microfluidic flow . . . 5

2.1.1 Governing equations . . . 5

2.1.2 Pressure driven flow in a rectangular microchannel . . . 6

2.2 Droplet formation in microfluidic T–junctions . . . 8

3 Principle of microfluidic fabrication with MeV ions **11**

3.1 Mechanisms of MeV ion interaction with matter . . . 11

3.1.1 Energy loss . . . 11

3.1.2 Nuclear stopping . . . 12

3.1.3 Electronic stopping . . . 15

3.1.4 Multiple scattering . . . 16

3.2 Chemical effects in ion beam irradiated polymers . . . 16

3.2.1 Ion–polymer interaction . . . 16

3.2.2 Radiation G–value . . . 17

3.3 Poly(methyl methacrylate): PMMA . . . 19

3.4 Poly(dimethylsiloxane): PDMS . . . 19

3.5 Amorphous silica: silicon dioxide (SiO_2) . . . 20

3.6 Lithography and soft–lithography . . . 21

3.6.1 MeV ion beam lithography (MeV–IBL) . . . 21

3.6.2 Soft–lithography . . . 24

4 Ion beam lithography systems **27**

4.1 Programable proximity aperture lithography at JYU . . . 27

4.1.1 PPAL system . . . 27

4.1.2 MeV ion beam exposure . . . 30

4.2 Programmable proximity aperture lithography at CMU . . . 32

4.2.1 CMU–MeV IBL system . . . 32

4.2.2 Fluence monitor . . . 35

5 Experimental results and discussions **39**

5.1 Characterization of ion beam exposure characteristics for poly(methyl methacrylate) . . . 39

5.2 Exposure characteristic of amorphous silica (SiO_2) . . . 41

5.3 Study of dose spreading at edges . . . 42

5.4 Microstructure fabrication by the PPAL technique . . . 44
5.4.1 "Positive" tone PMMA structures . . . 45
5.4.2 "Negative" tone PMMA structures . . . 45
5.4.3 SiO_2 microfluidic structure . . . 45
5.5 PDMS replication . . . 46
5.6 Test microfluidic device . . . 47
5.7 Summary of the Papers . . . 48
5.7.1 Paper I . . . 48
5.7.2 Paper II . . . 49
5.7.3 Paper III . . . 50
5.7.4 Paper IV . . . 50
5.7.5 Paper V . . . 51
5.7.6 Paper VI . . . 52
5.7.7 Paper VII . . . 52
5.7.8 Paper VIII . . . 53

6 Conclusions 55

7 Future vistas 57

Appendix: Publications not included in the thesis 59

References 61

1 Introduction

During the past few decades, an interdisciplinary field including physics, engineering, biotechnology, chemistry, etc., so called "Microfluidics", has been intensively investigated. This is a science and technology that deals with manipulation of a small quantities of fluids, typically nL–aL (10^{-9} to 10^{-18} liters), flowing in a tens to hundreds of micrometer size channels [Whitesides06]. Microfluidic devices have recently been used in many applications such as pharmaceuticals, biotechnology, life sciences etc. due to their advantages i.e., small volume of reagent, low cost for production, and high sensitive and fast analysis. Moreover, there is a possibility to integrate a whole laboratory in to a single chip giving rise to the acronym "Lab–on–a–chip" or "Micro–total–analysis–system (μ–TAS)" [Ouellette03].

In the beginning of development in microfluidics, the devices were mostly fabricated in glass and silicon materials. Consequently, production was expensive and time consuming [Shao07]. This gave a driving force to many researchers and companies to find cheaper materials and approaches. This lead to fabrication of microfluidic devices in polymeric materials are versatile alternatives because of their biocompatibility, low cost and disposability. Furthermore, mass production of the polymer–based microfluidic chips can be achieved by many techniques such as soft–lithography, nanoimprint lithography, injection molding, etc. [Whitesides01, Guo07, Becker02].

Lithographic microstrucutures have been written by using conventional lithographies e.g. photolithography (EUV), electron beam lithography (EBL), X–ray lithography (LIGA), focused ion beam (FIB) lithography and MeV ion beam lithography (MeV–IBL) [Madou02]. Among the conventional lithographies, MeV–IBL is considered to be an interesting technique due to its unique advantages [Van Kan08]. A comparison between the MeV–IBL and other methods has previously been reported by Watt et al. [Watt05] based on the dose distributions schematically shown in Fig. 1.1. The main advantage of using MeV ions for patterning materials is that their trajectory is straight with a long well–defined penetration depth. This means that MeV–IBL can be used to fabricate structures with straight and vertical side walls [Chiam07]. Moreover, three dimensional (3D) high aspect ratio structures in thick polymer resist can also be produced by using the MeV–IBL technique [Van Kan07]. In contrast, the electron beam lithography technique is limited to use for fabricating essentially 2–dimensional (2D) structures in thin polymer resist films since the electron trajectories have large spread except close to the surface (∼100 nm) (see Fig. 1.1). In focused ion beam (FIB) lithography, low energy heavy ions are used to sputter atoms from the surface.

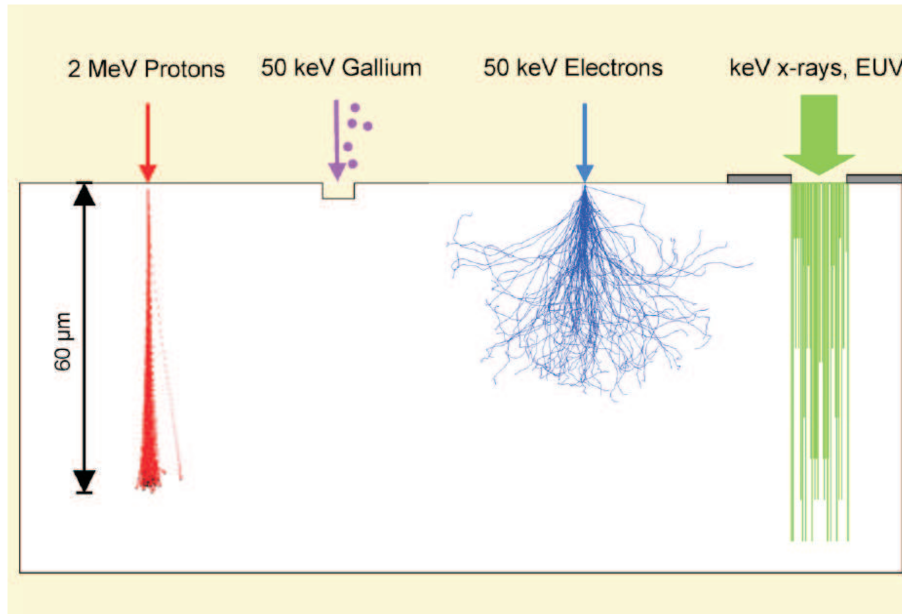

Figure 1.1: Comparison of predicted modification profiles among 4 different lithographic techniques (After [Watt05] used with permission).

However, the sputtering is very low. Therefore, it is very time consuming to produce 3D high aspect ratio structures [Munnik03] and also it introduces significant atomic displacement damage. In the case of photo– and X–ray lithography, the penetration depth is not well defined and the absorption leads to an exponentially decreasing dose with depth. For this reason, the thickness of the structure cannot be well–controlled. In addition, masks are needed for the exposure process. This leads to a high production cost for these techniques.

There are two basic approaches for MeV–IBL. One approach is well–known as proton beam writing (PBW), which was largely pioneered at the Center for Ion Beam Applications (CIBA) of the National University of Singapore [Watt07]. This technique utilizes a focused 2 MeV proton beam of sub–100 nm spot size [Chatzichristidi08] which by scanning the beam is used to write a 3D structure in a polymeric resist. The second approach, which is developed in this thesis, is called programmable proximity aperture lithography (PPAL) [Paper I]. In this technique, the MeV ion beams are shaped to a rectangle with side lengths of 0.2–500 μm by a pair of L–shaped aperture blades mounted on motorized motion slides. By combining exposures with different sized rectangular beam with programmed motion of the X–Y stages on which the sample is mounted, complex patterns can be written by this technique. Although the PPAL technique does not have the resolution of the focused proton beam writing technique, it has the significant advantage that is much faster especially for large areas because each pattern element is written in a single exposure [Sangyuenyongpipat09].

This thesis is divided into six chapters. An introduction to MeV ion beam lithography and microfluidics are discussed in Chapter one. Chapter two describes details of basic fluid flow in microfluidic devices. In addition, micro–droplet generation using a T–junction microfludic device is also included in this chapter. Chapter three explains the principle of fabrication of microfluidic device using MeV ion beam lithography. The MeV ion beam lithography and soft–lithography techniques are demonstrated in this chapter. Chapter four introduces the programmable proximity aperture lithography systems used in this thesis. The two similar facilities, which are developed at both the University of Jyväskylä (JYU) in Finland and the Chiang Mai University (CMU) in Thailand, are presented in detail. Chapter five presents the results and discussions of the experiments and also a summary of the papers. Chapter six concludes this thesis. Finally, Chapter seven presents the future vistas of this study.

2 Microfluidic devices

This chapter presents an overview of fluid flow along a rectangular microchannel. Pressure–driven fluid flow, which has been used to propel fluids in this study, is also described. Moreover, generation of micro–droplets using T–junction pattern microfluidic devices is described in detail.

2.1 Fundamentals of microfluidic flow

2.1.1 Governing equations

As previously mentioned in the introduction section, microfluidics is a science and technology that is concerned with manipulation of fluid flowing in microchannels by internal or external forces. On a microscale, the physical phenomena are quite different from a macroscopic scale. Typical dominant effects are laminar flow, diffusion, fluidic resistance, surface area to volume ratio and surface tension [Beebe02, Squires05].

The behavior of fluid flow is generally described by two main governing equations, which can be derived from the laws of conservation of mass, momentum and energy. The first governing equation can be expressed in terms of a continuity equation as shown in Eq. (2.1) [Bruss08],

$$\frac{\partial \rho}{\partial t} + \nabla \cdot (\rho \mathbf{v}) = 0, \tag{2.1}$$

where $\frac{\partial \rho}{\partial t}$ is the time derivative of the mass density ρ and $\mathbf{v}$ is the fluid velocity field. This continuity equation represents the conservation of mass of fluid flow through a fixed boundary region. In a typical microfluidic device, the fluid can be treated as an incompressible fluid because the velocity of fluid flow is negligibly small when compared with the velocity of pressure waves (sound) in the liquid [Bruss08]. In this case, the mass density (ρ) is constant and independent of space and time. Therefore, the continuity equation reduces to:

$$\nabla \cdot \mathbf{v} = 0. \tag{2.2}$$

The second governing equation is a general equation for describing a fluid in motion. It is the well known Navier–Stokes equation, which is expressed as [Squires05, Bruss08],

$$\rho \left[\frac{\partial \mathbf{v}}{\partial t} + (\mathbf{v} \cdot \nabla)\mathbf{v} \right] = -\nabla p + \eta \nabla^2 \mathbf{v} + \mathbf{f}, \tag{2.3}$$

where p represents the applied pressure, η is the fluid viscosity and $\mathbf{f}$ is the body force densities. The Navier–Stokes equation is equivalent to Newton's second law where the left hand side refers to the product of mass per unit volume and the acceleration which balance the three forces on the right hand side of the equation which are pressure gradient, viscosity, and forces on the volume of fluid.

2.1.2 Pressure driven flow in a rectangular microchannel

The main techniques to drive fluid flow in microchannels can be categorized into pressure–driven, electrokinetic and capillary actuation [Sia03, Hetsroni05, Bruss08]. In pressure–driven fluid flow, a positive displacement pump such as a syringe pump is commonly used for fluid flow actuation in the microchannels. The syringe pump has many advantages; it can provide a sufficient pressure for handling fluid flow in a complicated microfluidic circuit, which usually has a high fluidic resistance R_h. Furthermore, it is suitable for use with both electrolytes and dielectric liquids [Sia03].

Infinite parallel–plate microchannel case

Here for simplicity we consider first the simpler infinite parallel–plate microchannel case. Subsequently, we consider the case of a finite closed microchannel.

A pressure difference $\triangle p$ is applied as the main source of driving force in pressure–driven flow. A simplified schematic drawing of the pressure driven flow in a closed infinite parallel–plate of length L and height h is depicted in Fig. 2.1. In order to solve the Navier–Stokes equation, the boundary conditions are very important. In this fluid flow, no–slip boundary conditions, where fluid velocity components at the walls are zero ($\mathbf{v} = 0$), are applied. Solution of the Navier–Stokes equation gives a fluid velocity field for fluid flow. For the pressure driven fluid flow in x–direction, this velocity field can be given by [Bruss08],

$$v_x(z) = \frac{\Delta p}{2\eta L}(h - z)z, \tag{2.4}$$

where η is a viscosity of fluid. This implies that the velocity field follows a parabolic profile across the channel. Generally, the fluid velocity field can be used to determine a volumetric flow rate Q from the following relation [Bruss08],

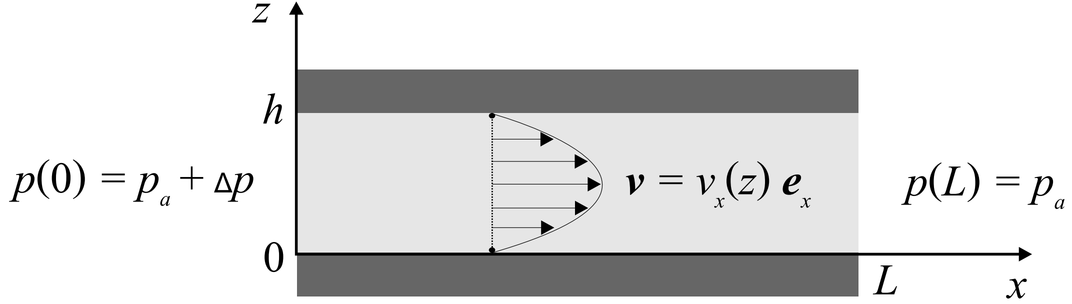

Figure 2.1: A pressure–driven fluid flow through an infinite parallel–plate channel of length L and height h where $\mathbf{e}_x$ is the unit vector of the flow direction (After [Bruss08]). This diagram implies that there is a pressure difference Δp between the two ends of the microfluidic channel.

$$Q = \int \mathbf{v} \cdot d\mathbf{a}, \tag{2.5}$$

where $d\mathbf{a}$ is a differential surface. Here, the volumetric flow rate through a section of the infinite parallel–plate of width w can be expressed by,

$$Q = \frac{h^3 w \triangle p}{12\eta L}. \tag{2.6}$$

Closed rectangular microchannel case

For fluid flow in a closed rectangular[1] microchannel of length L, width w, and height h as depicted in Fig. 2.2, the fluid velocity field can be expressed as [Bruss08]:

$$v_x(y,z) = \frac{4h^2\Delta p}{\pi^3 \eta L} \sum_n^{\infty} \frac{1}{n^3} \left[1 - \frac{\cosh(n\pi \frac{y}{h})}{\cosh(n\pi \frac{w}{2h})}\right] \sin(n\pi \frac{z}{h}), \tag{2.7}$$

where n are odd integers. In this case, the volumetric flow rate can be determined to be [Bruss08],

$$Q = \frac{h^3 w \triangle p}{12\eta L} \left[1 - \sum_n^{\infty} \frac{192h}{n^5 \pi^5 w} tanh\left(\frac{n\pi w}{2h}\right)\right]. \tag{2.8}$$

The volumetric flow rate can also be express as $Q = \Delta p / R_h$. Therefore, the fluidic resistance R_h of the rectangular microfluidic channel can be represented by,

$$R_h = \frac{12\eta L}{h^3 w [1 - \sum_n^{\infty} \frac{1}{n^5} \frac{192h}{\pi^5 w} tanh(\frac{n\pi w}{2h})]}. \tag{2.9}$$

[1] In this thesis only microfluidic channels of rectangular cross section are considered. This is because PPAL is suited to fabricate microchannels with rectangular cross section. Analytical solutions exist where the cross section is round or elliptical [Bruss08].

In case of $h < w$, the fluidic resistance can be approximated [Bruss08] as:

$$R_h = \frac{12\eta L}{[1 - 0.63(h/w)]h^3 w}. \tag{2.10}$$

In the limit of a high aspect ratio rectangular microfluidic channel ($h \gg w$), which can be achieved using MeV ion beam lithography, the fluidic resistance reduces to,

$$R_h = \frac{12\eta L}{h^3 w}. \tag{2.11}$$

There are many advantages of using high aspect ratio microchannel in microfluidic structures:
(i) high volume per unit area – important for reservoirs and capillary pumps
(ii) high packing density – important to minimise chip area consumption and achieve high functionality at low cost
(iii) large surface area per volume – important for surface specific bonding of markers in bioanalytical applications
(iv) low evaporation from small exposed surface.
The use of MeV ions to fabricate such structures is discussed in the next chapter.

2.2 Droplet formation in microfluidic T–junctions

Flow of two or more of immiscible fluids in a microchannel represents a multiphase fluidic flow. Multiphase flow is important for microfluidic devices because it can be used to create nanolitre droplets which are important in practical applications such as emulsification and encapsulation, microreactors, mixing, and bioassays [Shui07]. They also represent the flow of various biological fluids such as blood, serum etc which can contain cells, viruses in a liquid medium. For realizing droplet formation a T–junction

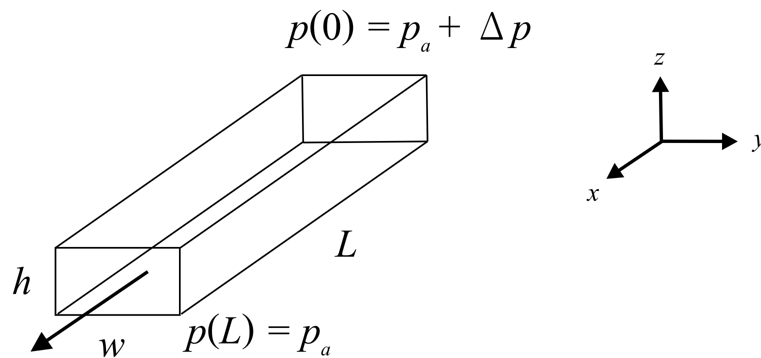

Figure 2.2: Schematic of a rectangular microchannel of height h, width w, and length L.

geometry is commonly used. Fig. 2.3 shows a schematic drawing of a T–junction microfluidic device for droplet generation. In this geometry, the main inlet channel of width w carries the flow of oil with volumetric flow rate Q_{oil}. Whereas, the second inlet channel of width d, which is orthogonal to the main inlet, is used to introduce a flow of water of volumetric flow rate Q_{water}. By solving the ratio of the volumetric flow rates of flow of the oil and water, the length of the droplets (L) can be determined by [Bruss08, Garstecki06],

$$L = \left(1 + \frac{d}{w}\frac{Q_{water}}{Q_{oil}}\right) w. \tag{2.12}$$

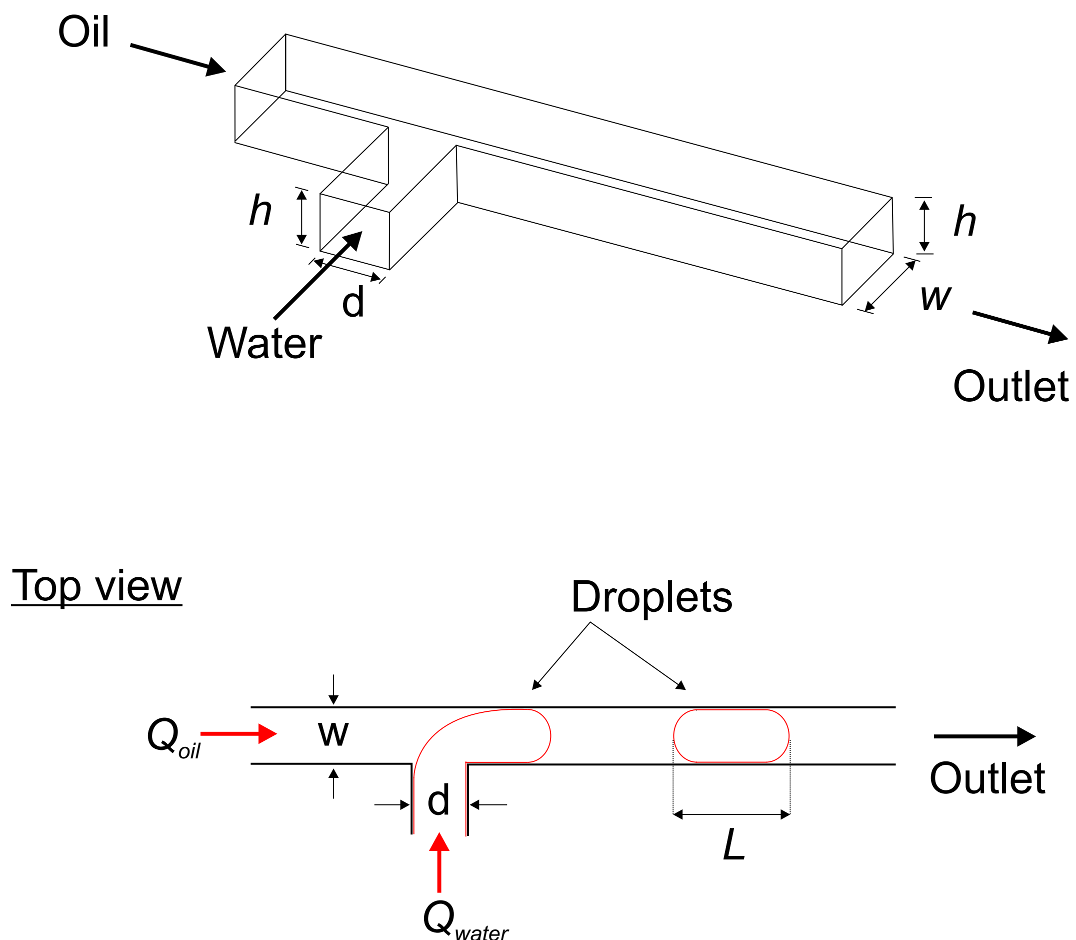

Figure 2.3: A schematic illustration of T–junction microfluidic device for generation of water droplets in an oil phase (Following: [Garstecki06]).

3 Principle of microfluidic fabrication with MeV ions

This chapter presents the interaction of MeV ions with materials and chemical effects in polymeric materials after ion beam exposure. The process used to fabricate three dimensional (3D) microstructures using MeV ion beam lithography is also presented. Furthermore, a process to produce poly(dimethylsiloxane), PDMS microfluidic devices is discussed.

3.1 Mechanisms of MeV ion interaction with matter

3.1.1 Energy loss

When an energetic ion traverses through matter, it interacts with nuclei and electrons of the target, typically through more than thousand collisions [Watt07], before coming to rest. One of the most important quantities associated with this slowing down process is the energy loss $\mathrm{d}E/\mathrm{d}x$, which is by the average energy loss $\mathrm{d}E$ of the incoming ion per unit travelling depth $\mathrm{d}x$. This is the *stopping force* [Sigmund04, Hellborg09]. Often terms such as the "linear energy transfer (LET)" and "stopping power" are used synonymously to mean stopping force. This quantity is an important parameter used for calculation of the ion's penetration depth or range, R, according to the following relation [Lindhard63],

$$R = \int_{E_0}^{0} \frac{1}{\mathrm{d}E/\mathrm{d}x} dE, \tag{3.1}$$

where E_0 denotes an incident ion energy and the sign of the dE/dx is negative.

Fig. 3.1 shows a schematic illustration of energetic ion interactions with the target material. The ion transfers its kinetic energy to the medium by two main processes i.e., *nuclear stopping* and *electronic stopping*. More details of these processes will be given in the following sections. The nuclear and electronic stopping not only reduce the speed of the ion (denoted as *stopping*) but is also associated with deflection of the ion trajectory from the initial direction (denoted as *scattering*) [Nastasi96]. The

total energy loss, $\mathrm{d}E/\mathrm{d}x|_{tot}$, can simply be expressed by,

$$\frac{\mathrm{d}E}{\mathrm{d}x}|_{tot} = \frac{\mathrm{d}E}{\mathrm{d}x}|_n + \frac{\mathrm{d}E}{\mathrm{d}x}|_e, \tag{3.2}$$

where subscripts n and e refer the nuclear and electronic stopping, respectively. Typical energy losses are of the order of a few to many 100 eV/nm depending on the target material [Nastasi96]. The stopping force can easily be estimated by using the computer predictor code SRIM [SRIM].

The energy loss is also related to the stopping cross–section S (eV$\cdot cm^2$/atoms) through the relation, given by [Nastasi96],

$$S(E) = \frac{1}{N}\frac{\mathrm{d}E}{\mathrm{d}x}, \tag{3.3}$$

where N is the number of target atoms per unit volume in atoms/cm^3. This parameter is often more useful than the stopping force because it is independent of target density.

3.1.2 Nuclear stopping

In a nuclear collision, an energetic ion loses its kinetic energy to a target atom by scattering in a screened coulombic interaction. The collision can be considered to be a binary collision, or two body collision since its mean free path is much larger than the interatomic distance [Nastasi96]. The nuclear stopping or nuclear energy loss is an elastic collision process. This process is predominant when the incident ion has low energy E_0 and high atomic number Z_1 [Nastasi96].

The nuclear stopping and associated scattering is small, but persistently present even at high energies. The nuclear stopping is the main contributor to angular deflection of the ion's trajectory. Atomic displacement of the target atom can take place when the energy transfer from the ion to the target atom is larger than some displacement energy (E_d), which is the effective average energy for displacing the target atom from its original lattice site. The transferred energy results in vibration of the target atom when the energy transfer is less than the displacement energy. In both regimes, phonons can be released instead of the energy dissipation [Nastasi96, Lee99].

As previously mentioned, the collision between the ion and the target atom is elastic so that the total momentum and energy are conserved. Using the principle of momentum and energy conservation, a kinetic energy transfer T of the ion to the target atom can be written as [Nastasi96]:

$$T = \Lambda E_0, \tag{3.4}$$

$$\Lambda = \frac{4M_1M_2}{(M_1+M_2)^2} sin^2(\frac{\theta_c}{2}), \tag{3.5}$$

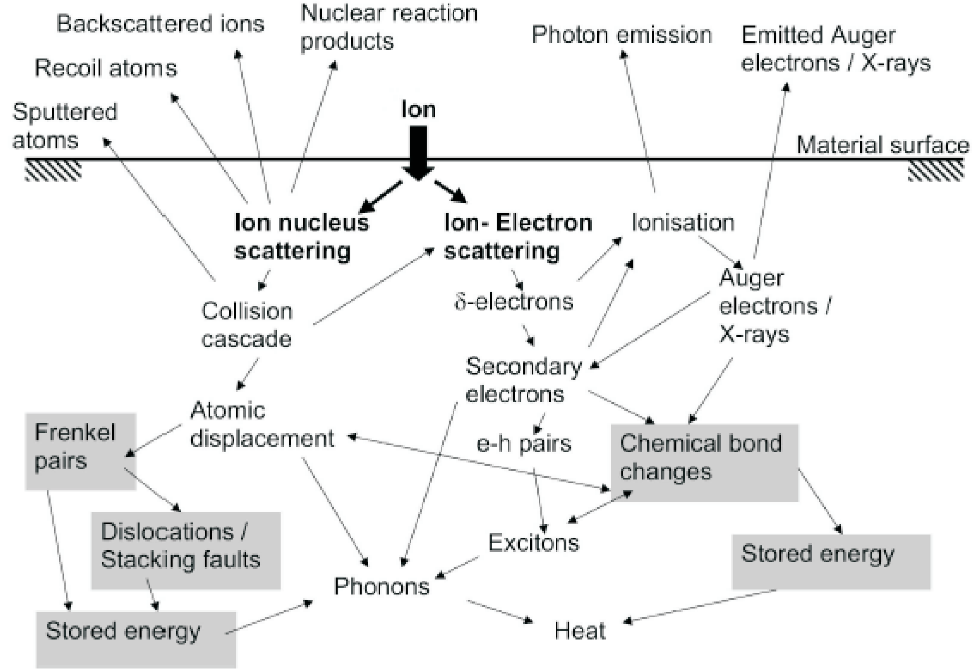

Figure 3.1: Schematic illustration of an incoming ion interactions with nuclei and electrons of the target material (From: [Zhang05] used with permission).

where Λ is the kinematic factor, θ_c is the center–of–mass scattering angle of the ion, and M_1 and M_2 are the masses of the ion and the target atom, respectively. In scattering by a central potential $V(r)$, the center–of–mass scattering angle θ_c can be determined from the equation [Nastasi96, Fink04, Sigmund06],

$$\theta_c = \pi - 2b\int_{r_0}^{\infty} \frac{\mathrm{d}r}{r^2[1 - V(r)/E_c - (b/r)^2]^{1/2}}, \tag{3.6}$$

in which $E_c = \frac{M_2}{M_1+M_2}E_0$ is the center–of–mass total energy, b is the impact parameter and r_0 is the closest distance between the ion and the target atom.

For an infinitesimal penetrating depth $\mathrm{d}x$ in the target material, the nuclear energy loss ($\frac{dE}{dx}|_n$) can be expressed by [Nastasi96],

$$\frac{\mathrm{d}E}{\mathrm{d}x}|_n = N\int_{T_{min}}^{T_{max}} T\frac{\mathrm{d}\sigma(E)}{\mathrm{d}T}\mathrm{d}T, \tag{3.7}$$

where N is the density of the target material, $\mathrm{d}\sigma(E)/\mathrm{d}T$ is the differential cross–section of the energy transfer, and T_{min} and T_{max} are the minimum and maximum energy transfers, respectively. T_{min} can be taken to be zero $\mathrm{d}\sigma(E)/\mathrm{d}T \to 0$. This is generally the case for a screened Coulomb interaction potential (discussed below). From the Eq. (3.4), the maximum energy transfer is given by $T_{max} = \frac{4M_1M_2}{(M_1+M_2)^2}E_0$,

which occurs in a head–on collision ($\theta_c = 180°$).

Using the relationship in the Eq. (3.3), the nuclear stopping cross–section $S_n(E)$ can also be written as:

$$S_n(E) = \int_{T_{min}}^{T_{max}} T \frac{\mathrm{d}\sigma(E)}{\mathrm{d}T} \mathrm{d}T. \tag{3.8}$$

The scattering angle θ_c is a function of the interatomic potential $V(r)$ as follows Eq. (3.5). Many analytically tractable empirical potentials such as the hard–sphere, square–well, inverse–power, and Lennard–Jones potentials have been used for calculation of the interatomic potential [Nastasi96]. For the screened Coulomb potential, $V(r)$ can be written as [Fink04]:

$$V(r) = \frac{Z_1 Z_2 e^2}{4\pi\epsilon_0 r} \Phi\left(\frac{r}{a}\right), \tag{3.9}$$

where Z_1 and Z_2 are the atomic numbers of the incident ion and the target atom, respectively, $\Phi(\frac{r}{a})$ is the screening function, and a is a screening length. The screening length is related to the Bohr radius a_0 through this relation [Ziegler85],

$$a = \frac{0.8854 a_0}{Z_1^{0.23} + Z_2^{0.23}}. \tag{3.10}$$

By using the Ziegler, Biersack, and Littmark (ZBL) universal screening function, a practical calculation of the nuclear energy loss ($\frac{dE}{dx}|_n$), of an incident ion mass M_1 and atomic number Z_1 with the incident energy E_0 impinging on the target atom of mass M_2 and atomic number Z_2, can be approximated by [Nastasi96],

$$\frac{dE}{dx}|_n = N \frac{8.462 \times 10^{-15} Z_1 Z_2 M_1 S_n(\varepsilon)}{(M_1 + M_2)(Z_1^{0.23} + Z_2^{0.23})} \quad eV/nm, \tag{3.11}$$

where $S_n(\varepsilon)$ is the reduced stopping cross–section which is given by:

$$S_n(\varepsilon) = \frac{0.5\ell n(1 + 1.1383\varepsilon)}{\varepsilon + 0.01321\varepsilon^{0.21226} + 0.19593\varepsilon^{0.5}} \qquad \text{for } \varepsilon \leq 30, \tag{3.12}$$

and

$$S_n(\varepsilon) = \frac{\ell n(\varepsilon)}{2\varepsilon} \qquad \text{for } \varepsilon > 30, \tag{3.13}$$

where the reduced energy ε is given by,

$$\varepsilon = \frac{32.53 M_2 E_0}{Z_1 Z_2 (M_1 + M_2)(Z_1^{0.23} + Z_2^{0.23})}. \tag{3.14}$$

3.1.3 Electronic stopping

In electronic stopping, the ion's energy is transferred to the electrons of the target atom by two main mechanisms; electronic excitation and ionization through a coulomb interaction. It should be emphasized that both excitation of the projectile and target atoms contribute. The electronic stopping mechanism is essentially an inelastic process; which is dominant when the ion has high energy (E_0) and low atomic number (Z_1) [Nastasi96]. When the ion velocity v_0 is much smaller than the Bohr velocity v_b ($v_b = 2.2 \times 10^6$ m/s) ∼10 keV or less, the ion mainly loses energy by the nuclear stopping process. At low energies the electronic stopping force is proportional to velocity ($\frac{dE}{dx}|_e \propto \sqrt{E}$) up to $v_0 = Z_1^{2/3} v_b$. For a very fast ion, or when the ion velocity $v_0 \geq Z_1^{2/3} v_b$, the electronic stopping decreases with increasing energy proportional to Z_1/E_0 [Nastasi96]. Between the two regions there is a broad maximum that is often called the Bragg maximum, or peak.

The electronic stopping force is given by,

$$\frac{\mathrm{d}E}{\mathrm{d}x}|_e = NZ_2 \int_{T_{min}}^{T_{max}} T \frac{\mathrm{d}\sigma(E)}{\mathrm{d}T} \mathrm{d}T, \tag{3.15}$$

and the electronic stopping cross section is determined by,

$$S_e(E) = Z_2 \int_{T_{min}}^{T_{max}} T \frac{\mathrm{d}\sigma(E)}{\mathrm{d}T} \mathrm{d}T, \tag{3.16}$$

where Z_2 is the atomic number of the target material. T_{min} in this case is the smallest excitation an electron energy.

The electronic energy loss, in SI units, can be estimated from the following equation [Sigmund04, Whitlow09],

$$\frac{\mathrm{d}E}{\mathrm{d}x}|_e = \frac{NZ_1^2 Z_2 e^4}{4\pi\varepsilon_0^2 m_e v_0^2} L_e, \tag{3.17}$$

where e is the electronic charge, ε_0 is the vacuum permittivity, m_e is the rest mass of electron, and L_e is the electronic stopping number. Generally, there are two categories for the electronic energy loss i.e. fast light ions and slower heavy ions. For the fast light ion in the Bethe region where the $1st$ Born approximation is valid, the electronic stopping number is defined as:

$$L_e = L_{Bethe} = \ell n(\frac{2m_e v_0^2}{I}), \tag{3.18}$$

in which $I = 10Z_2$ is the average excitation energy in eV [Nastasi96]. Whereas, the electronic stopping number of the slow heavy ion, follows the earlier estimate based

on Bohr's stopping theory [Sigmund04, Whitlow09],

$$L_e = L_{Bohr} = \ell n(\frac{1.12292 e_e v_0^3}{Z_1 e^2 \omega}). \tag{3.19}$$

3.1.4 Multiple scattering

As discussed in the previous section, when an energetic ion passes through matter, it collides with the nuclei and electrons of the target material. In each collision, not only its energy is transferred but also the ion's trajectory is deflected through a small angle relative to the initial direction (*scattering*). Single scattering corresponds to the situation in a very thin layer of the substrate when the ion experiences just one collision. The ion can undergo many collisions as the thickness of the substrate is increased, namely multiple scattering [Whitlow09, Amsel03].

The angular and lateral spreading from multiple scattering are important in many applications e.g., ion beam analysis (IBA), ion implantation, particle detection, MeV ion beam lithography, etc. In some applications of MeV ion beam lithography such as metal lift–off [Whitlow04], optical waveguides [Bettiol06] and narrow micro– and nanofluidics [Wang07, Shao07], an almost perfect vertical side wall of the patterns is required. The deflection of the ion's trajectory can give rise to an increasing deposited energy outside the irradiated area leading to a deviation from a perfect vertical side wall.

3.2 Chemical effects in ion beam irradiated polymers

3.2.1 Ion–polymer interaction

Polymers are macromolecules consisting of a set of regularly repeated chemical units bonded covalently together. Typically, they are classified according to the structure i.e. linear, branched and network polymers as schematically shown in Fig. 3.2. A kind of polymer, which is commonly used in lithographic applications, is a so called "resist". These are sensitive to radiation such as visible or UV light, X–rays, electrons and ions [Fink04]. When an energetic ion passes through a polymeric medium, it is slowed down by its energy transfer in nuclear and electronic scattering as discussed above. The interaction between the ion and the polymer can lead to two main effects, namely chain scission and cross–linking. Bond cleavages of polymer chains can take place both in the main chain and side chain upon ion irradiation [Fink04]. The chain scissioning processes cause the degradation (lower average molecular weight) of the

polymer and the formation of free radicals and gaseous products [Dong99, Chapiro98]. This leads to an increase in solubility of the polymer, where the shorter chains are the more soluble [Fink04]. On the contrary, cross–linking takes place if two free dangling ions or radical pairs on the neighboring chains are readily able to bond with each other [Lee99]. This process results in an increase of molecular weight by formation of a network polymer (Fig. 3.2(c)), which reduces the solubility of the polymer, and also increases hardness and wear resistance [Dong99].

The resist, in which chain scission predominates, is called a "positive" resist. In contrast, a "negative" resist corresponds to a resist in which cross–linking predominates. A general rule for considering if the structure of the polymer corresponds to a "positive" or "negative" resist is shown in Fig. 3.3. The "negative" resists usually have a structure, in which carbon atom of the backbone has at least one hydrogen atom (either $\mathbf{R}_1$ or $\mathbf{R}_2$). In contrast, if the polymer is a "positive" resist, neither $\mathbf{R}_1$ nor $\mathbf{R}_2$ bonded to the backbone carbon atom is hydrogen. This model for considering either positive or negative resist is a rule of thumb proposed by Dong et. al. [Dong99]. A summary of some "positive" and "negative" resists is depicted in Table 3.1.

3.2.2 Radiation G–value

One of general parameters used to determine the effect of high energy ion modification of polymers is the radiation G–value. It is determined by the number of chain scission (G_s) and cross–linking (G_x) events produced per 100 eV energy absorbed by the polymer. The scissioning radiation G_s–value can be calculated according to [Adesida83],

$$\frac{1}{M_n^*} = \frac{1}{M_n} + \frac{DEG_s}{ke\rho t N_A}, \tag{3.20}$$

where M_n^* and M_n are the average molecular weight of the initial and irradiated

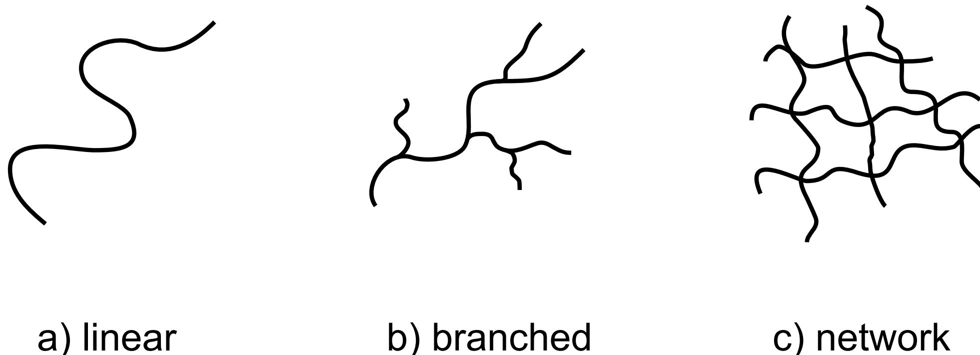

Figure 3.2: Schematic illustration of (a) a linear polymer, (b) a branched polymer and (c) a network polymer (After [Bower02]).

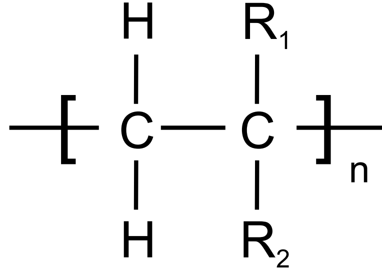

Figure 3.3: A general structure of monomer for the consideration as "positive" or "negative" resist (after [Dong99]).

polymer, respectively, D is the irradiation dose in C/cm^2, E is the absorbed energy in eV, k = 100 eV, e is the electronic charge, ρ is the density of the target polymer in g/cm^3, t is the thickness of the polymeric film in cm, and N_A is Avogadro's number.

On the contrary, the number of cross–linking bonds generated per 100 eV energy absorbed (G_x) is determined by [Herden98],

$$G_x = \frac{100N_A}{2M_w D_{gel}}, \tag{3.21}$$

where M_w represents the average molecular weight before irradiation and D_{gel} is the

Table 3.1: Positive resists versus negative resists [Dong99].

Chain scission polymers (positive resist)	Cross–linking polymers (negative resist)
Polyisobutylene	Polyethylene (PE)
Poly(α–methylstyrene)	Polypropylene (PP)
Polymethacrylates	Polystyrene (PS)
Polymethylmethacrylates (PMMA)	Polyacrylates
Polymethacrylamide	Polyacrylamide
Poly(vinylidene chloride)	Polyvinyl chloride (PVC)
Cellulose and derivatives	Polyimide (PI)
Polytetrafluoroethylene	Polyesters
Polytrifluorochoroethylene (PTFE)	Polyvinylpyrrolidone
	Rubbers
	Polysiloxanes
	Polyvinylalcohol (PVA)
	Polyacroleine

absorbed dose for gelation which is defined as:

$$D_{gel} = \frac{\Phi t_{gel}(dE/dx)}{\rho}, \tag{3.22}$$

where Φt_{gel} denotes the gelation fluence and dE/dx is the stopping force of the ion to the polymeric medium. In practise there are no clear experimentally accessible signals for the number of main–chain scissions and cross–linking bonds formed per ion. This makes interpretation of exposure characteristics using the G–values non trivial.

3.3 Poly(methyl methacrylate): PMMA

Poly(methyl methacrylate), PMMA, is a common positive resist that has been widely used in conventional lithography methods such as UV–lithography, electron beam lithography (EBL), MeV ion beam lithography (MeV–IBL), etc. The molecular structure of PMMA is schematically illustrated in Fig. 3.4(a). It has a high hardness and rigidity; however, it is brittle [Fink04]. Furthermore, it is highly transparent to visible light and near UV. PMMA also is known under the tradenames as Plexiglas® and Lucite®. The main effect in PMMA, when irradiated with low ion fluences, is chain scission. However, the modification can transform from chain scission dominated to cross–linking dominant at high ion fluences.

3.4 Poly(dimethylsiloxane): PDMS

Poly(dimethylsiloxane) or PDMS is an elastomeric polymer. Fig. 3.4(b) shows the molecular structure of PDMS. Recently, it has been used as an alternative material to silicon and glass for microfluidic applications. This is because it has many advantageous properties; for example it is inexpensive and flexible and its optical transparency extends to ∼230 nm [Sia03]. For this reason, the PDMS microfluidic devices can be used for analysis based on optical detection. PDMS is also biocompatible; it is thus suitable for biomedical microfluidic devices [Sia03]. Moreover, micro–structures can be easily transferred to PDMS by replicating from the master mold in a straightforward way with sub 100 nm precision [McDonald02] by using soft–lithography. This makes it suitable for mass production.

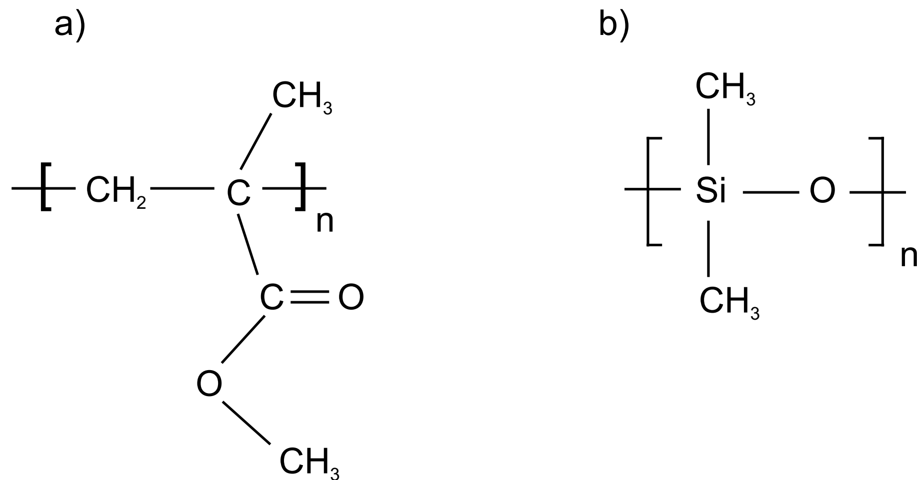

Figure 3.4: Molecular structures of (a) Poly(methyl methacrylate) PMMA. (b) Poly(dimethylsiloxane) PDMS.

3.5 Amorphous silica: silicon dioxide (SiO_2)

Amorphous silicon dioxide (SiO_2), also known as silica, is a common material used in many applications. These include the semiconductor industry (with uses ranging from the gate dielectric, furnace tubes to optical devices) and as the stationary phase in chromatography etc. This is due to the fact that it has many advantageous properties e.g. high chemical inertness, mechanical rigidity, high temperature resistance and optical transparency extending to deep ultraviolet [Klauk02, Wibbeler98, Teng07, Martin82]. Silicon dioxide occurs as an amorphous structure and a range of crystal structures. The crystalline structure is commonly known as quartz, whereas; fused silica or fused quartz refers to the amorphous structure. The molecular structure of amorphous silicon dioxide is schematically shown in Fig. 3.5. Pattern transfer to amorphous silicon dioxide can be achieved by many techniques such as ion track lithography [Jensen06], X–ray lithography [Mekaru10] and electron beam lithography [Beaumont10]. Silica is commercially available with extremely high purity e.g. synthetic fused silica. This makes it suitable for use as the stationary phase in chromatographic applications.

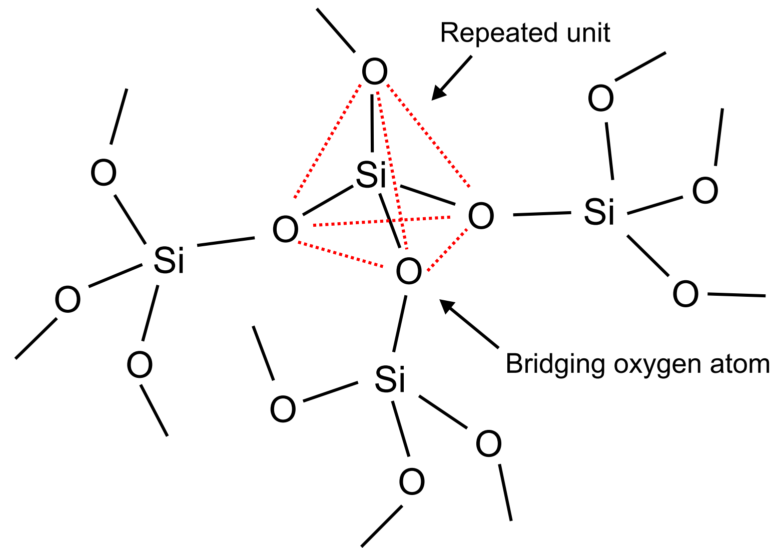

Figure 3.5: Chemical structure of amorphous silica (SiO_2). Amorphous silicon dioxide can be considered to be a network polymer.

3.6 Lithography and soft–lithography

3.6.1 MeV ion beam lithography (MeV–IBL)

In recent years MeV ion beam lithography (MeV–IBL) has emerged as a new tool for fabricating micro– and nano–structures in polymeric materials e.g., PMMA, SU–8 and HSQ [Watt07, Van Kan04, Gorelick09]. Fig. 3.6 shows a schematic diagram of the basic principle of micro– and nano–fabrication using MeV ions. At first, a polymer resist film is prepared by spin coating on a cleaned substrate such as Si or SiO_2. Next, the resist is exposed to high energetic ions such as protons, helium ions or heavy ions. There are two types of exposure techniques (i) where a scanned focused beam is used to paint the exposed region in the structure and (ii) where a beam shaped by a variable aperture is used to expose pattern elements as depicted in Fig. 3.6(b). Proton Beam Writing (PBW) is commonly used to describe the first case where MeV proton beams are commonly used. It employs a focused MeV ion beam that is scanned directly across a resist to produce the structures. In the second case, which is often termed programmable proximity aperture lithography (PPAL) a pair of L-shaped aperture blades are mounted on computer controlled motorised positioners. These are used to shape the exposing beam to a rectangular form with 0.2–500 μm size. By combining sample and aperture movements, the micro–nano structures can be created by using this technique [Paper I]. After exposure, the exposed sample is subsequently developed in a suitable developer. If the polymer resist is a positive resist, only the exposed area is removed by the developer leaving the unexposed areas. Whereas, for

the negative resist, the developer removes the unexposed area while the exposed area remains (see Fig. 3.6(c)). The MeV ion beam lithography technique can be used to fabricate a master mold for casting poly(dimethylsiloxane) or PDMS. This process will be discussed in the following section.

The MeV ion beam lithography technique can also be used for direct writing microstructures in amorphous silica (SiO_2). Swift ion irradiation of silica introduces network damage by breaking the Si–O bonds. This network damaged area is subsequently more susceptible to removal by selective etching in a 4% v/v aqueous hydrofluidic acid (HF) solution. A process of direct microfabrication in silica using the MeV ion beam lithography technique is schematically illustrated in Fig. 3.7.

One of the most important parameters in exposure of polymer resists with ion beams is the ion fluence (Φ). In ion matter interactions it is generally taken to be the number of ions $\mathrm{d}N$ passing through the area $\mathrm{d}A$ ($\Phi = \mathrm{d}N/\mathrm{d}A$). This has units ions per unit area. This does not explicitly define the direction as discussed in [Hellborg09]. However, $\mathrm{d}A$ is generally taken to be normal to the ion direction. There are several techniques for determining the ion fluence. However, a standard method is based on

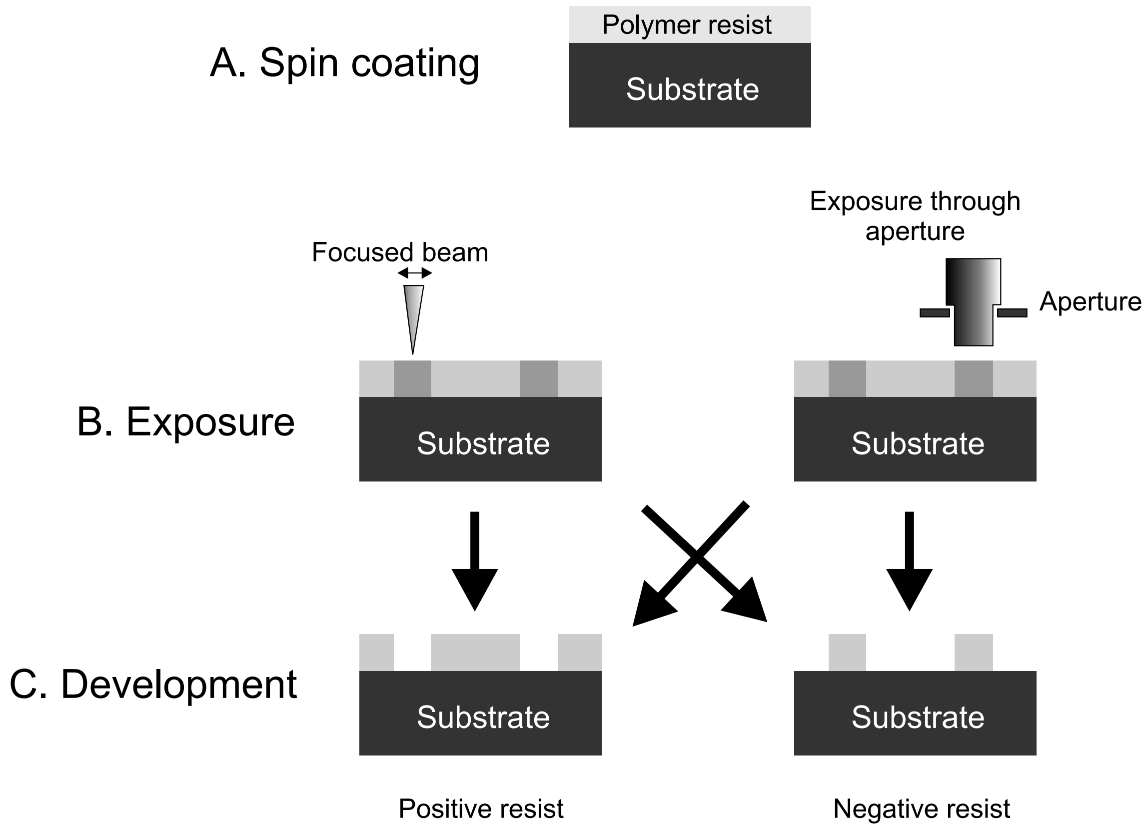

Figure 3.6: Principle of microfabrication in polymer resist using MeV ion beam lithography.

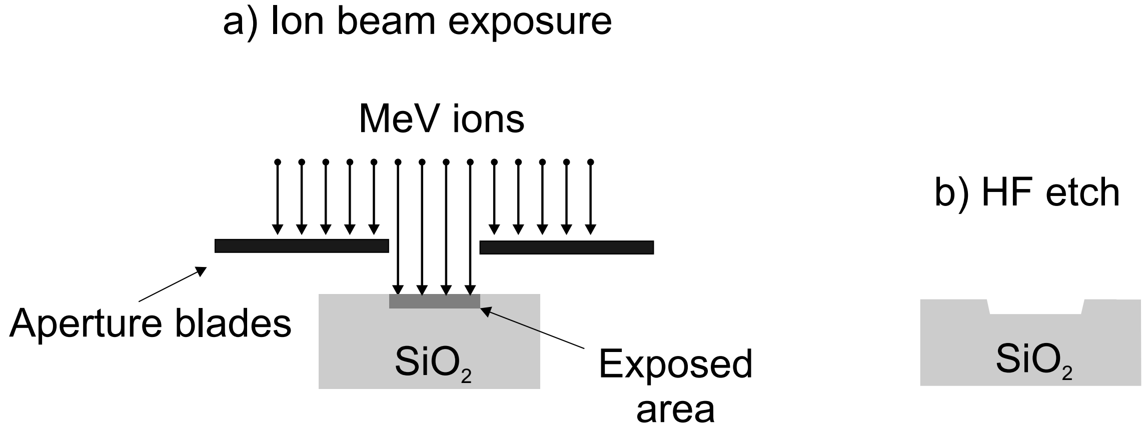

Figure 3.7: Schematic illustration of direct writing microstructures in silica using MeV ion beam lithographic technique (After [Paper VIII]).

measurement and integration of the current on a target [Pászti90, Redondo07]. In this method, the number of impinging ions N is given by,

$$N = \frac{\int_0^t idt'}{qe}, \tag{3.23}$$

where i is the measured current on the target during a period of exposure time t, q is the charge state, and e is the electronic charge. Therefore, the accumulated ion fluence can be determined by [Hellborg09],

$$\Phi = \frac{N}{A}, \tag{3.24}$$

in which A is the area.

A Faraday cup is a simple and common device used for measuring the ion current. However, an unstable beam which gives rise to beam current fluctuations commonly occurs in many electrostatic accelerators. In this case, an alternative way for measuring the ion fluence can be realised by using a precision gold–coated dual–vane rotator that periodically chops the beam in conjuction with synchronous current measurement [Paper III]. This approach is based on measuring the yield of backscattered ions from the vane that are proportional to the ion fluence and calibrating this against a pulsed current integrator. The number of backscattered ions, Y_g, is defined as [Chu78]:

$$Y_g = n_{vane}G, \tag{3.25}$$

where n_{vane} is the number of ions that hit on the vane and $G = (Nt)\omega\sigma_r(E, \theta)$, in which Nt is the number of atoms per unit volume×thickness of the gold film, ω is the small angle subtended by the silicon surface barrier (SSB) detector, and σ_r is the

average differential scattering cross section of the incident ion beam. The relationship between the number of backscattered ions and the ion fluence is then defined as:

$$Y_g = \gamma\Phi, \tag{3.26}$$

where γ is the geometric constant. More details of calculations can be found in [Paper III].

3.6.2 Soft–lithography

Soft–lithography is a standard technique used for fabricating poly(dimethylsiloxane), PDMS, microfluidic devices because it is simple, flexible and inexpensive [Whitesides01, McDonald02, Sia03]. This technique is straightforward and based on a replication of PDMS from a master mold as shown schematically in Fig. 3.8. First, the master mold is fabricated by MeV ion beam lithography as discussed in the previous section. Then, a 10:1 (v/v) base:curing agent ratio of PDMS mixture (Sylgard 184 silicone elastomer kit, Dow Corning, Midland, MI, USA), is degassed under vacuum for 20 minutes, and subsequently poured over the master mold. The sample is subsequently cured at 70 °C for 1 hour. Next, the replica is peeled off the master. Then, the micro–channels are enclosed by sealing the replica with a PDMS film, which is spin coated on a clean glass substrate and pre–cured at 70 °C for 6 minutes. This bonding process is made under a coarse vacuum. To completely harden the PDMS, the microfluidic chip is subsequently cured again at 70 °C for 45 minutes.

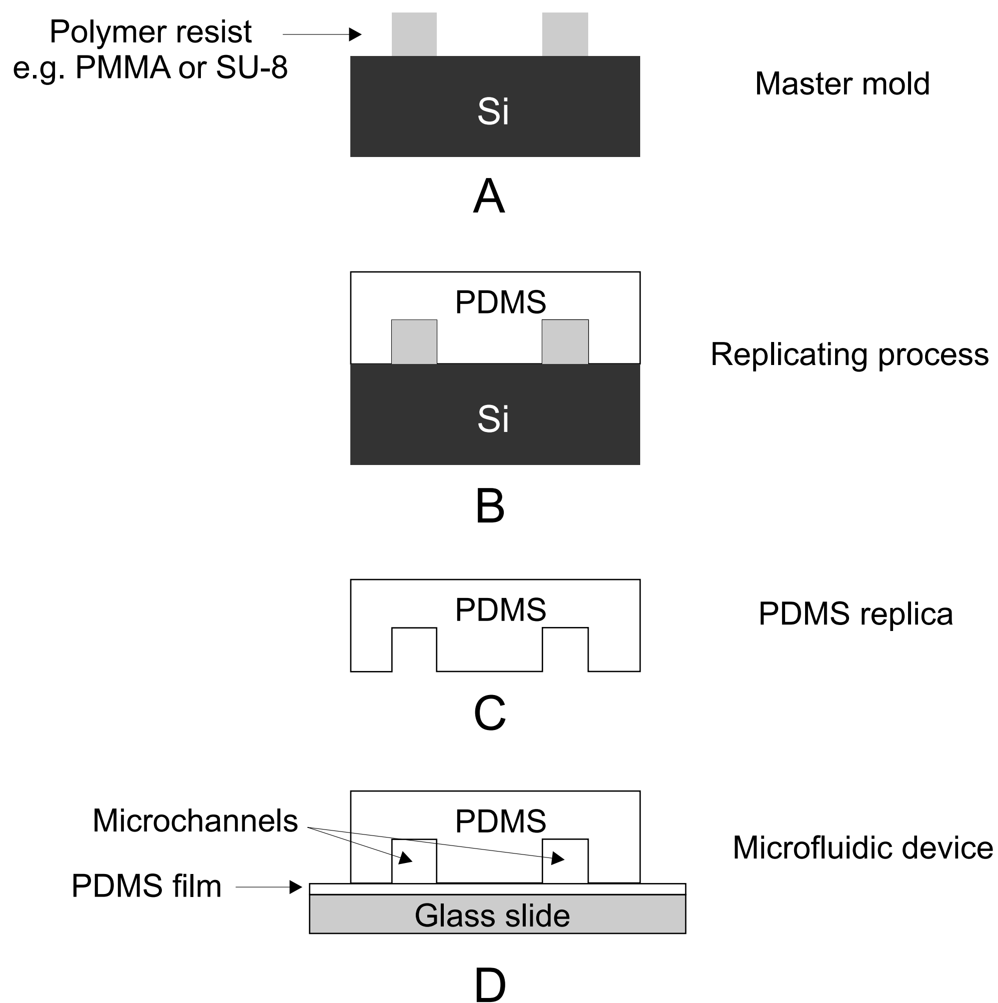

Figure 3.8: Fabrication of a microfluidic device by soft–lithography: (A) lithography of master mold, (B) PDMS replica molding, (C) separation of PDMS from the master mold, and (D) sealing.

4 Ion beam lithography systems

MeV ions from electrostatic accelerators have been widely used not only for ion beam analysis applications e.g., Rutherford backscattering spectrometry (RBS), particle induced X-ray emission (PIXE), ionoluminescence (IL), etc. [Chu78, Kamwanna08] and for ion beam modification of materials [Intarasiri07] and more recently for ion beam lithographic applications [Watt07, Paper I]. In this work, programmable proximity aperture lithography (PPAL) systems have been developed at two facilities; in the University of Jyväskylä (JYU) and Chiang Mai University (CMU). At JYU, a 1.7 MV Pelletron was used to produce MeV ions of proton, helium, carbon and oxygen ions; whereas MeV nitrogen ions were produced from a cyclotron accelerator. For the CMU system, MeV hydrogen and helium ion beams were produced by a 1.7 MV Tandetron accelerator. Overviews of these systems are presented in this chapter.

4.1 Programable proximity aperture lithography at JYU

4.1.1 PPAL system

A PPAL system was developed at JYU in this study for lithographic applications and creating nano–scale patterns of ion tracks. This system was designed to use with both Pelletron and cyclotron accelerators. A $40 \times 40 \times 40$ cm lithographic vacuum chamber that can be mounted on two different supporting frames to accommodate the different beam height of the two accelerators, as shown in Fig. 4.1. A schematic diagram of the PPAL principle is depicted in Fig. 4.2. In the PPAL system, MeV ions from the accelerators are shaped to a rectangular pattern by a pair of computerized L–shaped aperture blades (see Fig. 4.2) each made from two tantalum sheets. The thickness of each Ta sheet was 100 μm and can completely stop up to 6 MeV per nucleon helium ions [Paper I]. To give extremely straight aperture edges one edge of the Ta sheets was carefully polished. The Ta foils were mounted on a stainless steel polishing jig and then polished with 150, 600, 800, 1500, and 2000 grade SiC papers followed by a diamond paste of 6 and 0.5 μm grain size. Experimental results showed that the edge roughness of the Ta sheets was close to 100 nm [Gorelick07]. Each L–shaped aperture was made of two Ta sheets that were glued on a supporting block with a

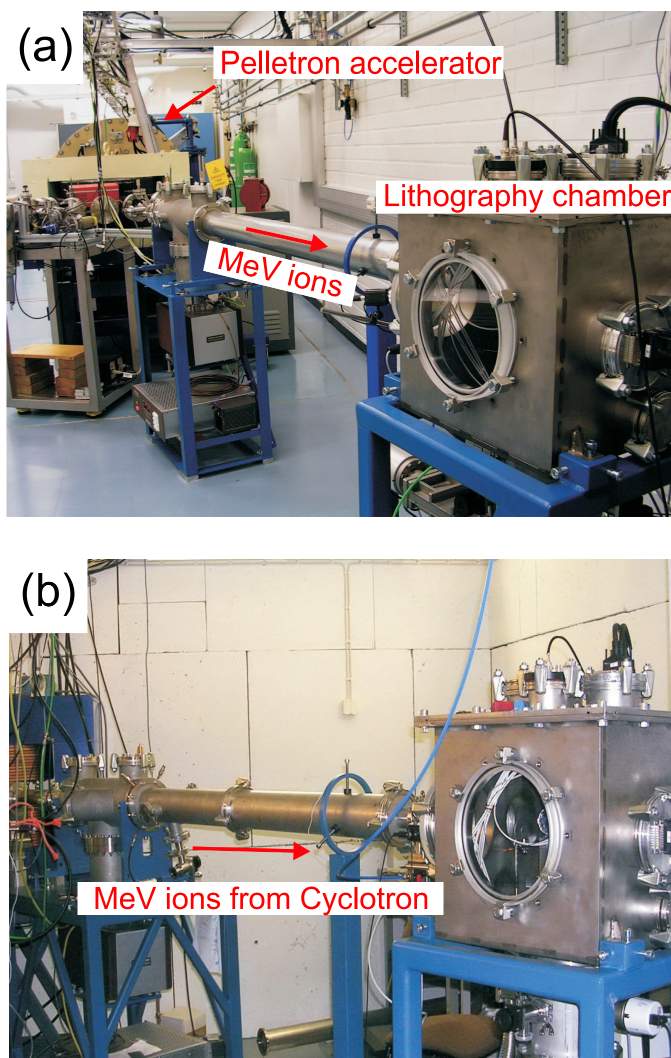

Figure 4.1: Programmable proximity aperture lithography (PPAL) set–up with (a) Pelletron and (b) cyclotron accelerators.

vacuum epoxy adhesive (Torrseal^{TM}) under an optical microscope. Then, two of the L–shaped blades were mounted on an upper aluminum block and a lower aluminum block, respectively, as shown in Fig. 4.2. The aperture blocks were mounted on motorized positioners and the sample holder was mounted on a motorised X–Y–Z stage. The motorized linear positioners were fitted with vacuum–compatible dc servomotors (Newport MFA–CCV6). Newport ESP 300 controllers were used to control the linear motion drives. A computer program, which was used to control the controllers, was written in LabVIEW using a standard RS–232 serial ports for interfacing to the motion controllers. A beam blanker was used to turn on and off the beam. This comprised a pair of parallel Cu plates 20 cm long and with 5 mm separation. It was biased up to 3 kV potential difference that was delivered via a high voltage relay. A TTL

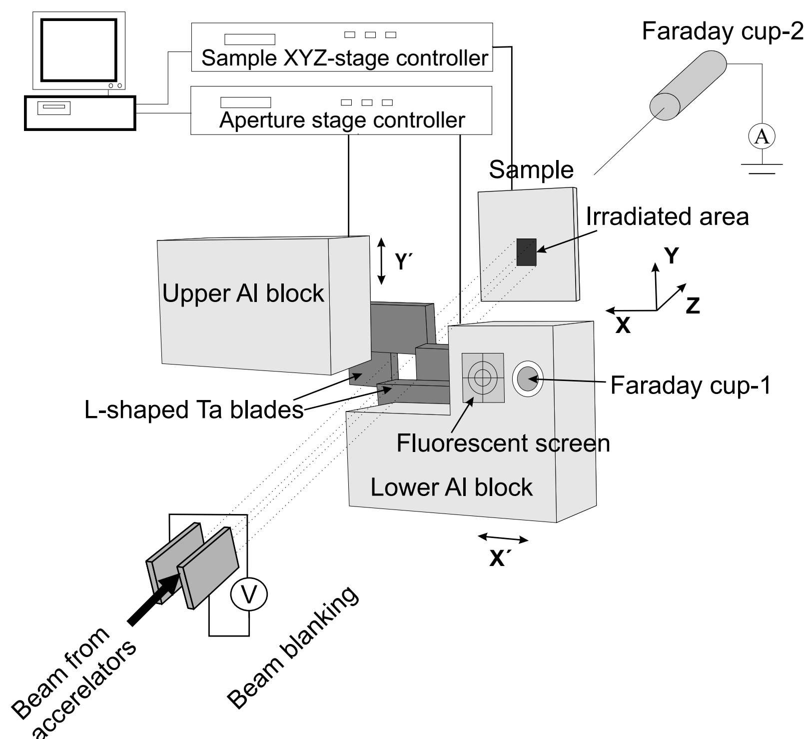

Figure 4.2: A simplified schematic diagram of the PPAL system at JYU (After [Paper I]).

logic signal, which was generated by the control computer via a National Instruments PCIe–6251 multifunction data acquisition (DAQ) card, was used to control the relay. The beam shape was determined by a fluorescent screen that was mounted on the lower Al block (see Fig. 4.2). The beam current was measured using two Faraday cups that were mounted before and after the aperture. More details of the PPAL system are described in [Paper I]. An ASCII format file was used to control the PPAL system. The data structure for each rectangular pattern element consisted of six sequential records as shown in Fig. 4.3. The first record is the keyword for writing a rectangle or square. The upper left x (X_1) and y (Y_1) coordinates of the pattern are the second and third records, respectively. The fourth and fifth records are used to specify the lower of x (X_2) and y (Y_2) coordinate, respectively. The final record is used to determine the fluence exposure time in seconds.

A schematic diagram of the PPAL geometry and penumbra broadening at JYU Pelletron is shown in Fig. 4.4. A primary aperture was located at 2.85 m from the L–shaped aperture blades. The distance between the apertures and the sample was typically about 1 mm (or less). From this geometry, the beam divergence is in order of few mrad. This beam divergence leads to a penumbra broadening. This can be minimized by close proximity of the L–shaped apertures to the sample. Typically, the beam current profile of the focused beam can be considered to be a Gaussian distri-

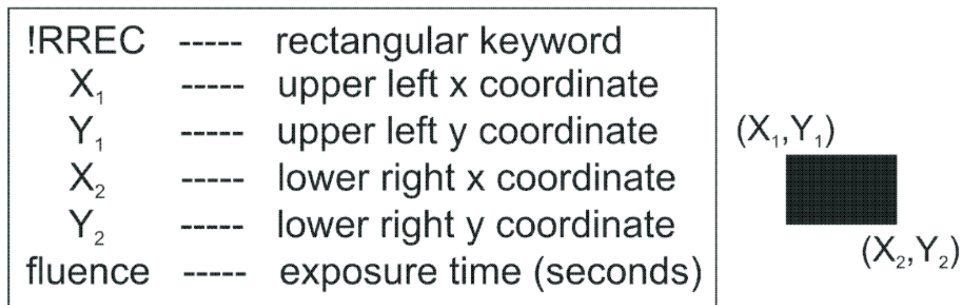

Figure 4.3: The structure of the PPAL file for writing rectangular or square pattern as shown on the right (After [Paper I]).

bution. A small part of the Gaussian beam selected by the L–shaped apertures will then have an approximately rectangular beam current profile.

The smallest feature that can be written is governed by the penumbra broadening, aperture roughness and the positional accuracy of the aperture motor control. Features of the size of a few hundred nm in 7.5 μm thick PMMA resist have been written [Gorelick].

4.1.2 MeV ion beam exposure

MeV ions from a 1.7 MV Pelletron (National Electrostatics Corp.) and the Jyväskylä K=130 cyclotron accelerators were used in this work. The ion source for the Pelletron was generally a RF positive ion source coupled to a Rb–vapour charge exchange oven (Alphatros). A negative ion source (SNICS) was also connected to the Pelletron. In

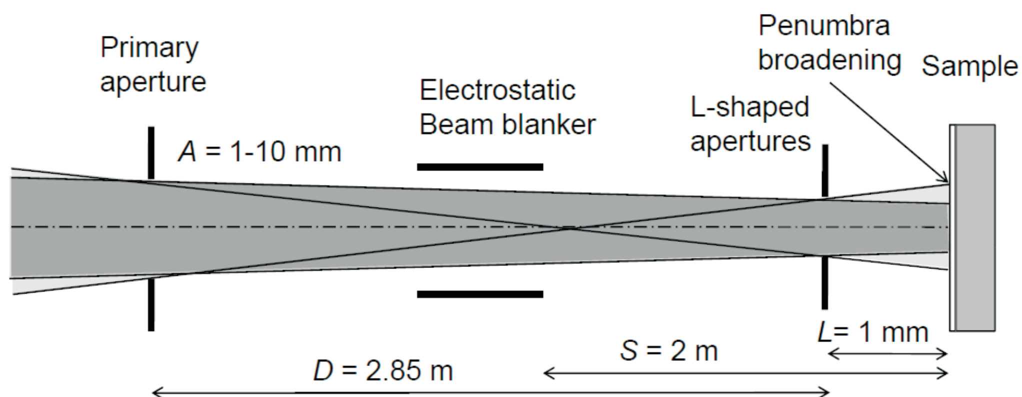

Figure 4.4: Illustration of the PPAL geometry and penumbra broadening (not scale).

this thesis, the Alphatros ion source was utilized for producing helium ions. Hydrogen ions and heavy ions such as carbon and oxygen ions were produced using the SNICS ion source.

The Alphatros ion source works by first producing positive ions and then converting them by electron capture to negative ions. In this ion source, a gas, typically hydrogen or helium, is fed into a silica tube at low pressure. A plasma is produced by capacitive coupling of the plasma to a 100 MHz radio frequency oscillator, as shown schematically in Fig 4.5. Hydrogen or helium ions are extracted from the plasma and then accelerated to a charge exchange cell by a potential difference, typically 2–6 kV. Some of the positive ions are then converted in electron capture reactions to negative ions in a rubidium vapor inside the charge exchange cell. The charge exchange process is described in more detail in the next section.

The SNICS ion source was the other type ion source used in this work. It has been widely used as an injector for tandem electrostatic accelerators because it can directly generate negative ions of many elements in a solid form. The principle of the negative Cs sputter ion source is shown in Fig 4.6. A Cs reservoir is heated to about 100 °C to generate Cs vapor. The Cs vapor fills a region between a cooled cathode and a heated ionizer. The Cs atoms impinge onto the surface of the ioniser and become ionised. They are then accelerated by a potential to the cathode where they sputter atoms of the cathode materials and ionise them negatively. Finally, the negatively charged beams are extracted and injected to the accelerator by an extractor electrode.

In both Pelletron and cyclotron accelerators, the beam current density was determined by measuring the current that passes through a 1×1 mm^2 aperture opening

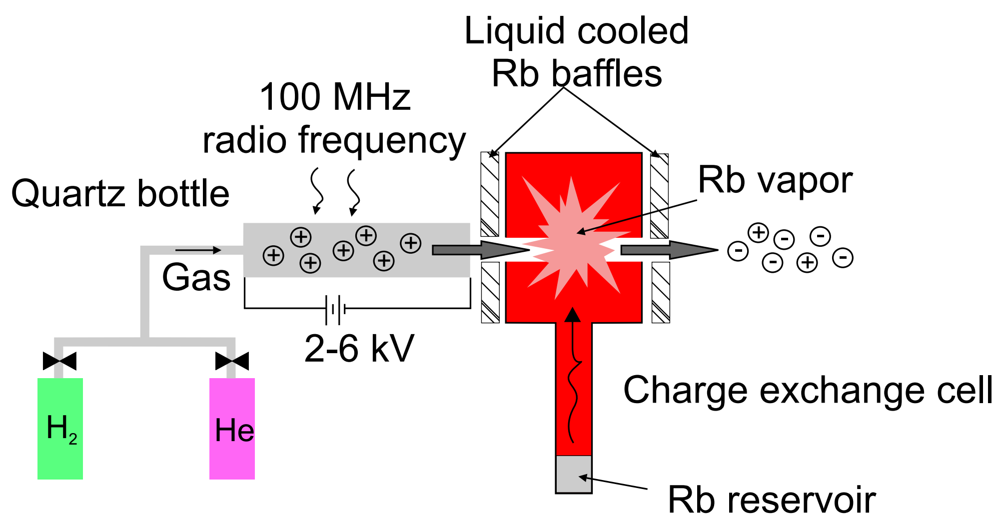

Figure 4.5: A schematic diagram of the RF ion source (After [Pelletron]).

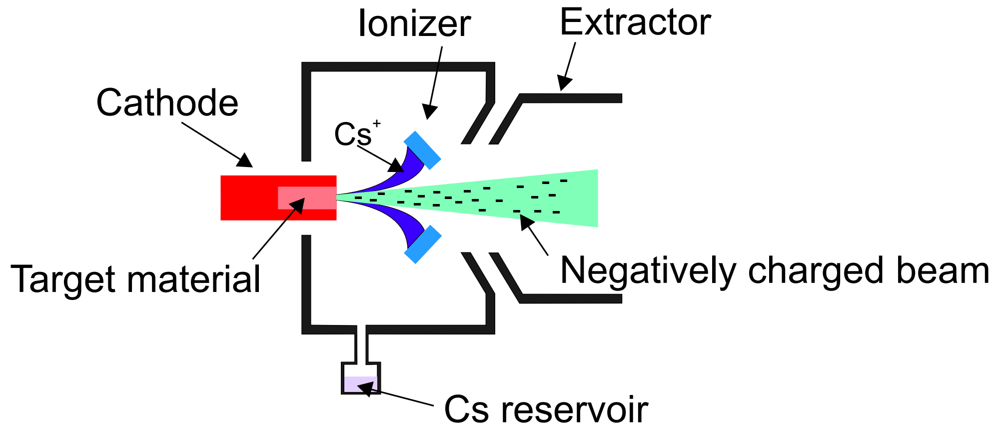

Figure 4.6: A schematic drawing of the negative Cs sputter ion source (After [Pelletron]).

area with a Faraday cup after the aperture system (see Fig. 4.2). In early tests with the cyclotron, 56 MeV $^{14}N^{3+}$ ions from the JYFL cyclotron accelerator were used to expose PMMA. This beam was chosen because it was easy to optimize and also can provide a sufficient beam current. We estimated that 2.1×10^{12} ions/cm^2 was required in this irradiation. This means that each pattern was irradiated for 100 s. However, for comparison when 3 MeV $^4He^{2+}$ was used for lithography in the same PMMA layer, we determined 6.25×10^{12} ions/cm^2 was needed to expose PMMA which was equivalent to $\sim$ 20 s irradiation per pattern element. Typically, exposure times are between 10 and 100 s per pattern element.

4.2 Programmable proximity aperture lithography at CMU

4.2.1 CMU–MeV IBL system

A similar approach to the PPAL system at JYU was developed at the Plasma and Beam Physics Research Facility (PBP) of Chiang Mai University for the purpose of fabrication of 3D micropatterns in polymeric materials such as PMMA. The structures fabricated by this technique were used as a master mold for soft–lithography applied in microfluidics. A main equipment, which was a 1.7 MV Tandetron accelerator from High Voltage Engineering Europa (HVEE), was used for producing the energetic ions. Fig. 4.7(a) illustrates a view of the tandem accelerator at the PBP. The negative ions that are injected into the tandem accelerator are supplied by two ion injectors, which are a duoplasmatron ion source and Cs sputter ion source as shown in Fig. 4.7(b). However, only the duoplasmatron ion source was used for this study.

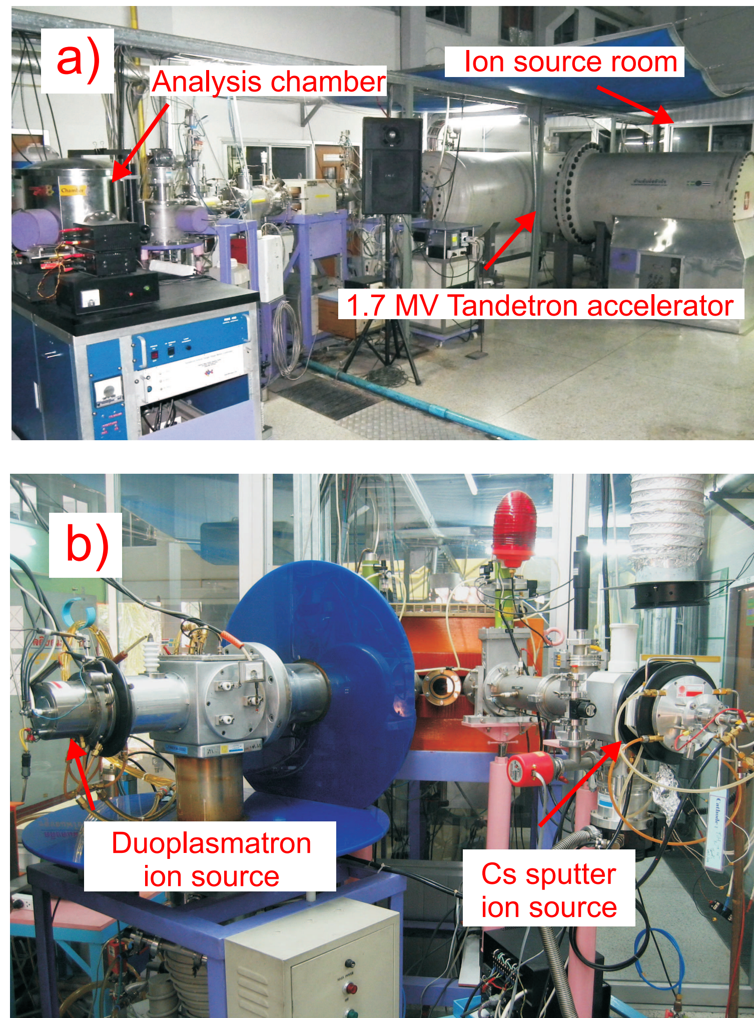

Figure 4.7: (a) A view of 1.7 MV HVEE tandem "Tandetron" accelerator at CMU. (b) The CMU duoplasmatron and Cs sputter ion sources.

The duoplasmatron ion source (PSX–100, Peabody Scientific) first creates positive ions such as H^+ or He^{++} from hydrogen and helium gases, respectively. This ion source has advantage over the Cs sputter ion source that it can generate a helium ion beam which the latter can not produce. Fig. 4.8 illustrates a schematic representation of a typical duoplasmatron ion source. A plasma composing of ions, electrons and neutral particles is generated by a gas discharge. A magnetic field is used to confine the plasma away from the ion source wall thereby increasing the plasma density. Positive ions inside the plasma are extracted by an extraction electrode biased with several kV potential difference relative to the plasma potential (typically, 10 kV is used in our system). The positive ions are converted to negative ions by collisions with an alkali metal vapour as for the RF ion source described above. An Einzel lens is used to focus the ten's of keV positive ions into the charge exchange canal. In our system, potas-

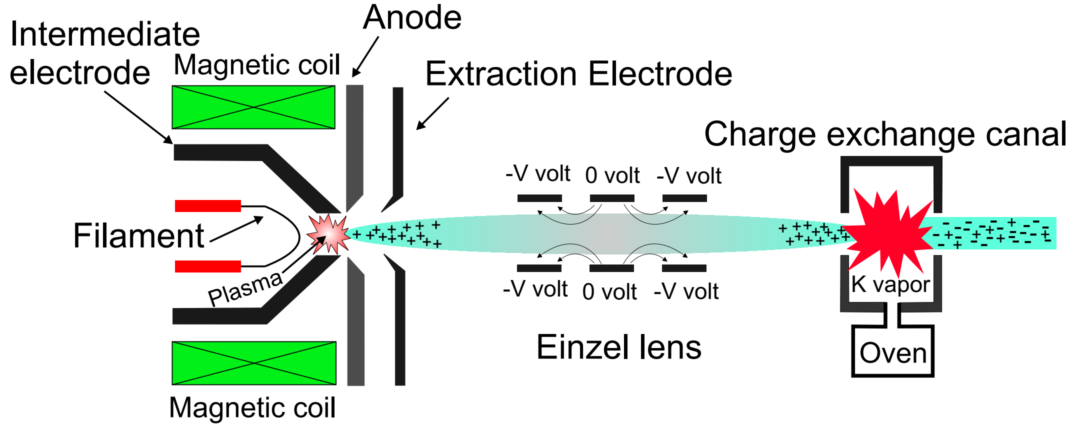

Figure 4.8: Schematic diagram of a duoplasmatron ion source (After [Hellborg09, Kamwanna08]).

sium vapour is used as the charge exchange medium. During the collision processes between the positive ion and the potassium vapor, the positive charge of the ion is transformed to the negative charge by the following reactions [Alton05],

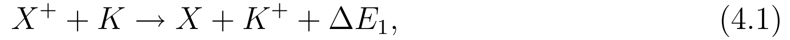

$$X^+ + K \rightarrow X + K^+ + \Delta E_1, \tag{4.1}$$

and

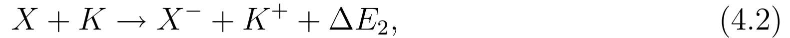

$$X + K \rightarrow X^- + K^+ + \Delta E_2, \tag{4.2}$$

where X and K refer as the ion and the potassium (or rubidium) vapour, respectively, ΔE_1 is the ionization energy difference of the ion and the alkali metal vapor, and ΔE_2 is the difference between the electron affinity of the ion and the ionization energy of the potassium vapour.

Fig. 4.9 shows a schematic diagram of the Tandetron accelerator system. Like the JYU Pelletron, this accelerator is a "Tandem accelerator" because it uses a high positive potential at the terminal to accelerate ions twice. In the first stage, negative ions which are preaccelerated to δE keV from the ion source are accelerated by a potential difference, U, between ground potential at the low energy end to the positive potential at the high voltage terminal (HV), as shown in Fig. 4.9. In this process, the ions gain an energy which is equal to eU where e is the elementary charge (for singly charged ions). In the HV terminal, nitrogen gas is used as a stripper. During the collisions between the negative ions and the stripper gas, some negative ions are converted to positive ions. Subsequently, these positive ions are accelerated in the second stage from the positive HV terminal to zero potential. The total kinetic energy (E) of the ions in all of the processes of the Tandem accelerator is given by $E = (e + q)U + \delta E$, where q is the charge state of the positive ions which can be single or multiple.

The PPAL system in Chiang Mai for fabricating $3D$ microchannels in PMMA using the PPAL system at CMU is schematically shown in Fig 4.10 (a). In this system,

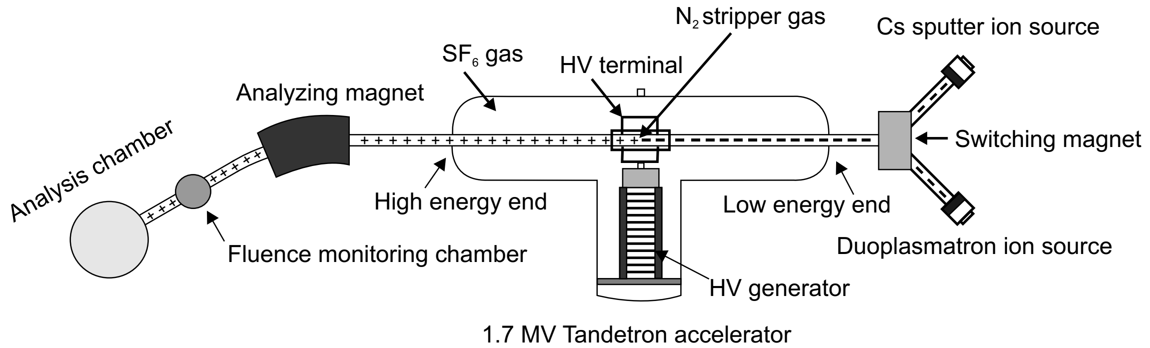

Figure 4.9: Schematic of the 1.7 MV Tandetron accelerator system used for CMU–MeV IBL.

the MeV ion beam from the 1.7 MV Tandetron accelerator was collimated to a micrometer rectangular or square shaped for irradiating the sample. This shape was controlled by a pair of computerized L–shaped aperture blades with well–polished edges. The two apertures were mounted onto MM–3M–F–1 Motorized MicroMini^{TM} stages with 0.49609 μm/step and 25.4 mm travel range. A picture of the aperture system is illustrated in the close–up view in Fig. 4.10 (b). This system was installed inside the analysis chamber (see also Fig. 4.9). One of the motorized stages can move in the X direction and the other in the Y direction. The sample was mounted on the X–Y stage that was normally used as a 6–axis goniometer for RBS and channeling studies. A beam shutter to start or stop the beam was also controlled by a computerized rotation motor. A fluence monitoring system including a rotating dual–vane and a silicon surface barrier (SSB) detector will be discussed in the next section.

4.2.2 Fluence monitor

At the CMU system, two approaches were developed for determination of the ion fluence Φ $(ions/cm^2)$. The first approach was an in–situ ion beam fluence monitoring system. This system allows the unpredictable beam fluctuations to be taken into account. It was attached to the Tandetron accelerator inside the fluence monitoring chamber (see Fig.4.9). The approach used in this technique was based on a measurement of the yield of backscattered ions, by Rutherford Backscattering Spectrometry (RBS), from a gold coated dual–vane rotator in combination with synchronous current measurement. In order to establish the current calibration a 8 mm inner diameter and 65 mm deep Faraday cup was placed in the sample position. The configuration of the fluence monitor, is shown in Fig. 4.11. In this set–up, the gold coated dual vane rotator, of 30° angular span for each vane in 5 cm length with total mass of 3.82 g, was rotated with a constant angular speed of 6.15 rad/s by a unipolar stepper motor to periodically chop the beam. A SSB detector connected to a pre–amplifier, amplifier, multichannel analyser (MCA), and PC, respectively, was used to collect the

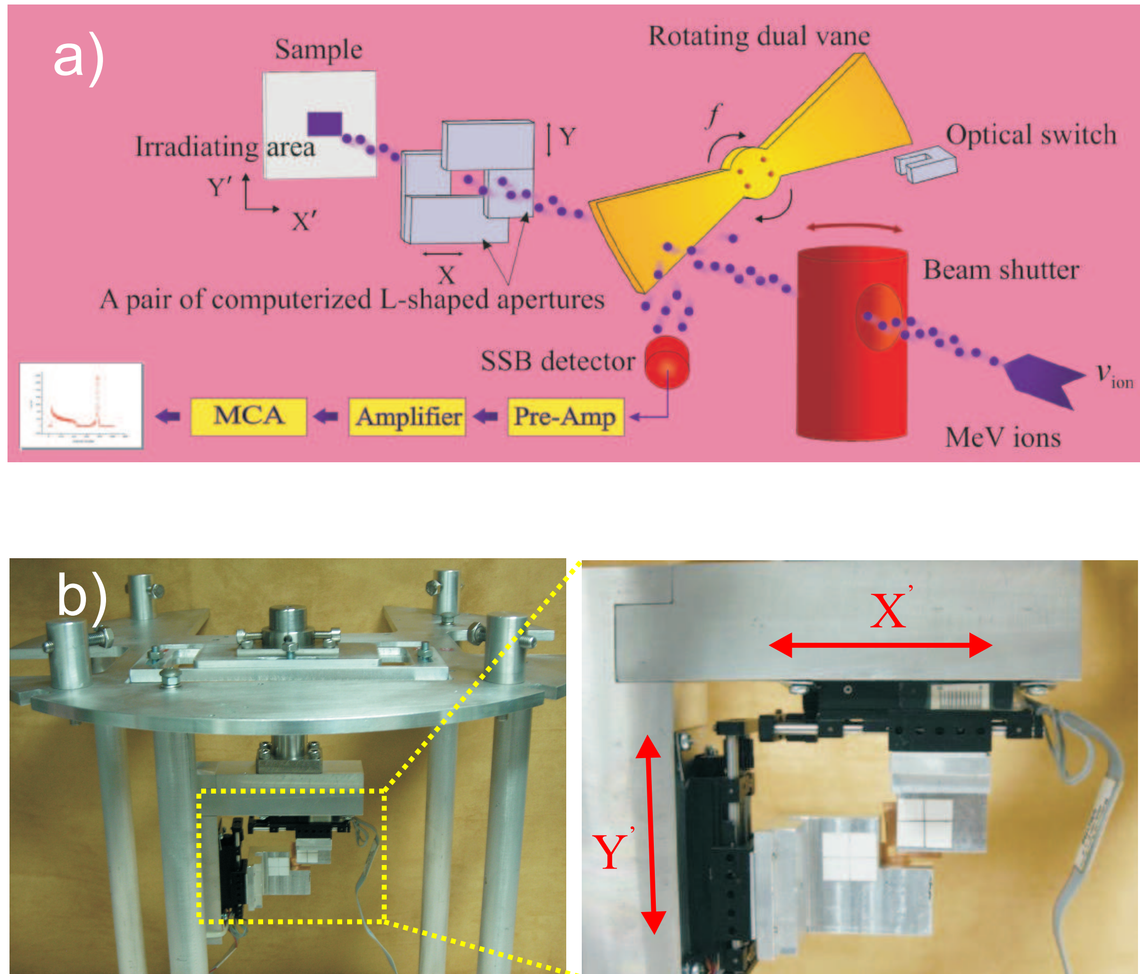

Figure 4.10: a) Schematic of the CMU MeV–IBL system at the 1.7 MV Tandetron accelerator. b) View of the aperture positioning system in a close–up view in the right pane.

number of backscattered ions at 150 degrees when the beam was blocked by the vane. The detector subtended a solid angle (Ω) of 8.11 msr. The beam impinged at about 4 cm from the rotating center of the vane. This implies that 83.3 % of the beam can pass through the vane. The FC was directly connected to a purpose–designed pulsed current integrator for converting the beam current to the ion fluence (Φ). More details of the in–situ ion fluence monitor can be found in [Paper III].

The second approach was based on a measurement of the ion charge that is intercepted by the L–shaped aperture blades during the exposure by a purpose–built current integrator with a resolution of 4.8 pC. For calibration purposes, a Cu Faraday cup of 65 mm long and 8 mm inner diameter can be moved into the sample position (see Fig. 4.12). A relationship between the total charge that is incident on the aperture blades (Q_A) and the charge that passes through the fixed opening aperture area A (Q_F) is determined by this calibration. The irradiating ion fluence on the sample is

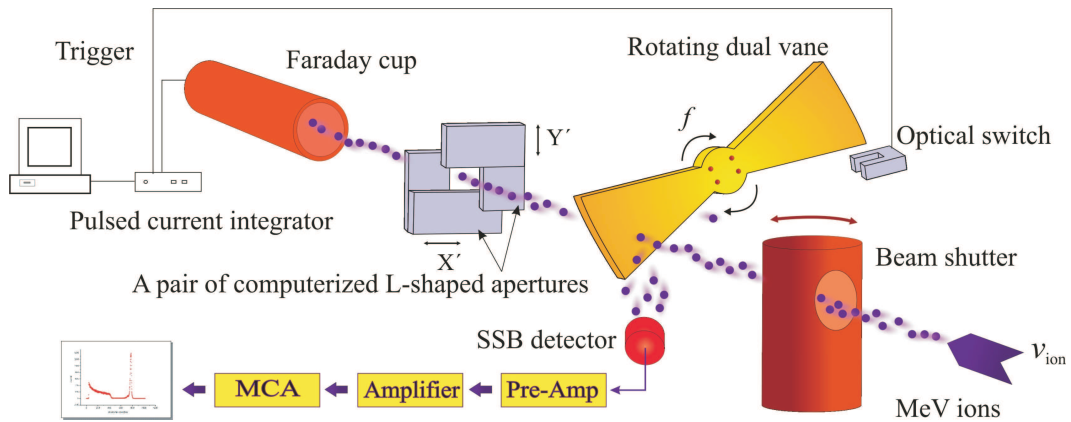

Figure 4.11: Schematic of the first approach for ion beam fluence monitoring at CMU (After [Paper III]).

then estimated by transforming the Q_A to the Q_F from the calibration relation and dividing by the known aperture area size. More discussions about this approach can be found in [Paper IV, Paper VII].

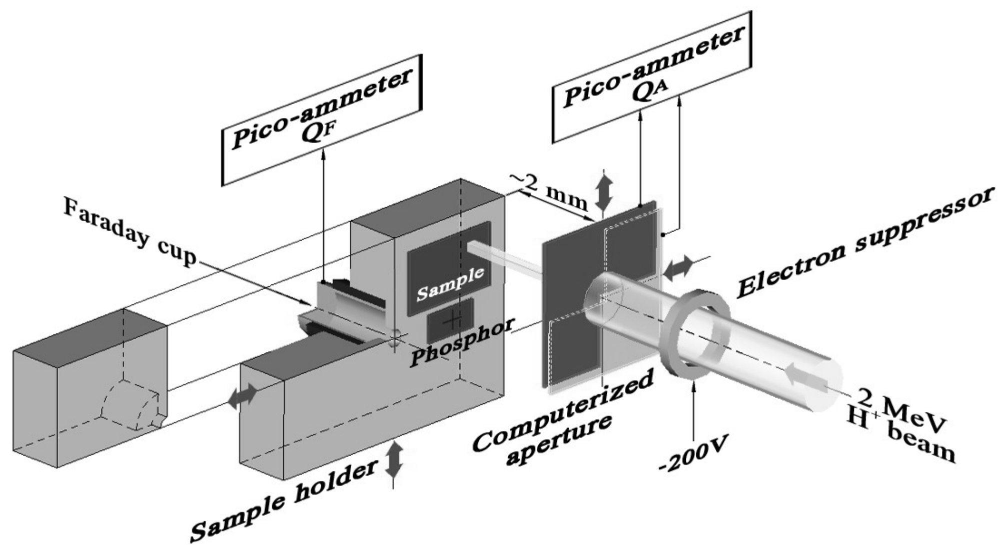

Figure 4.12: Schematic diagram of the second approach for fluence monitoring at CMU and similarly at JYU (After [Paper VII]).

5 Experimental results and discussions

5.1 Characterization of ion beam exposure characteristics for poly(methyl methacrylate)

The exposure characteristics in term of ion fluence Φ of poly(methyl methacrylate), PMMA, for MeV ion beam lithography was investigated in this study [Paper I, Paper III, Paper IV]. In order to produce micro–structures in "positive" resist tone of PMMA, the ion fluence must satisfy the condition,

$$\Phi_0 \leq \Phi < \Phi_{\mathrm{x0}}, \tag{5.1}$$

where Φ_0 and Φ_{x0} are the clearing and onset of cross–linking ion fluences, respectively. In this ion fluence range, the primary effect in the PMMA is chain scission in which the molecular weight is reduced by ion irradiation, as previously discussed in section 3.2.1. As a result, the exposed region is more susceptible to dissolution in mild solvents such as a 7:3 by volume, propan-2-ol: deionised water mixture (IPA:DI) [Yasin02].

At the ion fluences below the clearing ion fluence ($\Phi < \Phi_0$), the irradiated ion tracks are too far apart so that the local dose[1] does not uniformly exceed Φ_0. In this case, the developer cannot completely dissolve the PMMA in the exposed region. This gives a nanometer–scale rough surface as shown in Fig. 5.1. At sufficiently large fluences the ion tracks are so close together that the clearing fluence (Eq. 5.1) is uniformly exceeded. Here, the developer can completely dissolve the exposed regions. This gives straight and vertical PMMA side walls as depicted in Fig. 5.2. At ion fluences above the cross–linking fluence ($\Phi \geq \Phi_{x0}$), the PMMA can undergo cross–linking. This allows PMMA to be used as a lithographic "negative" tone resist when the ion fluence is,

$$\Phi_{x\infty} \leq \Phi, \tag{5.2}$$

where $\Phi_{x\infty}$ is the full cross–linking ion fluence. In this case, the IPA:DI water (7:3) developer can not dissolve the cross–linked regions in the exposed areas. In contrast, the PMMA pattern can be developed in acetone. The developer was found to dissolve

[1] Dose is strictly defined as energy deposited per unit mass. This can be conveniently expressed in term of eV/(ρ nm^3) where ρ is the density.

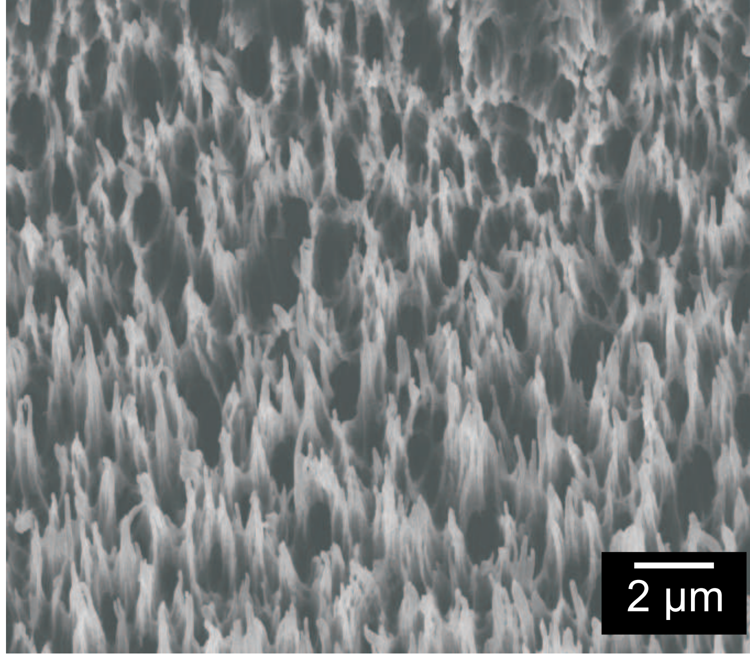

Figure 5.1: SEM image of a nanometer–scale rough pattern in PMMA fabricated with ion fluence $\Phi < \Phi_0$ using 56 MeV $^{14}N^{3+}$ ions (After [Paper I]).

only the unexposed regions leaving the exposed regions proud of the substrate surface, as discussed in sect. 3.5 above. Fig. 5.3 shows an example of the negative PMMA patterns fabricated by the PPAL technique after development in acetone.

Table 5.1 summarizes the clearing (Φ_0), onset of cross–linking (Φ_{x0}) and fully cross–linking ($\Phi_{x\infty}$) fluences for 2 MeV protons, 3 MeV $^4He^{2+}$ and 6 MeV $^{12}C^{3+}$ ions. Details of the measurements of these fluences can be found in [Paper IV].

Table 5.1: Fluences for clearing (Φ_0), onset of cross–linking (Φ_{x0}) and fully cross–linking ($\Phi_{x\infty}$) fluences for 2 MeV protons, 3 MeV $^4He^{2+}$ and 6 MeV $^{12}C^{3+}$ ions in PMMA [Paper IV]. The stopping force data is from SRIM [SRIM] ($\rho = 0.95$ g/cm^3).

Ion	dE/dx (eV/nm)	Φ_0	Φ_{x0} (ions/cm^2)	$\Phi_{x\infty}$
2 MeV proton	15.2	3.3×10^{13}	3.5×10^{14}	7.0×10^{14}
3 MeV $^4He^{2+}$	121	2.4×10^{13}	5.4×10^{13}	1.5×10^{14}
6 MeV $^{12}C^{3+}$	816.6	1.8×10^{12}	3.4×10^{12}	8.1×10^{12}

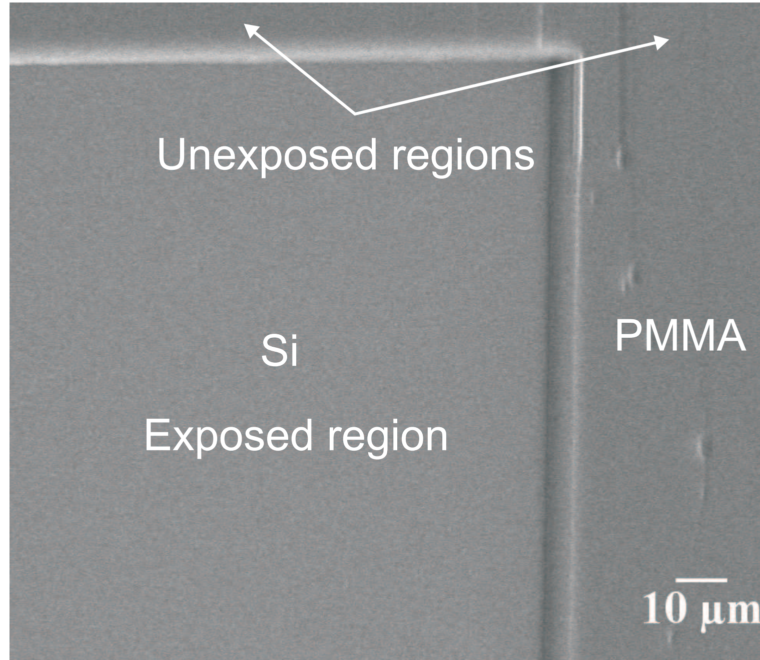

Figure 5.2: SEM micrograph of a pattern in PMMA produced with a clearing fluence ($\Phi_0 \leq \Phi < \Phi_{x0}$) (After [Paper I]).

5.2 Exposure characteristic of amorphous silica (SiO_2)

The 6.8 MeV $^{16}O^{3+}$ ion beam was used to study the lithographic exposure characteristic of amorphous silica (SiO_2). Here, the relationship between the *effective etched depth z*, which is the difference in etch depth between irradiated and unirradiated areas, and the ion fluence (Φ) was investigated. Fig. 5.4(a) shows an optical micrograph of 8 square patterns (200 $\times$ 200 μm) irradiated with different ion fluences of 6.8 MeV $^{16}O^{3+}$ ions, after development in an aqueous solution of 4% v/v HF for 60 minutes. A stylus profilometer (KLA–Tencor P–15 Profiler) was used to measure the etch depths. The ion fluence and the effective etch depth of each pattern element in Fig. 5.4.(a) is summarized in Table 5.2. The relation between the effective etch rate and the ion fluence is illustrated in Fig. 5.4(b). Empirically, the effective etch depth z(μm) asymptotically approaches a constant value with increasing ion fluence following the relation: $z(\mu m) = 2.9[1 - exp(-1.5\Phi)]$, where Φ is in units of 10^{14} ions/cm^2. We found that the effective etch depth approaches the asymptotic value at fluences above 1.6×10^{14} ions/cm^2. The wet etching behavior of SiO_2 is complex because unirradiated SiO_2 is etched at a lower rate than irradiated. Furthermore, the asymptotic behavior may indicate an overlapping ion track effect. For this reason, the absence of more data, no detailed analysis can be put forward at this stage. More details of this investigation can be found in [Paper VIII].

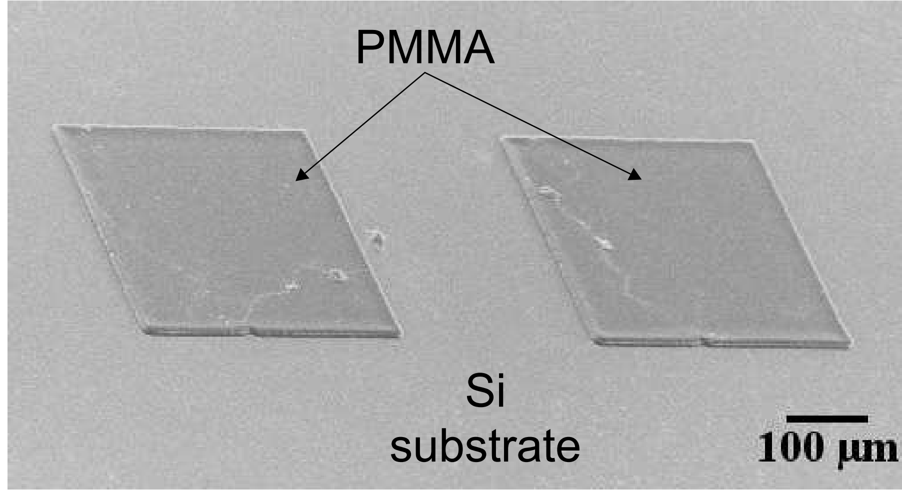

Figure 5.3: SEM image of the negative PMMA pattern made with high fluence ($\Phi_{x\infty} \leq \Phi$) after developing in acetone (After [Paper VII]).

5.3 Study of dose spreading at edges

Multiple scattering of the incident ion gives a deviation in the ion's trajectory. This leads to a deposition of the ions' kinetic energy outside the irradiated area that affects spreading and the wall straightness in the developed pattern. In this study, a combination of computational results from the SRIM code [SRIM] and a simple integral transformation was used to study the ion fluence distributions across the straight edge of a semi–infinite irradiated area and along the bisectors of the internal and external 90° corners of semi–infinite irradiated areas for 2 MeV protons and 3 MeV helium ions passing through a 7.5 μm thick PMMA film. The detail of calculations is described in [Paper I]. Fig. 5.5 shows the fluence distribution along the transverse distance d (nm), where $d = 0$ corresponds to the edge or corner location. It is clearly seen that the shape of the curves in Fig. 5.5 is similar to a complimentary error function, cerf(x).

Table 5.2: The ion fluence (Φ) parameters and the effective etch depth (z) of each pattern element (after development in 4% v/v HF for 60 minutes) [Paper VIII].

Pattern no.	Φ (ions/cm^2)	z (μm)	Pattern no.	Φ (ions/cm^2)	z (μm)
A1	3.3×10^{13}	0.93	A5	1.6×10^{14}	2.67
A2	7.0×10^{13}	1.98	A6	1.9×10^{14}	2.72
A3	1.0×10^{14}	2.34	A7	2.2×10^{14}	2.72
A4	1.3×10^{14}	2.57	A8	2.5×10^{14}	2.72

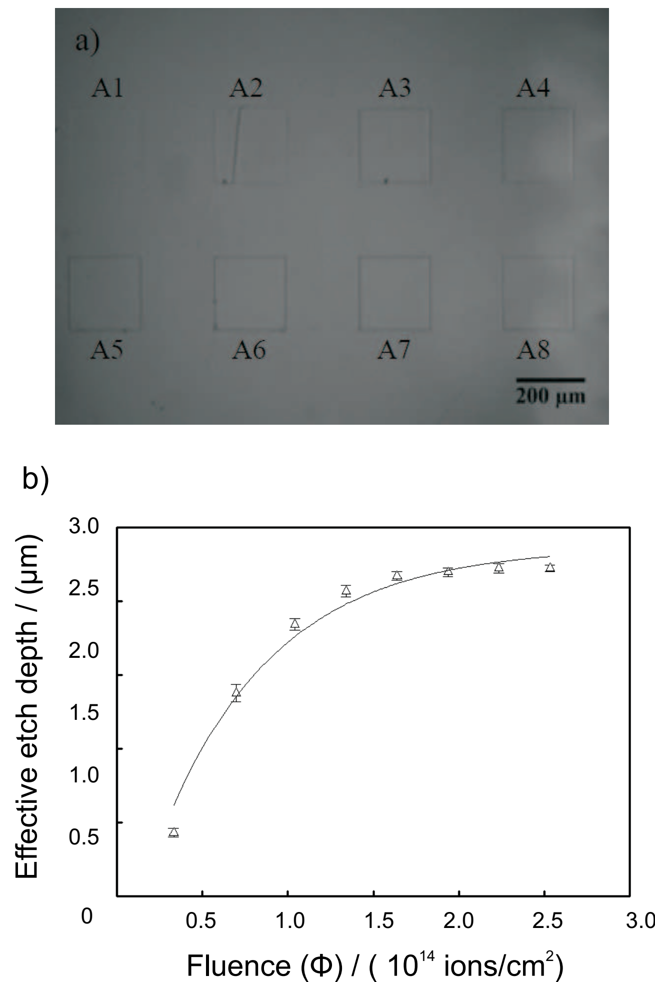

Figure 5.4: (a) Optical micrograph of 8 square patterns in silica irradiated with different ion fluences of 6.8 MeV $^{16}O^{3+}$ ions, after development in 4% v/v HF for 60 minutes. (b) The effective etch depth (z) vs fluence (Φ) (After [Paper VIII]).

We found that the spreading widths after penetrating 7.5 μm thickness of PMMA are $\sim$ 50 and $\sim$ 64 nm for 2 MeV protons and 3 MeV helium ions, respectively. This implies that the spreading of the fluence for 2 MeV protons is less than for 3 MeV helium ions in a 1–10 μm thick PMMA film [Paper I]. Furthermore, from Fig. 5.5, it can be seen that it did not depend significantly on if the edge was straight or an internal or external 90° corner.

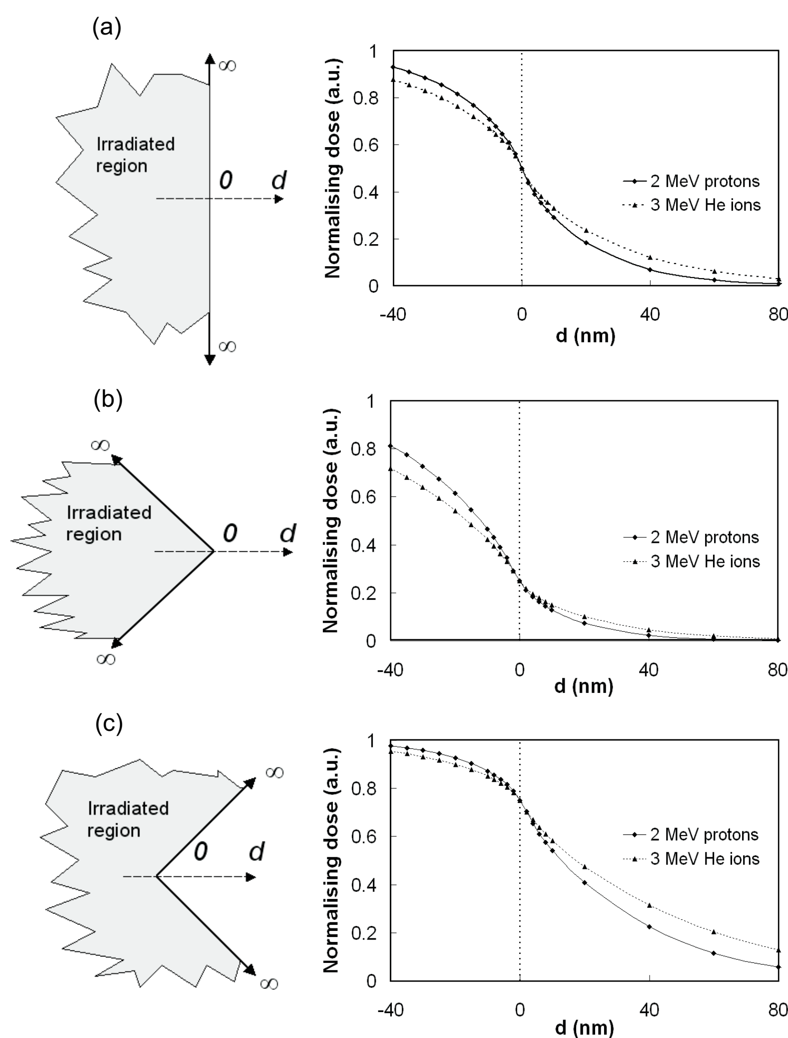

Figure 5.5: The distributions of ion fluence along the transverse distance d (nm) for unirradiated areas with (a) straight edge, (b) external 90° corner, and (c) internal 90° corner (After [Paper I]).

5.4 Microstructure fabrication by the PPAL technique

The PPAL technique was found very suitable for microfabrication of microfluidic devices. An entire microfluidic circuit usually consists of large reservoirs which are interconnected by microchannels and also to external pumps and sensors etc. PPAL is a very useful technique for fabricating the microfluidic structures compared to PBW with a scanned focused beam since the large reservoir can directly be written by one exposure. In this work, we used the PPAL approach to produce three dimensional (3D) micro–structures using both positive and negative resist modes of PMMA. Some microfluidic prototypes were produced in the positive PMMA tone. Whereas, negative

resist tone was used to produce the master mold that was used for replication of PDMS by standard soft–lithography. Moreover, a test microfludic prototype pattern was produced in natural fused silica (SiO_2) using the PPAL technique.

5.4.1 "Positive" tone PMMA structures

Exposure with a clearing ion fluence in the range $\Phi_0 \leq \Phi < \Phi_{x0}$ was used to fabricate 3D micro–structures in PMMA by using positive characteristic. Here, we have used the PPAL systems at the University of Jyväskylä and Chiang Mai Universiy (CMU) to produce some microfluidic prototypes. Fig. 5.6(a) shows SEM image of a prototype of a sorting device produced in "positive" resist tone PMMA by using the PPAL technique. The device consists of 22, 12, 5 and ~1.6 μm wide channels. A close–up of a ~1.6 μm width channel is illustrated in Fig. 5.6(b). We realized that this sorting prototype can be used for cellular and sub–cellular studies [Paper I, Paper V, Paper VI]. Fig. 5.6 (c) and (d) reveal SEM micrographs of 20 μm wide grooves and an array of 40 μm squares produced in ~9 μm thick PMMA using 3 MeV $^4He^{2+}$ ions at the CMU.

5.4.2 "Negative" tone PMMA structures

PMMA can be used as a negative resist by high ion fluence exposures so that the total cross–linking dose is uniformly exceeded. A micro–channel in poly(dimethyl siloxane), PDMS, can be made by casting a micro–ridge from a master mold. In this study, we have used the PPAL approach to fabricate negative PMMA master molds. Fig. 5.7 shows a test pattern consisting of a T–junction microfluidic structure of the negative master mold fabricated using a high fluence of 2 MeV protons. The structure consists of a main straight ridge, an inlet ridge, two inlet reservoirs and one outlet reservoir. The main ridge is perpendicular to the second inlet reservoir as depicted in Fig. 5.7. Some stitching errors can be observed in this pattern. However, these errors could be reduced by careful alignment of the L–shaped aperture blades. During the fabrication, it was found that stability of the proton beam is very important since only one imperfection of the pattern element can cause the entire mold to fail (see the details of the fabrication in [Paper VII]).

5.4.3 SiO_2 microfluidic structure

Fig. 5.8 shows an SEM image of a test microfludic prototype produced by 6.8 MeV $^{16}O^{3+}$ ions using the PPAL technique after development in 4% v/v HF for 60 minutes. The ion fluence used for this structure was 3×10^{14} ions/cm^2. This ion fluence was

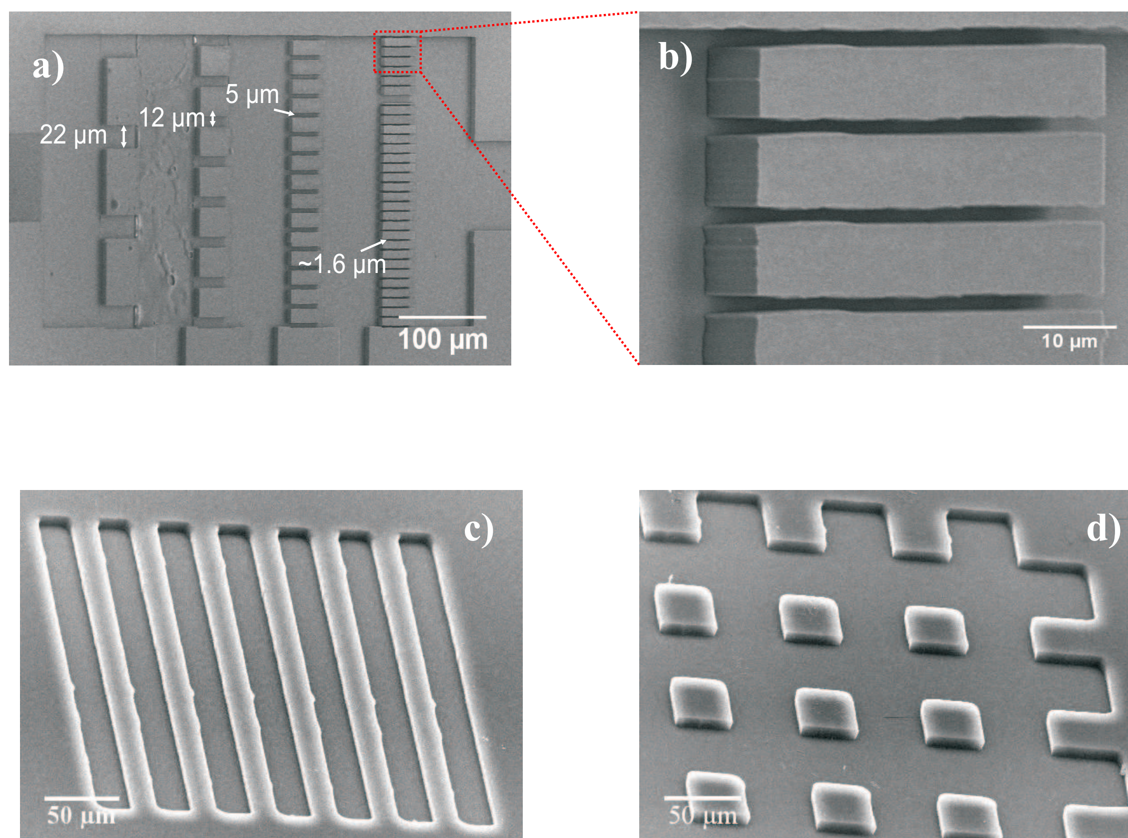

Figure 5.6: SEM images of (a) a prototype of cell–organelle sorting device, (b) a closed–up of ∼1.6 μm channel width in Fig.(a) (After [Paper I]), (c) 20 μm wide grooves, and (d) 40 μm square arrays, fabricated using the PPAL systems at the JYU and CMU.

chosen to give an effective etch depth approaching the asymptotic value as discussed in the section 5.2. The depth of this pattern was ∼2.5 μm. This pattern consists of three inlet reservoirs (200 × 200 μm) connected with an outlet reservoir (200 × 200 μm) through ∼20 μm wide channels. More details of the fabrication can be found in [Paper VIII].

5.5 PDMS replication

At Chiang Mai University, we have developed a combination of MeV-IBL with PDMS casting. Often the latter is referred to as soft–lithography. The technique has advantages for making microfluidic devices because it is simple and it is possible to use in mass production. In this technique, micro–structures in poly(dimethylsiloxane) PDMS were transferred from a master mold which is made by the PPAL technique. Fig. 5.9(a) shows a SEM micrograph of a PDMS replica of 20 μm wide bars. This

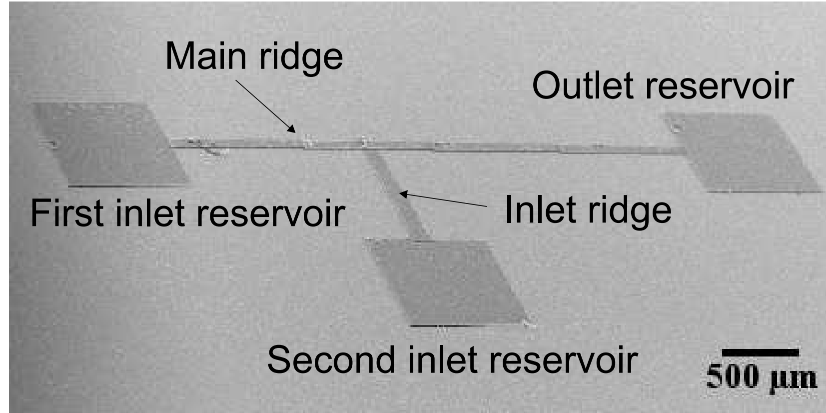

Figure 5.7: SEM images of T–junction negative PMMA microstructure fabricated by PPAL technique with high fluence protons (After [Paper VII]).

PDMS structure is replicated from the master mold shown in Fig. 5.6(c). A SEM image of the 40 μm grid pattern PDMS replica, which is transferred from the mold depicted in Fig. 5.6(d), is illustrated in Fig. 5.9(b). Both of these PDMS replicas have replicated well the master mold that was produced in the positive resist tone of PMMA. In addition, the PDMS replication can also be produced from a negative PMMA master mold. Fig. 5.9(c) shows the PDMS replica of the T–junction microfluidic device replicated from the negative PMMA master mold as shown in Fig. 5.7. A close–up of the outlet reservoir of the Fig. 5.9(c) is depicted in Fig. 5.9(d).

5.6 Test microfluidic device

Fig. 5.10 shows an example of PDMS microfluidic device made by a soft lithography method as described in section 3.6.2. The microfluidic chip is composed of two injection inlets and one outlet. In this experiment, fluids are propelled through microchannels by pressure–driven flows using syringe pumps. A Zeiss optical microscope (100$\times$ maximum) fitted with a Sony CCD camera (30 fps) was used to characterize the fluid flows in the microfluidic device. Here, we have tested the PDMS T–junction microfluidic device by injecting oil into the first inlet and red–dyed DI water into the second inlet. The main channel for flowing the oil stream is 95 μm wide whereas, the width of the second inlet for red–dyed DI water flow is 150 μm, measured using the ImageJ image analysis software [ImageJ]. The formation of water droplets in the oil phase is illustrated in the optical micrographs shown in Fig. 5.11. Equal volumetric flow rates of both water and oil ($Q_{water} = Q_{oil} = 0.16$ μL/min) were used in this experiment. By calculating from the Eq. 2.12, the length of the droplets is $L_{dcal} =$ 245 μm. Experimental results showed that the droplet has a length of $L_{dexp} = 237.5$ μm. This agrees well with the calculation with a difference of 3% [Paper VII]. It can

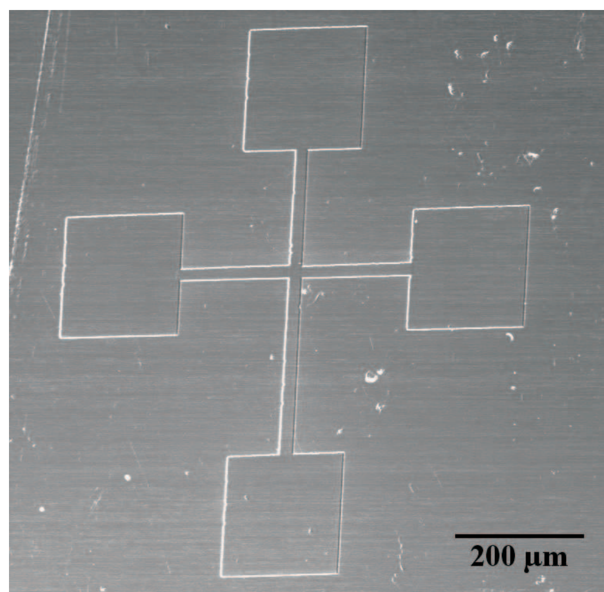

Figure 5.8: SEM image of a test microfluidic prototype in silica fabricated using 6.8 MeV $^{16}O^{3+}$ ions with 3×10^{14} ions/cm^2 (After [Paper VIII]).

be observed that there were small perturbations in the replica at some connecting spots. These could be associated with stitching errors, see Fig. 5.11. However, these perturbations were not strong enough to break the droplets.

5.7 Summary of the Papers

5.7.1 Paper I

Programmable proximity aperture lithography with MeV ion beams

A novel MeV ion beam programmable proximity aperture lithography system was developed at the Accelerator Laboratory of the University of Jyväskylä, Finland. In this paper, the basic principle of the PPAL technique is described. This paper also reports on technical development of the PPAL system, the controlling software, the calibration procedures and investigations of multiple scattering effects. Here, a 3 MeV $^{4}He^{2+}$ ion beam from a 1.7 MV Pelletron accelerator was used to fabricate channel structures. In addition, 56 MeV $^{14}N^{3+}$ ion beam from K130 cyclotron accelerator was used to produce lithographically defined regions with nanometer–scale ion–track structures. It was found that the smallest pattern produced by the PPAL system at this stage was an approximately 700–800 nm wide wall in 7.5 μm thick PMMA. This corresponds to the aspect ratio of the structure about 10.

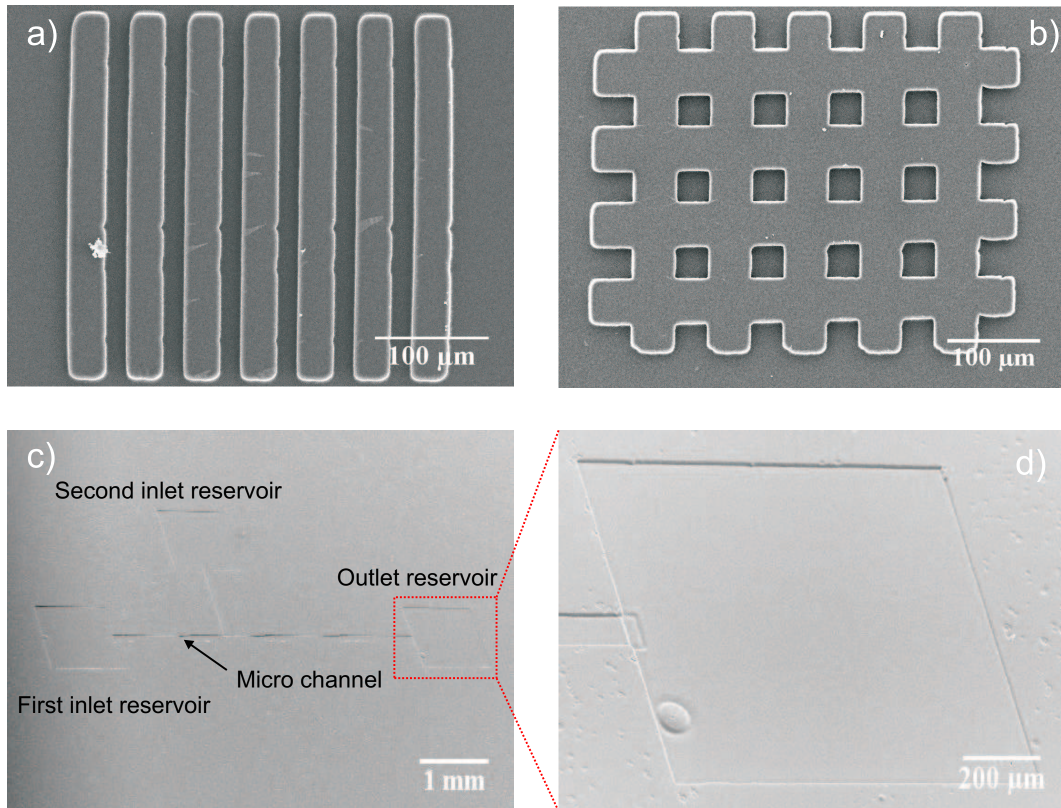

Figure 5.9: SEM images of PDMS replicas of (a) 20 μm wide bars, (b) 40 μm grid pattern, (c) the T–junction microfluidic device and (d) a close–up of the outlet reservoir in the previous image (c).

5.7.2 Paper II

Resolution Performance of Programmable Proximity Aperture MeV Ion Beam Lithography System

In this paper, the resolution performance of the PPAL system was investigated. This investigation primarily studied effects associated with scattering from the proximity aperture using a Monte Carlo approach. The beam divergence, aperture blade straightness, and secondary and scattered particle from the aperture blade edges defined the pattern edge sharpness. The beam spatial resolution on the sample defined by the proximity aperture was investigated by ray–tracing simulations using object oriented toolkit GEANT4 [GEANT4]. Experimental results show that the edge–scattering does not significantly affect the pattern edge sharpness.

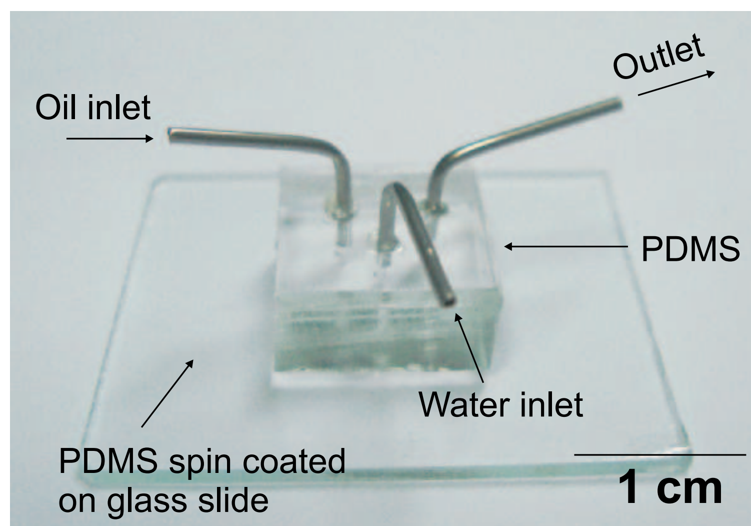

Figure 5.10: A test microfluidic device of the T–junction geometry fabricated using a standard soft lithography (After [Paper VII]).

5.7.3 Paper III

In–Situ Ion Beam Fluence Monitoring System For MeV Ion Beam Lithography at CMU

An in–situ ion beam fluence monitoring system was developed at Chiang Mai University. This approach was based on Rutherford Backscattering Spectrometry (RBS) using a gold–coated dual–vane rotor. In this system, the computer controlled dual–vane rotor was installed in front of the sample holder. A built–in Faraday cup connected to a synchronous pulsed current integrator was used to calibrate the monitoring system. The system development and some preliminary results were presented in this paper.

5.7.4 Paper IV

Lithography exposure characteristics of poly(methyl methacrylate) (PMMA) for carbon, helium and hydrogen ions

Poly(methyl methacrylate) is well–known as a positive resist for lithographic applications. The clearing ion fluence (Φ) required for this application lies in the interval $\Phi_0 \leq \Phi < \Phi_{x0}$, where Φ_0 and Φ_{x0} are the clearing and cross–linking onset fluences, respectively. Here, the programmable proximity aperture ion beam lithography systems in Chiang Mai and Jyväskylä were used to determine the exposure characteristics of PMMA in terms of fluence for 2 MeV protons, 3 MeV $^{4}He^{2+}$ and 6 MeV $^{12}C^{3+}$ ions,

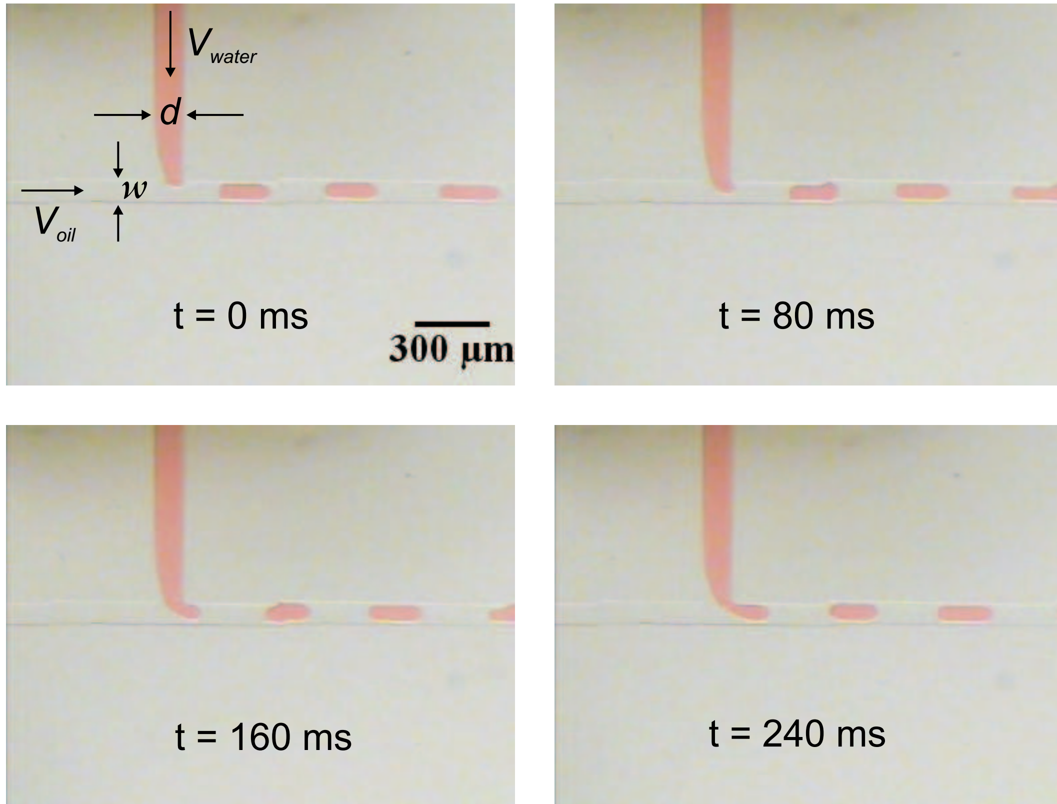

Figure 5.11: Optical images of water droplets generated using the T–microfluidic PDMS chip shown in Fig. 5.10 (After [Paper VII]).

respectively. Experimental results showed that the threshold for both clearing and the onset of cross–linking decreases with increasing electronic stopping force. The exposure latitude was considerably greater for protons than for heavy ions. It was also observed that at fluences less than the clearing fluence, the PMMA is incompletely removed, leaving a surface that is rough on a nanometer scale. This is associated with a spatial dose non–uniformity presumably resulting from individual ion impingements.

5.7.5 Paper V

3D Micro–channel fabrication in PMMA based on MeV ion beam lithography

This paper demonstrated use of the PPAL technique for fabricating three–dimensional (3D) micro–channels in PMMA. A comparison between MeV ion beam lithography and electron beam lithography (EBL) is described. Here, we have shown that the quality of the L–shaped aperture blade defined the quality of the pattern features. Moreover, a prototype 3D micro–channel pattern in 7.5 μm thick PMMA was demon-

strated in this paper using 3 MeV $^{4}He^{2+}$ ions.

5.7.6 Paper VI

Fabrication of microfluidic devices using MeV ion beam Programmable Proximity Aperture Lithography (PPAL)

Microfluidic patterns were produced in PMMA using 56 MeV $^{14}N^{3+}$ and 3 MeV $^{4}He^{2+}$ beams from K130 cyclotron and a 1.7 MV Pelletron accelerators, respectively, at the University of Jyväskylä. A stitching issue, where the fluence was doubled in overlapping exposed regions was discussed in this paper. We have shown that the PPAL system can be used to lithographically define regions of ion tracks with nanometer–scale ion–track structures. This could be used for biomedical analytical and cellular applications.

5.7.7 Paper VII

Fabrication of a negative PMMA master mold for soft–lithography by MeV ion beam lithography

In this paper, poly(methyl methacrylate) (PMMA) was investigated as a negative resist by irradiation with a high–fluence 2 MeV proton beam produced from a 1.7 MV Tandetron accelerator at the Plasma and Beam Research Facility (PBP) of Chiang Mai University. It was observed that the PMMA transforms from being a positive to negative resist at the threshold fluence of 3.5×10^{14} ions cm^{-2} for 2 MeV protons. A negative PMMA master mold for a T–junction pattern was fabricated. This master mold was used for casting poly(dimethylsiloxane) (PDMS) following a standard soft–lithography process. The PDMS chip produced by this technique was tested as a microfluidic device for formation of water droplets in an oil phase. We also found that dozens of PDMS devices can be produced from the negative PMMA master mold without any deterioration.

5.7.8 Paper VIII

Direct writing of channels for microfluidics in silica by MeV ion beam lithography

The PPAL technique was used to investigate the lithographic characteristic exposure of amorphous silica (SiO_2) for 6.8 MeV $^{16}O^{3+}$ ions. The exposed samples were developed in 4% v/v HF for 60 minutes. The correlation of the effective etched depth (z) in term of ion fluence (Φ) was investigated in this work. The experimental results indicated that the effective etched depth asymptotically approaches a constant value with increasing the ion fluence as: $z = 2.9[1 - exp(-1.5\Phi)]$ in which the fluence Φ is in units of 10^{14} ions/cm^2. It was found that the etched depth approaches a constant value at ion fluences above 1.6×10^{14} ions/cm^2. In this paper, a test microfluidic pattern was fabricated in SiO_2 with 6.8 MeV $^{16}O^{3+}$ ions at a fluence of 3×10^{14} ions/cm^2.

6 Conclusions

The main objective of this thesis was to develop a novel MeV ion beam lithography technique, namely programmable proximity aperture lithography (PPAL) technique, at both the University of Jyväsklyä (JYU) in Finland and Chiang Mai University (CMU) in Thailand. The overall goal was to achieve a method to rapidly develop microfluidic devices. In this technique, a rectangular or square shape of ∼micrometre size exposure area is determined by a pair of L–shaped aperture blades, which are computer controlled by precise linear motion drivers.

We have shown that:

• The PPAL technique is capable of processing 3D micro–structures not only in "positive" resist tone but also in a "negative" resist tone of poly(methyl methacrylate) (PMMA) and also direct writing in amorphous silica.

• The patterns fabricated using this technique have useful properties i.e. straight and vertical side walls with high aspect ratio (about 10, or greater).

• The PPAL system can be used for both light ions such as protons and helium ions, and heavy ions such as carbon, oxygen and nitrogen ions.

• Two approaches were developed for determining the ion fluence.

• A sensitive and reliable ion fluence monitoring system is very important for reproducibility of the experimental results especially for fabrication of the negative PMMA master molds.

• It was demonstrated that the negative PMMA pattern can be used as a master mold for replicating poly(dimethylsiloxane).

• A microfluidic device fabricated from the negative PMMA master mold by using the standard soft–lithography was tested to produce water droplets in an oil phase.

• Direct writing of patterns into silica was demonstrated with PPAL using 6.8 MeV ^{16}O ions.

7 Future vistas

MeV ion beam lithography has truly outstanding possibilities in point form and applications. Here, as examples, few potential avenues for research are outlined as points below.

1. Fundamental studies

• Investigation of ultimate small–feature size limit in the PPAL technique to elucidate quantitative edge broadening, nanoroughness from breakdown of continuous slowing down model (CSDA) [Udalagama07].

• Characterization of MeV ion enhanced etching process for SiO_2 ion species, fluence, stopping force, etc.

• Optimisation of irradiated conditions ion species and energy for different resist materials (e.g. novolac, polyimide, PET).

• Establish statistical models for chain scission and cross–linking dependence on ion species, energy in PMMA under MeV ion irradiation.

2. Improvement of the PPAL system

• Fabrication of structures down to nm sizes.

- Improving the precision of motion drivers to work on nm scales.
- Improving the quality of the L–shaped aperture edges down to few nanometre e.g. magnetic float polishing, electrochemical polishing.
- Improving polynomial calibration over a limited range.

• Large area patterning.

- Replacing X–Y–Z sample stages to allow writing 110 × 76 mm areas.

3. Future applications

- Direct patterning in poly(dimethlysiloxane) (PDMS) using the PPAL technique (etching, optical changes etc.).

- Fabrication of durable nanoimprint lithography stamps in glass by direct writing.

- Integration of optical waveguides for readout of fluorescent markers.

- Develop MeV–ion produced rough surfaces for capillary pumps and optical absorbers.

- Construction of purposed–tailored microfluidic Lab–on–a–Chip (LOC) devices for diagnosis of diseases, pharmaceutical preparation, environmental monitoring, etc. (e.g. malaria, H5N1, dengue fever, soil pollution from industry, micro fuel–cells etc.).

- Optical waveguide devices base on liquid bubble array e.g. Bragg–grating waveguides, evanescent mode detector etc.

APPENDIX: Publications by the author not included in the thesis

1. *Microfluidics Pumping Mechanism Based on a Microliter Syringe Pump.* **N. Puttaraksa**, S. Unai, R. Pinchaipat, M.W. Rhodes, K. Singkarat, H.J. Whitlow, and S. Singkarat, (In manuscript).

2. *Influence of MeV H^+ Ion Beam Flux on Crosslinking and Blister Formation in PMMA resist.* S. Unai, **N. Puttaraksa**, N. Pussadee, K. Singkarat, M.W. Rhodes, H.J. Whitlow, and S. Singkarat, (Submitted to Maejo International Journal of Science and Technology).

3. *Fast and Blisters Free Irradiation Conditions for Complete Crosslinking of PMMA Induced by 2 MeV H^+ Ion Beam.* S. Unai, **N. Puttaraksa**, N. Pussadee, K. Singkarat, M.W. Rhodes, H.J. Whitlow, and S. Singkarat, (In manuscript to be submitted to Microelectronic Engineering).

4. *Why are hydrogen ions best for proton beam writing?.* R. Norarat, **N. Puttaraksa**, M. Napari, T. Sajavaara, and H.J. Whitlow, (In manuscript to be submitted to Microelectronic Engineering).

5. *Advanced time–stamped total data acquisition control front–end for MeV ion beam microscopy and proton beam writing.* H. Kivistö, M. Rossi, P. Rahkila, P. Jones, R. Norarat, **N. Puttaraksa**, T. Sajavaara, M. Laitinen, V. Hänninen, K. Ranttila, P. Heikkinen, L. Gilbert, V. Marjomäki and H.J. Whitlow, (In manuscript to be submitted to Microelectronic Engineering).

References

[Paper I] N. Puttaraksa, S. Gorelick, T. Sajavaara, M. Laitinen, S. Singkarat, and H.J. Whitlow, J. Vac. Sci. Tech. B 26(5) (2008) 1732.

[Paper II] S. Gorelick, T. Sajavaara, M. Laitinen, N. Puttaraksa, and H.J. Whitlow, Mater. Res. Soc. Symp. Proc. Vol. 1020–GG03–04 (2007).

[Paper III] N. Puttaraksa, M.W. Rhodes, T. Kamwanna, U. Tippawan, C. Thongleurm, W. Ginamoon, H.J. Whitlow, and S. Singkarat, *In–situ Beam Fluence Monitoring System for MeV Ion Beam Lithography at CMU*, Thai Physics Journal (Series 5, 2010).

[Paper IV] N. Puttaraksa, R. Norarat, M. Laitinen, T. Sajavaara, S. Singkarat, and H.J. Whitlow, Nucl. Instr. and Meth. B (2011), doi:10.1016/j.nimb.2011.01.056.

[Paper V] N. Puttaraksa, S. Gorelick, T. Sajavaara, S. Singkarat and H.J. Whitlow, *3D Micro–channel fabrication in PMMA base on MeV ion beam lithography*, Thai Physics Journal (Series 4, 2009).

[Paper VI] S. Gorelick, N. Puttaraksa, T. Sajavaara, M. Laitinen, S. Singkarat, and H.J. Whitlow, Nucl. Instr. and Meth. B 266 (2008) 2461.

[Paper VII] N. Puttaraksa, S Unai, M.W. Rhodes, K. Singkarat, H.J. Whitlow, and S. Singkarat, Nucl. Instr. and Meth. B (2011) doi:10.1016/j.nimb.2011.01.053.

[Paper VIII] N. Puttaraksa, M. Napari, O. Chienthavorn, R. Norarat, T. Sajavaara, M. Laitinen, S. Singkarat, and H.J. Whitlow, *Direct writing of channels for microfluidics in silica by MeV ion beam lithography*, Submitted to Advanced Materials Research.

[Adesida83] I. Adesida, Nucl. Instr. and Meth. B 79 (1983) 209.

[Alton05] G.D. Alton, *Electrostatic Accelerators*, (ed) R. Hellborg (Springer, Berlin, 2005).

[Amsel03] G. Amsel, G. Battistig and A. L'Hoir, Nucl. Instr. and Meth. B 201 (2003) 325.

[Beaumont10] A. Beaumont, C. Dubuc, J. Beauvais, and D. Drouin, J. Vac. Sci. Technol. B 28(5) (2010) 940.

[Becker02] H. Becker and L.E. Locascio, Talanta 56 (2002) 267.

[Beebe02] D.J. Beebe, G.A. Mensing, and G.M. Walker, Annu. Rev. Biomed. Eng. 4 (2002) 261.

[Bettiol06] A.A. Bettiol, S.V. Rao, T.C. Sum, J.A. van Kan and F. Watt, J. Cryst. Growth 288 (2006) 209.

[Bower02] D.I. Bower, *An Introduction to Polymer Physics*, Cambridge University Press, United Kingdom, 2002.

[Bruss08] H. Bruss, *Theoretical Microfluidics*, Oxford University Press, New York, 2008.

[Chapiro98] A. Chapiro, Nucl. Instr. and Meth. B 32 (1998) 111.

[Chatzichristidi08] M. Chatzichristidi, E. Valamontes. P. Argitis, I. Raptis, J.A. van Kan, F. Zhang, F. Watt, Microelectron. Eng. 85 (2008) 945.

[Chiam07] S.Y. Chiam, J.A. van Kan, T. Osipowicz, C.N.B. Udalagama, F. Watt, Nucl. Instr. and Meth. B 260 (2007) 455.

[Chu78] W.K. Chu, J.W. Mayer and M.A. Nicolets, *Backscattering Spectrometry*, Academic Press, New York, 1978.

[Dong99] H. Dong and T. Bell, Surf. Coat. Technol. 111 (1999) 29.

[Fink04] D. Fink, *Fundamentals of Ion–Irradiated Polymers*, Springer, Berlin, 2004.

[Garstecki06] P. Garstecki, M.J. Fuerstman, H.A. Stone and G.M. Whitesides, Lab on a Chip 6 (2006) 437.

[GEANT4] S. Agostinelli et. al., Nucl. Instr. and Meth. A 506 (2003) 250.

[Gorelick] S. Gorelick, "*MeV Ion Beam Lithography of High Aspect Ratio Structures With a Focused or Aperture–shaped Beam for Applications in Biomedical Studies and Microfludics*", PhD thesis, University of Jyväskylä (2008), http://www.jyu.fi/static/fysiikka/vaitoskirjat/2008/sergey–gorelick–2008.pdf.

[Gorelick07] S. Gorelick, T. Ylimäki, T. Sajavaara, M. Laitinen, A. Sagari A.R., and H.J. Whitlow, Nucl. Instr. and Meth. B 260 (2007) 77.

[Gorelick09] S. Gorelick, F. Zhang, P.G. Shao, J.A. van Kan, H.J. Whitlow and F. Watt, Nucl. Instr. and Meth. B 267 (2009) 2309.

[Guo07] L.J. Guo, Adv. Mater. 19 (2007) 495.

[Hellborg09] R. Hellborg, H.J. Whitlow, and Y. Zhang, *Ion Beams in Nanoscience and Technology*, Springer, 2009.

[Herden98] V. Herden, S. Klaumünzer and W. Schnable, Nucl. Instr. and Meth. B 146 (1998) 491.

[Hetsroni05] G. Hetsroni, A. Mosyak, E. Pogrebnyak, and L.P. Yarin, Int. J. Heat Mass Transfer 48 (2005) 1982.

[ImageJ] M.D. Abramoff, P.J. Magelhaes, S.J. Ram, Biophoton. Int. 11 (2004) 36.

[Intarasiri07] S. Intarasiri, L.D. Yu, S. Singkarat, A. Hallén, J. Lu, M. Ottosson, J. Jensen, and G. Possnert, J. Appl. Phys. 101 (2007) 084311.

[Jensen06] J. Jensen, A. Razpet, M. Skupiński, and G. Possnet, Nucl. Instr. and Meth. B 243 (2006) 119.

[Kamwanna08] T. Kamwanna, *Developments of Ion Beam Analysis Techniques for Micro and Nanoscale Materials*, Ph.D. Thesis, Chiang Mai University, 2008.

[Klauk02] H. Klauk, M. Halik, U. Zschieschang, G. Schimd, and W. Radlik, J. Appl. Phys. 92 (2002) 5259.

[Lee99] E.H. Lee, Nucl. Instr. and Meth. B 151 (1999) 29.

[Lindhard63] J. Lindhard, M. Scharff and H.E. Schiøtt, Mat. Fys. Medd. Dan. Vid. Selsk., 33, No. 14 (1963).

[Madou02] M.J. Madou, *Fundamentals of microfabrication: the science of miniaturization* 2nd ed., ISBN:0–8493–0826–7 (2002).

[Martin82] J.T. Martin, J.D. Barchas, and K.F. Faull, Anal. Chem. 54 (1982) 1806.

[McDonald02] J.C. McDonald and G.M. Whitesides, Acc. Chem. Res. 35 (2002) 491.

[Mekaru10] H. Mekaru, M. Fujimaki, K. Awazu, and M. Takahashi, Microsyst. Technol. 16 (2010) 1339.

[Munnik03] F. Munnik, F. Benninger, S. Mikhailov, A. Bertsch, P. Renaud, H. Lorenz, and M. Gmür, Microelectron. Eng. 67–68 (2003) 96.

[Nastasi96] M. Nastasi, J.W. Mayer, J.K. Hirvonen, *Ion-solid Interaction: Fundamentals and Applications*, Cambridge University Press, New York, 1996.

[Ouellette03] J. Ouellette, *A New Wave of Microfluidic Devices*, The Industrial Physicist 14–17 AUGUST/SEPTEMBER (2003).

[Pászti90] F. Pászti, A. Manuaba, C. Hajdu, A.A. Melo, and M.F. Dasilva, Nucl. Instr. and Meth. B 47 (1990) 187.

[Pelletron] URL://www.pelletron.com/tutor.htm.

[Redondo07] L.M. Redondo, J. Rocha, J.C. Soares, Nucl. Instr. and Meth. B 265 (2007) 576.

[Sangyuenyongpipat09] S. Sangyuenyongpipat, H.J. Whitlow, S.T. Nakagawa, E. Yoshida, AIP Conf. Proc. 1099 (2009) 282.

[Sia03] S.K. Sia and G.M. Whitesides, Electrophoresis 24 (2003) 3563.

[Shao07] P.G. Shao, J.A. van Kan, L.P. Wang, K. Ansari, A.A. Bettiol, and F. Watt, Nucl. Instr. and Meth. B 260 (2007) 362.

[Shui07] L. Shui, J.C.T. Eijkel and A. van den Berg, Adv. Colloid Interface Sci. 133 (2007) 35.

[Sigmund04] P. Sigmund, *Stopping of Heavy Ions A Theoretical Approach*, (Springer, Berlin, 2004).

[Sigmund06] P. Sigmund, *Particle penetration and radiation effects*, (Springer, Berlin, 2006).

[Squires05] T.M. Squires and S.R. Quake, Rev. Mod. Phys. 77 (2005) 977.

[SRIM] J.F. Ziegler, SRIM–2006, http://www.SRIM.org.

[Teng07] J.H. Teng, J.R. Dong, S.J. Chua, B.S. Foo, M.Y. Lai, Y.J. Wang, S.S. Ang, and R. Yin, Appl. Phys. Lett. 90 (2007) 171107.

[Udalagama07] C.N.B. Udalagama, A.A. Bettiol, and F. Watt, Nucl. Instr. and Meth. B 260 (2007) 384.

[Van Kan04] J.A. van Kan, A.A. Bettiol, K. Ansari, E.J. Teo, T.C. Sum and F. Watt, Int. J. Nanotechnology 1 (2004) 464.

[Van Kan07] J.A. van Kan, P.G. Shao, K. Ansari, A.A. Bettiol, T. Osipowicz, and F. Watt, Microsyst. Technol. 13 (2007) 431.

[Van Kan08] J.A. van Kan, F. Zhang, A.A. Bettiol, and F. Watt, Proc. of SPIE 6921 (2008) 69210K-1.

[Wang07] L.P. Wang, P.G. Shao, J.A. van Kan, K. Ansari, A.A. Bettiol, X.T. Pan, T. Wohland and F. Watt, Nucl. Instr. and Meth. B 260 (2007) 450.

[Watt05] F. Watt, A.A. Bettiol, J.A. van Kan, E.J. Teo, and M.B.H. Breese, Int. J. Nanosci. 4 (2005) 269.

[Watt07] F. Watt, M.B.H. Breese, A.A. Bettiol, and J.A. van Kan, Mater. Today 30 (2007) 20.

[Wibbeler98] J. Wibbeler, G. Pfeifer, and M. Hietschold, Sens. and Actua. A 71 (1998) 74.

[Whitlow04] H.J. Whitlow, M.L. Ng, V. Auželytė, I.A. Maximov, J.A. van Kan, A.A. Bettiol, and F. Watt, Nanotechnology 15 (2004) 223.

[Whitlow09] H.J. Whitlow and Y. Zhang, *Ion Beams in Nanoscience and Technology*, R. Hellborg, H.J. Whitlow and Y Zhang, Springer 2009.

[Whitesides01] G.M. Whitesides, E. Ostuni, S. Takayama, X. Jiang, and D.E. Ingber, Annu. Rev. Biomed. Eng. 3 (2001) 335.

[Whitesides06] G.M. Whitesides, *The origins and future of microfluidics*, Nature 442 (2006) 368.

[Yasin02] S. Yasin, D.G. Hasko, and H. Ahmed, Microeletronic. Eng. 61-62 (2002) 745.

[Ziegler85] J.F. Ziegler, J.P. Biersack, U. Littmark, *The Stopping and Ranges of Ions in Solids*, Vol 1 Pergamon, Oxford, New York, 1985.

[Zhang05] *Modification of materials by MeV ion beams*, In Eelectrostatic Accelerator ed by R. Hellborg (Springer, Berlin Heidelberg New York 2005) pp. 506-529. Y. Zhang and H.J. Whitlow,

Paper I

This article was published in Journal Vacuum Science and Technology, Section B, volume 26(5), Sep/Oct 2008,
Nitipon Puttaraksa, Sergey Gorelick, Timo Sajavaara, Mikko Laitinen, Somsorn Singkarat, and Harry J. Whitlow,
Programmable proximity aperture lithography with MeV ion beams,
pp. 1732-1739,

Reprinted with the permission from J. Vac. Sci. Tech. **B 26(5)**, 1732 (2008). Copyright 2008 American Vacuum Society.

Programmable proximity aperture lithography with MeV ion beams

Nitipon Puttaraksa[a)]
Department of Physics, University of Jyväskylä, P.O. Box 35 (YFL), Jyväskylä FIN-40014, Finland and Fast Neutron Research Facility, Department of Physics, Faculty of Science, Chiang Mai University, Chiang Mai 50200, Thailand

Sergey Gorelick, Timo Sajavaara, and Mikko Laitinen
Department of Physics, University of Jyväskylä, P.O. Box 35 (YFL), Jyväskylä FIN-40014, Finland

Somsorn Singkarat
Fast Neutron Research Facility, Department of Physics, Faculty of Science, Chiang Mai University, Chiang Mai 50200, Thailand

Harry J. Whitlow
Department of Physics, University of Jyväskylä, P.O. Box 35 (YFL), Jyväskylä FIN-40014, Finland

(Received 15 February 2008; accepted 4 August 2008; published 17 September 2008)

A novel MeV ion beam programmable proximity aperture lithography system has been constructed at the Accelerator Laboratory of the University of Jyväskylä, Finland. This facility can be used to fabricate three dimensional microstructures in thick (<100 μm) polymer resist such as polymethylmethacrylate. In this method, MeV ion beams from the 1.7 MV pelletron and K130 cyclotron accelerators are collimated to a beam spot of rectangular shape. This shape is defined by a computer-controlled aperture made of a pair of L-shaped Ta blades which are in close proximity to the sample to minimize the penumbra broadening. Here the authors report on development of the system, the controlling software, the calibration procedures, investigations of multiple scattering effects, and present illustrative results using 3 MeV $^4He^{2+}$ ion beams for lithography and 56 MeV $^{14}N^{3+}$ ion beams for creating patterns of regions with ion tracks. © *2008 American Vacuum Society.* [DOI: 10.1116/1.2978173]

I. INTRODUCTION

MeV ion beam lithography is a very useful technique for the fabrication of the three dimensional (3D) micro- and nanostructures with very high aspect ratio, i.e., the ratio between feature height and width in the etched patterns.[1–10] This maskless technique can be used for low-cost rapid and flexible prototyping in polymeric materials as well as for the production of master stamps for mass production, e.g., by hot-embossing. The most common form of MeV ion beam lithography is proton-beam writing (PBW) which uses a magnetic multielement lens focusing system to produce a micro- or nanobeam of MeV protons that is scanned directly across a polymer resist.[11,12] One of the advantages of PBW is that the demagnified beam spot can be used to machine patterns down to nanometer dimensions with straight and smooth vertical sidewalls in thick resists of about 1–30 μm. This is significantly better than can be achieved with electron beam lithography because of the smaller lateral spreading of secondary electrons produced by penetrating MeV ions which results in localization of the deposited energy around the ion tracks.[13] Structures made in polymers with PBW have been used for (i) fabrication of micromachined components by electrodeposition,[14] (ii) microfluidic devices,[15,16] (iii) cell growth substrates,[17] (iv) stamps for nanoimprinting and μ-contact printing,[18,19] and (v) maskmaking for using with x-ray lithography.[20]

In an alternative approach to PBW, namely, proton-beam lithographie galvanoformung abformung (LIGA),[7] rather than focusing the beam and scanning it across the sample, the sample is moved relative to a finely collimated fixed beam.[21–23] Driven by the needs of our biomedical research program which requires writing large areas with many pattern elements, we extended this technique to programmable proximity aperture lithography (PPAL) which, in addition to moving the sample relative to the collimated beam spot, also shapes the beam spot using a computer-controlled aperture in close proximity to the target. The aperture and target are maintained in close proximity to minimize broadening of the edges of the irradiated area because of penumbra broadening and scattering from the aperture edges.[21,24]

There are several advantages in the PPAL approach. It is considerably faster than lithography with focused or collimated beams [e.g., PBW, electron beam lithography (EBL), and P-beam LIGA] where the pattern is written serially pixel by pixel. This is because in PPAL an entire rectangular pattern element is written in one exposure. Our method is thus intermediate in speed between writing with rastered focused beams and a true parallel exposure method such as exposure through a mask. Furthermore, the PPAL method is not susceptible to distortions introduced by scanning and it is tolerant of poor beam energy stability and divergence, which is often the case when the ion beam is provided by a cyclotron.[25] A further key advantage is that it allows very high energy heavy ions up to the limit set by the thickness of the apertures[21] that define the exposed area. Such very high en-

[a)]Electronic mail: niputtar@cc.jyu.fi

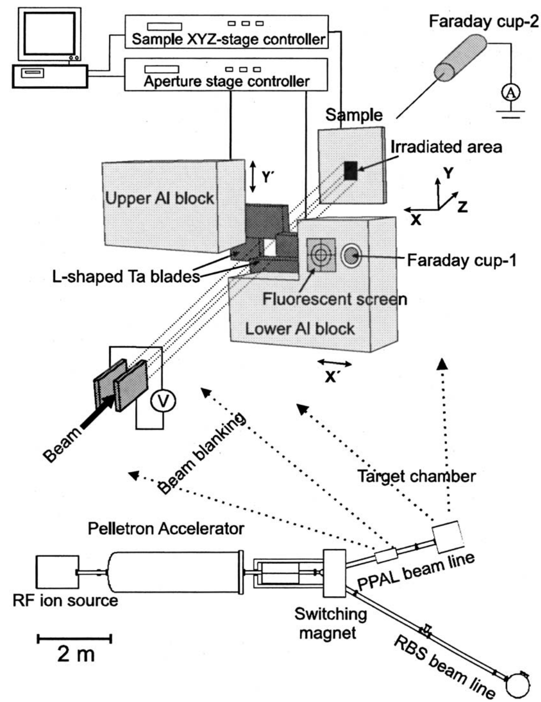

FIG. 1. Schematic of the MeV ion beam PPAL system at the University of Jyväskylä Pelletron Accelerator.

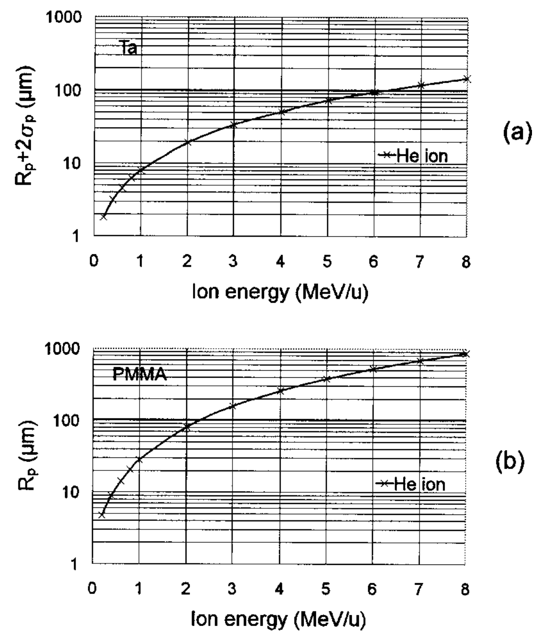

FIG. 2. (a) $R_p+2\sigma_p$ of He ion in Ta vs He ion energy and (b) projected range in PMMA vs He ion energy. [Data calculated using SRIM (Ref. 26).]

ergy heavy ions are difficult to focus with conventional quadrupole magnetic lens systems because of their high rigidity. However, these advantages are at the expense of not being able to focus the beam down to spot sizes of a few tens of nanometres, the need to write each pattern element sequentially, and the restriction to rectangular pattern elements.

Here, we report on the practical development of the PPAL method and calibration procedures using high energy $^4He^{2+}$ ions for microfabrication and high energy $^{14}N^{3+}$ ions for producing patterned areas made up of ion tracks.

II. PRINCIPLE

The basic principle of the PPAL system is that the shape and size of the incident ion beam are defined by an aperture formed by two L-shaped aperture blades that move over each other rather like a pair of scissors (Fig. 1). Tantalum was chosen as the aperture blade material because it has a high atomic weight, low coefficient of thermal expansion, and is not easily activated by high energy ions. The latter would lead to undesirable exposure of the resist from radiation emanating from the region of induced radioactivity.[21] Obviously the aperture blade must be sufficiently thick to completely stop incident ions outside the aperture opening. The penetration of He ions in Ta estimated using the SRIM code[26] is illustrated in Fig. 2(a), where the penetration depth at which the ions are completely stopped, was taken to be $R_p+2\sigma_p$. Here R_p and σ_p are projected range and projected range straggling, respectively. The projected range of He ions in polymethylmethacrylate (PMMA), which corresponds to the maximum film thickness that can be exposed, is also shown in Fig. 2(b). Reference to this figure shows that 100 μm of Ta will completely stop He projectiles of up to 6 MeV per nucleon while enabling patterns to be written in up to 450 μm thick PMMA resist. For 3 MeV He ions, which can be produced by many small accelerators, the projected range in PMMA is about 20 μm, which allows patterns in up to 10–12 μm thick PMMA to be written with sharp vertical edges. Swift MeV ions deposit energy in resist polymers such as PMMA through electronic excitation which creates mainly low energy δ-electrons.[27] These low energy (5–100 eV) secondary electrons have short ranges[5,28] and cause chain scission and cross-linking in resist polymers that modify the solubility in developer around the ion trajectories. The mean free path for ion-nucleus scattering is much longer than for ion-electron scattering[29] and the ion trajectories normally exhibit only a small divergence. Although this divergence which arises from multiple scattering is small, it governs the straightness of the vertical walls because it leads to a spreading of the dose into unirradiated areas from adjacent irradiated regions. This effect increases with the thickness of the material traversed by the ion.

III. MULTIPLE SCATTERING AND WALL EDGE STRAIGHTNESS

An important factor for some applications such as metal lift-off,[5] narrow microfluidic channels,[15,16] and optical waveguides[30] is the departure of the wall sides from perfect verticality. The deviation is primarily governed by multiple scattering which gives rise to an increasing deposition of energy outside the irradiated area as the penetration distance of the ions increases. This effect can be estimated by using a 3D simulation code, e.g., GEANT4;[24] however, it requires considerable expertise. Here we have used a more computation-

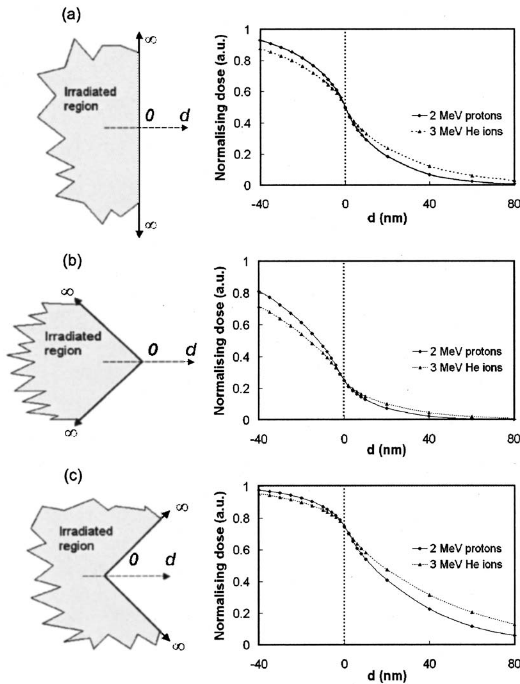

FIG. 3. The fluence distribution along the transverse distance d (nm) for unirradiated areas with (a) straight edge, (b) external 90° corner, and (c) internal 90° corner. The position $d=0$ corresponds to the edge or corner location.

ally easy approach by combining the SRIM code[26] with a simple integral transformation (Appendix).

Monte Carlo binary collision approximation codes such as SRIM (Ref. 26) generally provide fluence distributions for ions incident along the z axis at the origin of the (x,y) plane. For our purposes we are interested in the spreading of the ion fluence by multiple scattering across the edges of an irradiated area. This distribution can be obtained from the SRIM data by a simple integral transformation, which, because of its general application in ion-matter interaction work, is presented in the Appendix. Figure 3 presents the fluence distributions across the straight edge of a semi-infinite irradiated area and along the bisectors of the internal and external 90° corners of semi-infinite irradiated areas for 2 MeV protons and 3 MeV He ions that have traversed a 7.5 μm PMMA film.

The shape of the curves in Fig. 3 is similar to a complimentary error function, cerf (x). As one expects the distributions are symmetric in the case of a straight boundary to the irradiated area [Fig. 3(a)] and skewed in the case of the external and internal corners [Figs. 3(b) and 3(c), respectively]. Taking the 12%–88% width corresponds to the full width at half maximum of the Gaussian derivative of the cerf(x). The widths after penetrating 7.5 μm thick of PMMA are ~50 and ~64 nm for 2 MeV protons and 3 MeV He ions, respectively. The implication is that the spreading of the fluence for 2 MeV protons is less than for 3 MeV helium ions in a 1–10 μm thick PMMA film. It can be seen in Fig. 3 that the spreading of the fluence distribution (and hence dose) into the unirradiated regions where $d>0$ is accompanied by a corresponding reduction in fluence in the irradiated regions close to the boundary, where d is just smaller than zero. The implication is that for high contrast resists, the vertical profile of the wall and if it is over- or undercut at the bottom, will depend on both the multiple scattering and the exposure fluence. As one expects, comparing the fluence along the bisectors of corners in Fig. 3 shows that the spreading of the fluence outside the irradiated region is greater for the internal corner (c) than the external corner (b).

The intersection of the distribution for H and He ions in Fig. 3 at $d=0$ is a consequence of normalization to the same dose for $d \ll 0$.

IV. EXPERIMENTAL DETAILS

A. Preparation of aperture blades

The operating principle of the PPAL technique is shown schematically in Fig. 1. A rectangular beam spot is produced by a shadow casting by a pair of L-shaped Ta aperture blades. Each of these blades is made up from two 8×13 mm^2, or 9×13 mm^2, 100 μm thick Ta foils. The four Ta foils were stacked together and clamped vertically in a stainless steel polishing jig. The edges were milled flat so they were the same height as the surface of the polishing jig. Subsequently the edges were mechanically polished successively with 600, 800, 1500, and 2000 grade SiC papers followed by a diamond paste of 6 and 0.5 μm grain sizes.[31] The flatness of the Ta surface was investigated by using a profilometer, and the polishing was stopped when the desired Ta edge roughness [<100 nm (Ref. 21)] was reached. It was found that, after the blades were removed from the polishing jig, the separated debris tended to accumulate on the edges. The Ta blades were cleaned with acetone in an ultrasonic bath for 10 min, followed by a 2 min rinse in ethanol and de-ionized water to remove this debris. Each pair of blades were then glued under an optical microscope using vacuum-compatible epoxy glue at right angles on two separate aluminum blocks that mount onto the computer-controlled linear-motion stages, as shown in Fig. 1.

B. Description of the PPAL system

Our PPAL system is designed to be used with the 1.7 MV pelletron and K130 cyclotron accelerators at the University of Jyväskylä Accelerator Laboratory. The PPAL system can be moved between the two accelerators by changing the support frame to accommodate the different beam heights. A schematic layout of the PPAL system at the 1.7 MV pelletron is shown in Fig. 1. The beam blanking is achieved by biasing a pair of 20 cm long plates, separated by 5 mm with a potential difference of 3 kV delivered via a high voltage relay. The relay is controlled by transistor-transistor logic signals delivered by the control computer via a PCIe-6251 multifunction data acquisition (DAQ) card.[32] A fluorescent screen on one of the aluminum blocks, which support the aperture blades, is used for focusing the beam. For measurement of

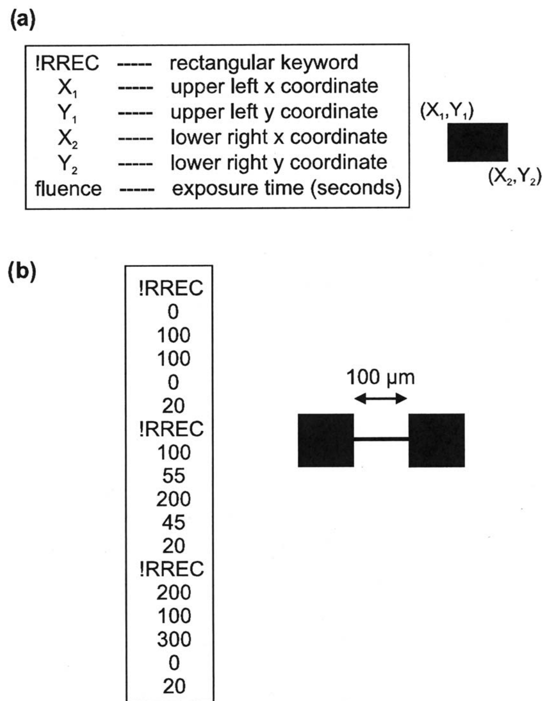

FIG. 4. (a) A PPAL file record structure for writing a rectangular or square pattern. (b) An example of a patterning file and the resulting pattern.

the beam current before and after the apertures, Faraday cups are installed both on the aperture block and behind the sample (see Fig. 1).

The sample is mounted on a computer-controlled *XYZ* stage that allows the beam spot to be positioned within a 20×20 mm^2 field on the sample and allows for precise adjustment of the aperture-sample distance. The *XYZ* stage and the aperture positioning use vacuum-compatible Newport MFA-CCV6 dc servomotor driven linear-motion drives.[33] According to the manufacturers specification, these have a 25 mm travel, with 100 nm minimum increment and a unidirectional setting accuracy of 180 nm, bidirectional setting accuracy of 2 μm, and accuracy in position of 4 μm (the latter is determined by the end-of-travel switch). The linear-motion drives are controlled using Newport ESP 300 controllers linked to the controlling PC using a standard RS-232 interface. A LABVIEW™ program is used to control the apertures, *XYZ* sample stage, exposure time, and beam blanking. The pattern is specified in a simple ASCII file arranged as sequential blocks of six records. The structure of the PPAL file is shown in Fig. 4(a). Figure 4(b) shows a typical example of the pattern file with the corresponding patterns. For compatibility, the LABVIEW™ program also accepts the Singapore group's emc file format.[34] In order to achieve optimum positioning accuracy the exposures were carried out when the sample and apertures were stationary. Furthermore, the final approach to the exposure position was always made in the same direction to minimize the detrimental effects of windup, backlash, and hysteresis in the mechanical components.

To ensure mechanical stability of the system, the sample and aperture stages are mounted on a small homemade optical mounting board in the vacuum chamber. At the pelletron accelerator, the $40\times40\times40$ cm^3 vacuum chamber is well isolated from building vibrations. It is mounted on a separated concrete floor that rests on a thick sand bed. The chamber is isolated from vacuum pump vibrations by edge-welded steel bellows and vibration damping sections. Additional information about PPAL system can be found elsewhere.[21]

C. Sample preparation

In this work we used PMMA as a resist material. This is a widely used positive electron beam lithography resist. The PMMA A11 solution[35] with a molecular weight of 950 000 Da was spun onto a clean Si wafer at 2500 rpm for 45 s. After spinning, the excess solvent was removed by a soft-bake on a hotplate at 160 °C for 5 min. This process was repeated three times to obtain an approximately 7.5 μm thick PMMA resist layer.

D. Sample exposure and development

For heavy ion irradiations, 56 MeV $^{14}N^{3+}$ ion beams from a cyclotron were used because sufficient current was available and this beam is easily optimized. The stopping power of 56 MeV $^{14}N^{3+}$ ions in PMMA is 423 eV/nm,[26] which is about 28 times larger than that of 2 MeV protons. While knowing that the required fluence of the 2 MeV protons to completely expose PMMA is 80 nC/mm^2,[12] we estimate that the fluence of 10 nC/mm^2 or 2.1×10^{12} ions/cm^2 is required for the 56 MeV $^{14}N^{3+}$ ions. The current of $^{14}N^{3+}$ ions transmitted through a 1×1 mm^2 aperture opening was measured by means of a Faraday cup positioned behind the sample (see Fig. 1). This current density translates into 100 s per pattern element exposures which was verified by a series of exposure and development tests.

For MeV ion beam lithography using ion beams from the pelletron accelerator, a 3 MeV $^4He^{2+}$ ion beam was used. In this case the stopping power is 121 eV/nm (Ref. 26) and the current, measured under the same conditions as above, was 1 nA. The exposure time was typically 10–20 s per pattern element. The stopping power of 3 MeV $^4He^{2+}$ ions in PMMA is about eight times larger than that of 2 MeV protons, so we estimate that in order to completely expose PMMA 20 nC/mm^2 or 6.25×10^{12} ions/cm^2 is required.

After exposure, the PMMA samples were developed in an isopropanol+water 7:3 mixture. This developer was chosen because it is reported to have good sensitivity, latitude, and contrast.[36] Moreover, its viscosity and toxicity are lower than that of conventional PMMA developers used for x-ray and EBL work. Subsequently, the samples were rinsed in deionized water twice and dried under the flowing helium gas.

V. RESULTS AND DISCUSSION

A critical first step when setting up the PPAL system to write patterns is to define the origin position where the apertures are just fully closed [i.e., X' and Y' (Fig. 1) are zero].

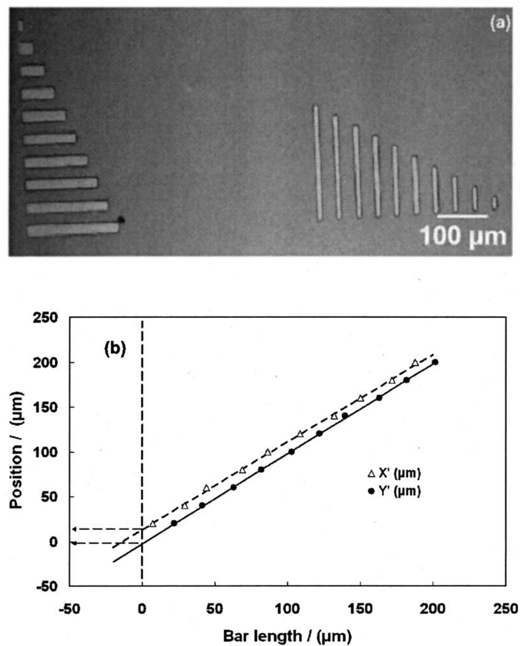

FIG. 5. An example of the set of calibration patterns produced by using 3 MeV $^{4}He^{2+}$ in 7.5 μm thick PMMA where the bar length is varied from 200 to 20 μm in 20 μm steps in x and y directions.

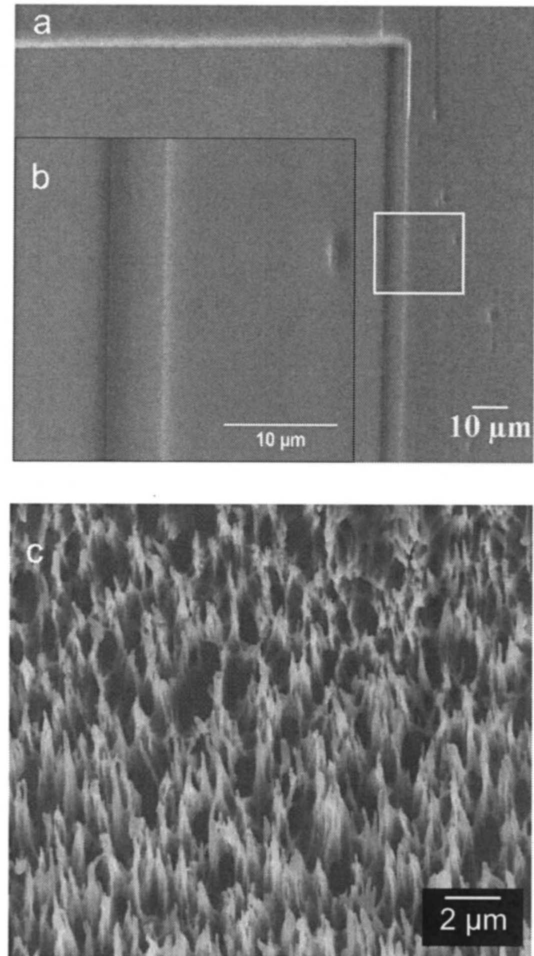

FIG. 6. (a) SEM image of a smooth sidewall pattern in 7.5 μm thick PMMA written using 56 MeV $^{14}N^{3+}$ ions. (b) A close-up of the area in (a) marked with a white square. (c) SEM image of the nanostructures obtained using a low fluence of 56 MeV $^{14}N^{3+}$ ions.

Measurement of the origin position for each run was found to be much more reproducible than the zero position derived from the end-of-travel limit switches. This calibration was done by exposing a test pattern consisting of sets of horizontal and vertical bars of different lengths. Figure 5(a) shows an example of the calibration patterns where the bar length is varied from 200 to 20 μm in 20 μm steps for both X' and Y' directions. It is then trivial to obtain the positions corresponding to $X'=0$, $Y'=0$, by straight line regression, as illustrated in Fig. 5(b). Inspection of the residuals in this plot (not shown) revealed no evidence of systematic deviation from straight lines. The standard errors in determining the zero position from the data in Fig. 5(a) were 1.4 and 0.8 μm in the X' and Y' directions, respectively. This uncertainty is mainly associated with the finite pixel width in the optical micrographs. The origin position can then be further refined using this procedure with shorter bars.

Figure 6(a) shows a scanning electron microscope (SEM) image of a smooth sidewall pattern produced in 7.5 μm thick PMMA with the 56 MeV $^{14}N^{3+}$ beam. A higher magnification SEM image of the pattern sidewall is shown in Fig. 6(b). In this case the fluence is sufficiently high that the ion tracks completely overlap so that the clearing dose within the irradiated area is exceeded and the PMMA is completely removed from the irradiated area. Lower fluences give a different result as shown in Fig. 6(c) where the clearing dose is only exceeded around the individual ion tracks. The stochastic variation in ion impingement then gives rise to a strong nanometer-scale texture. This situation is discussed in more detail elsewhere.[37] Similar structures were also obtained with a low fluence of He ions. This situation is in contrast to the case for 2 MeV protons[38] where the dose around individual ions is insufficient to exceed the clearing dose.

Figure 7 shows a SEM image of a pattern written using 3 MeV $^{4}He^{2+}$ ions in 7.5 μm thick PMMA. The pattern in Fig. 7(a) shows 1.6 μm wide channels between large reservoir areas (not shown). The smallest structure produced in PMMA so far is the 700–800 nm thick self-supporting wall shown in Fig. 7(b). The wall thickness to height aspect ratio is approximately 10. Inspection of the walls in Fig. 7(a) reveals that they are close to vertical as expected on the basis of SRIM estimations. Although no systematic study was made, this is consistent with the multiple scattering data in Fig. 3, which shows that the fluence broadening from multiple scattering is on a scale of 50 nm which is too small to be reliably measured. Moreover, the roughness features on corresponding edges are reproduced, indicating that the dominating contribution to pattern roughening originates from deviations in the straightness of the polished edges of the aperture blades.

It is an interesting question to consider the limits to the size of pattern features that can be written by the PPAL ap-

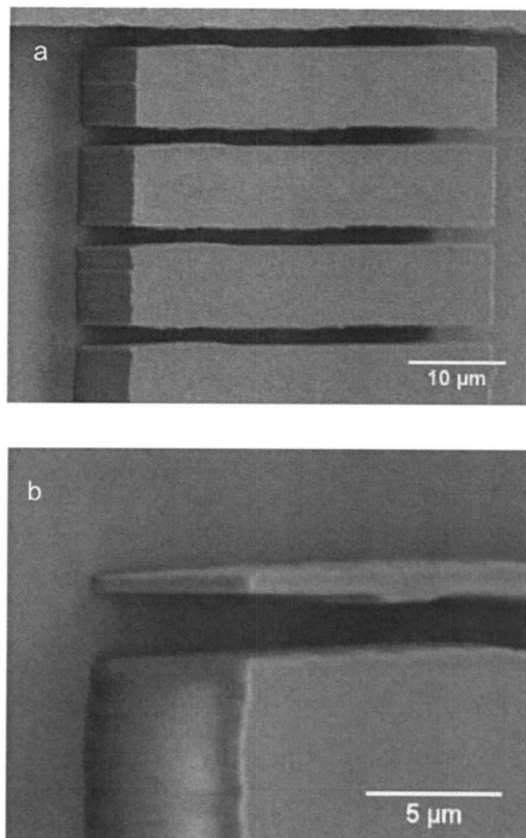

FIG. 7. (a) SEM image of 1.6 μm wide channels. (b) SEM image of a detail of the smallest structure (a 700–800 nm thick freestanding wall) produced by using 3 MeV $^4He^{2+}$ ions in a 7.5 μm thick PMMA.

proach. The limits are governed by (a) the roughness and alignment of the aperture blades, (b) the positioning accuracy of the aperture and the *XYZ* sample stage, (c) thermal effects, (d) spreading of the dose at the edges of the irradiated area associated with multiple scattering, (e) penumbra broadening, and (f) aperture edge scattering. Considering (a), close inspection of Fig. 7(a) reveals that ~100 nm roughness features on the edges of the aperture blades are faithfully reproduced. This roughness sets one limit to the minimum feature size and improvement of polishing technique; using e.g., electropolishing could reduce the roughness to 10 nm rms or so. Angular missalignment of the aperture blades will lead to a tapering of the rectangular pattern elements. Conventional metal machining practices can easily achieve an alignment accuracy of 0.1° over 20 mm. This corresponds to 10 nm over 5 μm. Thus the taper will not be a major problem for short pattern elements but becomes critical for long thin rectangular elements, e.g., a 100 nm wide and 500 μm rectangular line. The accuracy of the linear-motion drives (b) is of crucial importance. It is quite difficult to predict this performance because it depends on details of the control scheme and the position encoder and moreover, the data are generally given in terms of the entire range of travel rather than over small increments of motion. The minimum incremental motion is an indicator of this accuracy, which is 100 nm for our linear-motion drives. This could be improved by a factor of 10 if piezoelectric linear-motion drives were used instead. These are capable of fine movements with an accuracy of 10 nm or below. Thermal drifts (c) can also limit the accuracy and are difficult to estimate for our system because of the complex structure of the aperture blade mounting. A simple estimation, based on a thermal resistance of 0.5 K/W cm^2 (typical for a transistor mounting) between the aperture blade and the aluminum block, shows that a current of 10 nA of 3 MeV He ions will lead to an expansion of a Ta blade anchored 3 mm from the Al block edge by 100 nm. This corresponds about ten times greater current than that is usually employed.

The effect of multiple scattering is subtle because, as mentioned above, it can lead to over-and undercutting of the edge or even no effect at all. The penumbra spreading and edge scattering have potentially the largest contribution to the resolution. Penumbra broadening is associated mainly with beam divergence which can be minimized by close proximity of the aperture and target. For 1 mrad beam divergence, the fluence spreading at the edge of the irradiated area is 1 μm.[21,24,37] Similarly spreading from the aperture edges[21,24] also limits the broadening and hence the smallest sized features that can be written. However, by choice of a high contrast resist and careful control of fluence, the effects of broadening can be mitigated in a similar way to control the proximity effect in electron beam lithography. Thus on the basis of the above, with careful control of the divergence and mechanical movements, structures on a scale of hundreds of nanometers in thick resist should be achievable.

VI. CONCLUSIONS

We have developed a MeV ion beam PPAL system at University of Jyväskylä as a powerful lithographic instrument. This system enables the use of ion beam over a wide energy range to fabricate channel structures and lithographically defined regions with nanometer-scale ion-track structures. At present, the smallest structure produced by our system was an approximately 700–800 nm wide wall in 7.5 μm thick PMMA with a corresponding aspect ratio of about 10. In the future, the aspect ratio can be increased by producing structures in thicker resists or reducing structure dimensions. This system is suitable for making the structures for fundamental cellular or subcellular biomedical research in our group. Multiple scattering leads to a spreading of the fluence distribution at the edges of the irradiated regions on a scale of 50 nm after penetrating 7.5 μm of PMMA.

ACKNOWLEDGMENT

This work has been supported by the Academy of Finland Centre of Excellence in Nuclear and Accelerator-Based Physics (Ref. 213503). One of the authors (N.P.) also gratefully acknowledges financial support from the Royal Golden Jubilee Scholarship of the Thailand Research Fund and owes special thanks to the staff of the Accelerator Laboratory for their enthusiastic support and encouragement throughout his studies in Jyväskylä.

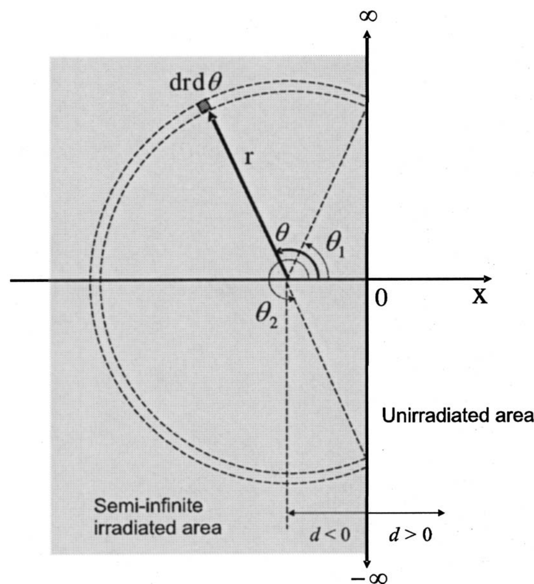

FIG. A1. Geometry for transformation of $N(r)$ to $N(d)$.

APPENDIX

SRIM (Ref. 26) and other simulation programs for particle-matter interactions [e.g., CASINO (Ref. 28)] mainly provide distributions $N(x,y)$ of physically interesting quantities (fluence, dose, ionization, displacement damage, etc.) in Cartesian coordinates. Generally, the distributions are in a plane perpendicular to the beam direction, z, where the origin (0, 0) in the plane of the surface corresponds to the point of the impingement of the ions.

A commonly met question in ion-matter interaction studies is that the quantity of interest is a distribution $N(d)$, where d is the perpendicular distance from the straight edge of an irradiated area, such as that defined by the edge of a scanned region or mask. This may be obtained from $N(x,y)$ using the transformation below. It is trivial to extend this approach to the bisectors of semi-infinite area bounded by two straight edges (e.g., the bisectors for internal and external corners).

The first step is to transform $N(x,y)$ to a radial distribution $N(r)$ according to $r=\sqrt{x^2+y^2}$ and subsequently apply proper normalization.

Then, using the symmetry property $N(r)=N(-r)$, the contribution to $N(d)$ from the arc of the circular shell of thickness dr is obtained by integrating along the arc $\theta_1 \rightarrow \theta_2$ inside the irradiated area (Fig. A1). Then integrating a second time over r we have

$$N(d) = \int_0^{\infty} \int_{\theta_1}^{\theta_2} N(r) d\theta dr, \qquad \text{(A1)}$$

where the limits of integration θ_1 and θ_2 are as follows: for $d<0$;

$$\theta_1 = \begin{cases} 0, & r \leq d \\ \cos^{-1}(d/r), & r > d, \end{cases}$$

$$\theta_2 = \begin{cases} 2\pi, & r \leq d \\ 2\pi - \cos^{-1}(d/r), & r > d \end{cases}$$

and for $d \geq 0$,

$$\theta_1 = \begin{cases} 0, & r \leq d \\ \pi/2 + \sin^{-1}(d/r), & r > d, \end{cases}$$

$$\theta_2 = \begin{cases} 0, & r \leq d \\ 3\pi/2 - \sin^{-1}(d/r), & r > d. \end{cases} \qquad \text{(A2)}$$

The distribution of lateral spreading $N(x,y)$ for a uniformly distribution of 10^4 projectiles of 2 MeV protons and 3 MeV helium ions traversing 7.5 μm of PMMA was determined using SRIM simulation.[26] To avoid uncertainties associated with the selection of mean free path at small impact parameters, which are expected to have a large influence on multiple scattering distributions, the calculation was set up to calculate scattering with each atomic layer. The distribution of lateral spread $N(d)$ across a straight edge of an irradiated area (Fig. 3) was then obtained by numerical integration of Eq. (A1). The transformation [Eq. (A1)] was extended to calculate $N(d)$ for internal and external corners of irradiated areas bounded by two straight lines by a trivial selection of different angular integration limits θ_1 and θ_2. The fluence distributions $N(d)$ along the bisectors of 90° forming external and internal corners are presented in Figs. 3(b) and 3(c).

[1]F. Watt, M. B. H. Breese, A. A. Bettiol, and J. A. van Kan, Mater. Today **30**, 20 (2007).
[2]L. Marot, F. Munnik, and S. Mikhailov, Appl. Surf. Sci. **252**, 7343 (2006).
[3]C. Debaes *et al.*, IEEE/LEOS, June 2005 (unpublished), Vol. 19, No. 3, pp. 12–14.
[4]V. Gomez, B. Volckaerts, H. Ottevaere, and H. Thienpont, Proceeding Symposium IEEE/LEOS, 2005 (unpublished), Benelux Chapter, Mons 301.
[5]H. J. Whitlow, M. L. Ng, V. Auzelyté, I. A. Maximov, J. A. van Kan, A. A. Bettiol, and F. Watt, Nanotechnology **15**, 223 (2004).
[6]J. A. van Kan, A. A. Bettiol, and F. Watt, Appl. Phys. Lett. **83**, 1629 (2003).
[7]F. Munnik, F. Benninger, S. Mikhailov, A. Bertsch, P. Renaud, H. Lorenz, and M. Gmür, Microelectron. Eng. **67–68**, 96 (2003).
[8]L. Cosentino, P. Finocchiaro, A. Pappalardo, A. Hermanne, H. Thienpont, M. Vervaeke, B. Volckaerts, and P. Vynck, Nucl. Instrum. Methods Phys. Res. B **209**, 340 (2003).
[9]L. Cosentino, P. Finocchiaro, A. Pappalardo, A. Hermanne, H. Thienpont, M. Vervaeke, B. Volckaerts, and P. Vynck, IEEE Trans. Nucl. Sci. **50**, 774 (2003).
[10]B. Volckaerts, L. Cosentino, A. Pappalardo, P. Vynck, M. Vervaeke, P. Finocchiaro, A. Hermanne, and H. Thienpont, LNS Activity Report, 2003.
[11]F. Watt, A. A. Bettiol, J. A. van Kan, E. J. Teo, and M. B. H. Breese, Int. J. Nanosci. **4**, 269 (2005).
[12]J. A. van Kan, A. A. Bettiol, K. Ansari, E. J. Teo, T. C. Sum, and F. Watt, Int. J. Nanotechnol. **4**, 464 (2004).
[13]S. Y. Chiam, J. A. van Kan, T. Osipowicz, C. N. B. Udalagama, and F. Watt, Nucl. Instrum. Methods Phys. Res. B **260**, 455 (2007).
[14]H. Nakajima, T. Noshiyuki, R. Hagiwara, K. Nitta, S. Inazawa, and K. Okada, Electrochim. Acta **53**, 24 (2007).
[15]L. P. Wang, P. G. Shao, J. A. van Kan, K. Ansari, A. A. Bettiol, X. T. Pan, T. Wohland, and F. Watt, Nucl. Instrum. Methods Phys. Res. B **260**, 450 (2007).
[16]P. G. Shao, J. A. van Kan, L. P. Wang, K. Ansari, A. A. Bettiol, and F. Watt, Nucl. Instrum. Methods Phys. Res. B **260**, 362 (2007).
[17]S. Gorelick, P. Rahkila, A. Sagari, A. R. T. Sajavaara, S. Cheng, L. B.

Karlsson, J. A. van Kan, and H. J. Whitlow, Nucl. Instrum. Methods Phys. Res. B **260**, 130 (2007).
[18]J. A. van Kan, L. P. Wang, P. G. Shao, A. A. Bettiol, and F. Watt, Nucl. Instrum. Methods Phys. Res. B **260**, 353 (2007).
[19]K. Ansari, J. A. van Kan, A. A. Bettiol, and F. Watt, J. Micromech. Microeng. **16**, 1967 (2006).
[20]J. A. van Kan, P. G. Shao, K. Ansari, A. A. Bettiol, T. Osipowicz, and F. Watt, Microsyst. Technol. **13**, 431 (2007).
[21]S. Gorelick, T. Ylimäki, T. Sajavaara, M. Laitinen, A. Sagari A.R., and H. J. Whitlow, Nucl. Instrum. Methods Phys. Res. B **260**, 77 (2007).
[22]J. van Erps *et al.*, IEEE Photonics Technol. Lett. **18**, 1164 (2006).
[23]M. L. Taylor, A. Alves, P. Reichart, R. D. Franich, S. Rubanov, P. Johnston, and D. N. Jamieson, Nucl. Instrum. Methods Phys. Res. B **260**, 426 (2007).
[24]S. Gorelick, T. Sajavaara, M. Laitinen, N. Puttaraksa, and H. J. Whitlow, *Resolution Performance of Programmable Proximity Aperture MeV Ion Beam Lithography System*, MRS Symposia Proceedings No. 1020 (Materials Research Society, Pittsburgh, 2007) p. 632.
[25]S. Kurashima *et al.*, Nucl. Instrum. Methods Phys. B **260**, 65 (2007).
[26]J. F. Ziegler, SRIM-2006, http://www.SRIM.org
[27]Y. Zhang and H. J. Whitlow, in *Electrostatic Accelerators* edited by R. Hellborg (Springer, Berlin, 2005), p. 507.
[28]P. Hovington, D. Drouin, R. Gauvin, D. C. Joy, and N. Evans, Scanning **19**, 29 (1997), http://www.gel.usherb.ca/casino/index.html
[29]H. J. Whitlow and S. T. Nankagawa, Nucl. Instrum. Methods Phys. Res. B **260**, 468 (2007).
[30]A. A. Bettiol, S. Venugopal Rao, T. C. Sum, J. A. van Kan, and F. Watt, J. Cryst. Growth **288**, 209 (2006).
[31]Diamond and tools PD0501/4HP, grain size $1/2-0$ μm.
[32]NI™ DAQ PCIe-6251, http://www.ni.com
[33]ESP300 1-3 axis motion controller/driver, MFA-CCV6 miniature linear stages, http://newport.com
[34]A. A. Bettiol, C. N. B. Udalagama, J. A. van Kan, and F. Watt, Nucl. Instrum. Methods Phys. Res. B **231**, 400 (2005).
[35]Nano™ PMMA and copolymer data sheet, MicroChem Corp., 1254 Chestnut Street, Newton, MA 02464, http://www.microchem. com/products/pdf/PMMA_Data_Sheet.pdf
[36]S. Yasin, D. G. Hasko, and H. Ahmed, Microelectron. Eng. **61–62**, 745 (2002).
[37]S. Gorelick, N. Puttaraksa, T. Sajavaara, S. Singkarat, and H. J. Whitlow, Nucl. Instrum. Methods Phys. Res. B **266**, 2461 (2008).
[38]H. J. Whitlow, J. A. van Kan, and F. Watt (unpublished).

Paper II

This article was published in Material Research Society Proceeding,
volume 1020-GG03-04,
Sergey Gorelick, Timo Sajavaara, Mikko Laitinen, Nitipon Puttaraksa,
and Harry J. Whitlow,
*Resolution Performance of Programmable Proximity Aperture MeV Ion
Beam Lithography System*,
Copyright Material Research Society (2008).

Reproduced with the permission of the publisher.

Mater. Res. Soc. Symp. Proc. Vol. 1020 © 2007 Materials Research Society 1020-GG03-04

Resolution Performance of Programmable Proximity Aperture MeV Ion Beam Lithography System

Sergey Gorelick[1], Timo Sajavaara[1], Mikko Laitinen[1], Nitipon Puttaraksa[2], and Harry J. Whitlow[1]
[1]Dept. of Physics, University of Jyväskylä, Jyväskylä, 40014, Finland
[2]Dept. of Physics, Chiang Mai University, Chiang Mai, 50200 (FNRF), Thailand

ABSTRACT

An ion beam lithography system for light and heavy ions has been developed at the University of Jyväskylä's Accelerator Laboratory. The system employs a programmable proximity aperture to define the beam. The proximity aperture is made up of four Ta blades with precise straight edges that cut the beam in the horizontal and vertical directions. The blade positions and dimensions are controlled by a pair of high-precision linear-motion positioners. The sample is mounted on a *X-Y-Z* stage capable of moving with 100 nm precision steps under computer control. The resolution performance of the system is primarily governed by the proximity aperture. Pattern edge sharpness is set by the beam divergence, aperture blade straightness, and secondary and scattered particles from the aperture blade edges. Ray tracing simulations using object oriented toolkit GEANT4 were performed to investigate the beam spatial resolution on the sample defined by the proximity aperture. The results indicate that the edge-scattering does not significantly affect the pattern edge sharpness.

INTRODUCTION

MeV proton beam writing (PBW) is a rapidly evolving lithography technique capable of patterning high 3D nanopatterns with very high line-width to resist-thickness aspect ratio (more than 100), and with a high resolution of better than 20 nm [1-3]. The PBW technique is analog to electron beam lithography (EBL). A beam of protons from an electrostatic accelerator is magnetically focused and scanned over the resist surface. However, the MeV protons, as opposed to keV electrons, can penetrate deep into the resist along a straight path with minimal scattering.

Proton beams from cyclotrons generally have higher energies (tens of MeV), which enables pattern writing in thicker resists (up to 400 μm for 6 MeV protons in PMMA [4]). However, even if large beam currents are available (up to 100's of μA), the rather large divergence (about 1 mrad) and poor energy resolution imply that it is not straightforward to use a focusing in order to reach μm beam spot sizes. An alternative approach is to raster the target relative to a small beam spot defined by an aperture [5,6]. In MeV ion programmable proximity aperture lithography (PPAL), which is used in our system, a rectangular beam spot is defined by a "shadow" of a computer-controlled variable aperture in close proximity to the sample (Fig. 1). The aperture is made up of two L-shaped Ta blades with straight edges (each blade is made up of two 100 μm thick Ta sheets glued together). Precise movement of each L-shaped blade in the *X'* and *Y'* directions defines the size of the beam spot (Fig. 1(a)). By combining *X'* and *Y'* movement of the defining aperture with *x* and *y* movement of the target, entire rectangular

pattern elements up to 500×500 μm^2 can be written in a single exposure over 20×20 mm^2 field. A technical overview of the PPAL system can be found elsewhere [7].

The PPAL approach considerably speeds up the writing time for large patterns compared to writing by scanning a small beam spot over the entire pattern element. This system is a valuable tool for our biomedical research programs at a cellular and sub-cellular level [8], where we are interested in rapidly exposing patterns with a large numbers of pattern elements of 10-300 μm size over a large area in thick (≤200 μm) resists in order to form cell-growth substrates. However, we believe that the PPAL system, besides production of cell culture substrates, may be also employed for a rapid production of 3D micro- and nanostamps, lab-on-chip and fluidic devices, micro- and nanophotonics structures.

The pattern edge sharpness is set by the beam divergence, aperture blade straightness, and secondary and scattered particles from the aperture edges. Ray tracing simulations were performed to investigate the beam spatial resolution on the sample as defined by the proximity aperture taking into account the beam divergence.

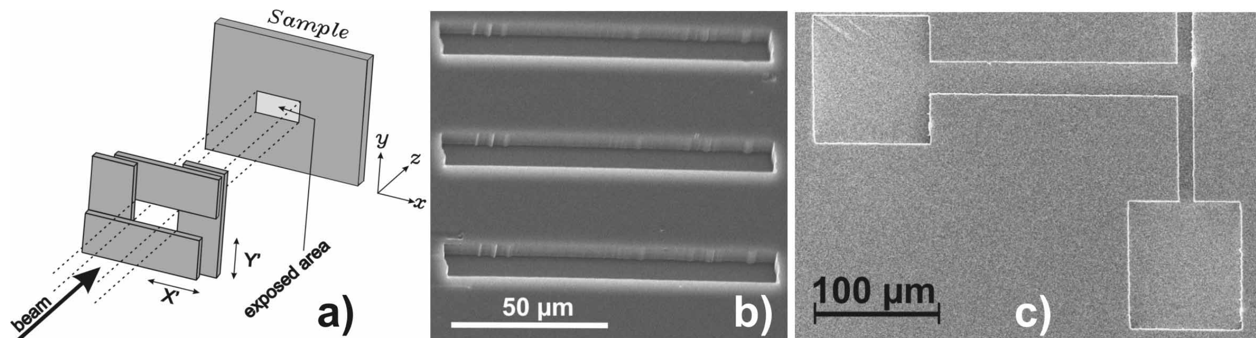

Figure 1. PPAL system. a) Two L-shaped aperture blades (each blade is made up of two 100 μm thick Ta sheets glued together). By combining the X' and Y' movement of the blades with x and y movement of the target entire rectangular pattern element of various sizes can be written in one step. b) and c) Examples of patterns written with PPAL system in 7.5 μm thick PMMA using 56 MeV ^{14}N beam.

SIMULATION OF THE EXPERIMENTAL SET-UP

The GEANT4 toolkit [9] was used to test the concept of the PPAL system. GEANT4 is an object-oriented Monte Carlo simulation tool written in C++ that provides comprehensive detector and physics modeling capabilities. Promising results of simulations at micrometer scale [10,11] made GEANT4 a natural choice to investigate the PPAL system resolution performance. In GEANT4 users can define their own materials and system geometry. We have defined four 100 μm thick Ta sheets combined together in space to form the defining aperture. The primary Ta circular aperture (2 mm thick and 1 mm diameter) was placed 1.76 m upstream from the defining aperture. Collisions with the residual gasses in the beam line were neglected in order to investigate a pure slit-edge scattering. The PPAL system was investigated using the latest release of GEANT4 (version 4.8.2) and its low energy extension (G4LOWEM3.0). Ion processes, such as multiple scattering and ionization, were simulated using standard EM physics provided by GEANT4 [12]. The general particle source (GPS) was used to produce proton beams with the desired energy, angular and spatial distributions. To provide reliable multiple scattering of the protons in the primary aperture and in the defining aperture's blades the maximal simulation step was set to 50 nm. The value of the secondary particle cut has been set to 100 μm in the primary

Ta aperture and in the four Ta sheets for 2 MeV protons. The values for the cut-value and the maximal simulation step have been optimized from a comparison between GEANT4 and SRIM 2006 [4] beam straggling simulations. In this calibration 2 MeV protons entering perpendicularly to the target surface passed through Ta foils of different thicknesses, and the positions of exiting protons were measured. Having position distributions of the transmitted protons it is possible to calculate quantities characterizing scatterings in the material, such as lateral projected range, lateral straggling, radial range and radial straggling. In this study, we used definitions of these quantities proposed by SRIM 2006 [4]. The GEANT4 and SRIM 2006 predictions show a reasonable agreement over the range of 1-15 μm of Ta foil thicknesses (Fig. 2). This suggests we can be confident in the predictions obtained in our calculations.

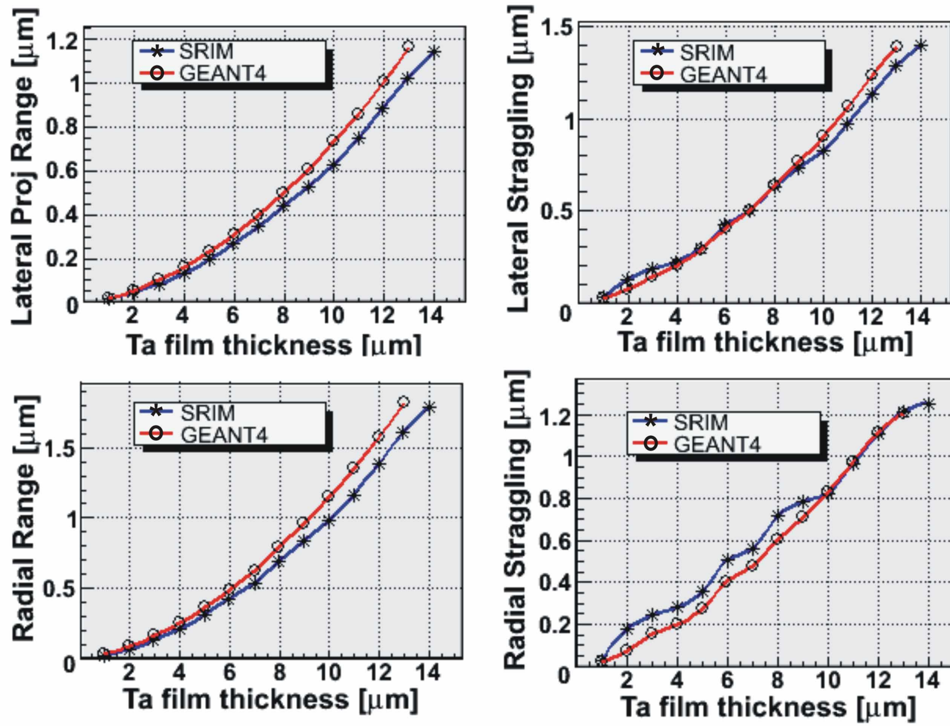

Figure 2. Comparison of 2 MeV proton beam straggling in Ta simulated by SRIM 2006 and GEANT4.

RESULTS AND DISCUSSION

To investigate the beam spot spatial resolution we modeled the target as a sensitive detector (sample) that could be placed at different distances behind the defining aperture. The detector recorded each proton's hit position coordinates (*x,y*) and its energy. This information could then be stored in files and processed by numerical analysis software, such as Matlab or ROOT [13]. In initial simulations we found out that the protons, that undergo scattering at the edges of the first aperture, have a negligible probability to transverse through the defining aperture. In these simulations the diverging (1 mrad) beam with a 600 μm radius was incident on the first collimator 1 mm in diameter. Fig. 3(a) shows the spatial distribution of protons transmitted through the first collimator and recorded 1 m downstream (0.76 m before the defining aperture). For 600 μm radius proton beam centered on 500 μm radius collimator with 3.4×10^6 incident protons we obtain 2.36×10^6 transmitted, giving 69.4% transmission efficiency

in the simulation, which is the proton beam spot to collimator opening surface ratio ($\pi\cdot500^2/\pi\cdot600^2$). Among the transmitted protons 0.29% or 6865 protons have been scattered by the collimator edges. Because the detector had a form of a 500×500 mm^2 square we estimate that the number of the scattered protons could be larger, since those hits further than 250 mm from the aperture center were not recorded.

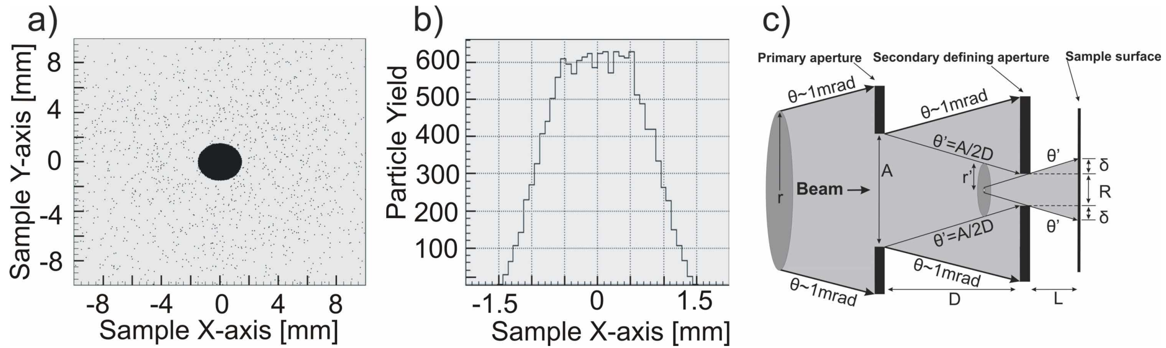

Figure 3. Transmission of 2 MeV protons through the first Ta aperture of 1 mm diameter and 2 mm thickness. a) Lateral distribution of the proton hits measured 1 m downstream b) 10 μm thick stripe cut from the previous distribution and presented in the histogram form, particle yield not normalized, c) Schematic presentation of the PPAL system made up of two apertures (not to scale). A proton beam with divergence θ=1 mrad is incident on the first aperture. Only that fraction of the beam having divergence set by the geometry of the system $\theta'=A/2D$, where A=1 mm is the diameter of the first aperture and D=1.76 m is the distance between the primary and secondary apertures, will be able to pass through the second aperture. R, which is the opening of the second aperture, is of the order of a few μm's and can be neglected.

It can be seen that the beam is well-confined at the target position (Fig. 3(a-b)), while scattering events are rare. The only fraction of the beam that is able to pass through the second aperture has a smaller divergence defined by the geometrical dimensions of the system. Therefore, we can approximate the system by neglecting the primary aperture, moving the proton source closer to the second aperture and making it smaller, and setting the maximal divergence to $\theta'=A/2D$=0.28 mrad instead of θ=1 mrad (see Fig. 3(c)). Such approximation allowed speeding up considerably (factor of 10) of the Monte Carlo calculations by allowing a smaller number of protons to be used. In our simulations we used a proton source of r'=50 μm radius with 0.28 mrad divergence placed 176 mm upstream the second aperture. Typically, 7.86×10^6 protons were simulated for aperture openings 1×10 μm^2 and 10×10 μm^2, while 26.5×10^6 protons for 0.1×10 μm^2 opening to ensure good statistics. The spatial distributions of the proton hits were measured at 0.5 mm, 1 mm, 2 mm and 5 mm distances behind the fourth Ta blade. For 7.86×10^6 incident protons, on average 9.5×10^4 and 9.5×10^3 are transmitted, and 2.6×10^4 and 1.8×10^3 are scattered through 10×10 μm^2 and 1×10 μm^2 apertures, respectively. For 26.5×10^6 incident protons, on average 3×10^3 are transmitted and 6×10^4 are scattered through 0.1×10 μm^2 aperture. Fig. 4(a) shows a typical spatial distribution of protons transmitted and scattered through the second aperture. The transmitted protons create rectangles well-confined within the intended locations (Fig. 4(b)). The scattered protons create a large "halo" spreading to several tens of mm. The protons are scattered mainly to the upper left corner of the sample (due to the geometry of the Ta blades). The scattered protons are separated by a few μm's and sometimes even by a few mm. The results

indicate that the slit-edge scattering will not degrade the pattern edge sharpness. The pattern dimensions will therefore be mainly set by the beam divergence and the Ta blades sharpness.

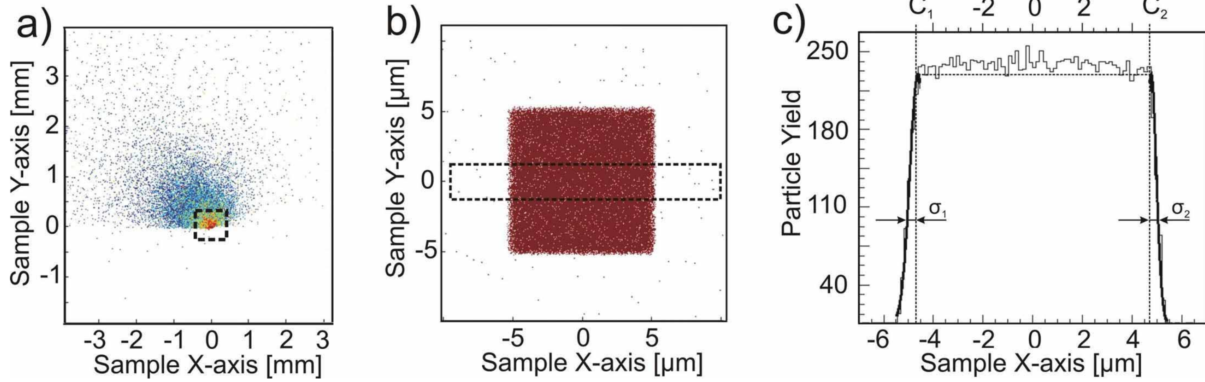

Figure 4. a) Spatial distribution and energy of the protons passing through 10×10 μm^2 second aperture measured 1 mm behind the fourth Ta blade. b) Distribution of the transmitted particles. c) Histogram built from 2 μm thickness stripe cut from the transmitted proton data, particle yield not normalized. FWHM of the beam spot can be found from Gaussian fits to the histogram tails, $FWHM=(C_2+1.7741\cdot\sigma_2)-(C_1-1.7741\cdot\sigma_1)$.

Stripes of 2 μm thickness from the hits distributions were "cut" and plotted in histogram form. The FWHM's of the beam spots were found from the Gaussian fits to the histograms' tails (e.g. see Fig. 4(c)). Fig. 5(a-c) show FWHM of the beam spots "shadowed" by the 10×10 μm^2, 1×10 μm^2, and 0.1×10 μm^2 aperture openings plotted against the distance between the sample and the fourth Ta blade. Linear functions were fitted to the results.

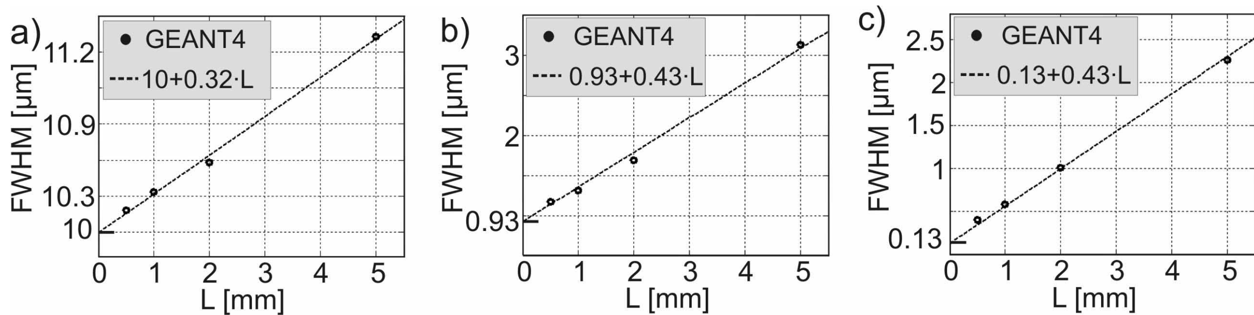

Figure 5. FWHM of beam spots measured at different sample-aperture separation *L* for a) 10×10 μm^2, b) 1×10 μm^2 and c) 0.1×10 μm^2 aperture openings.

From the linearity of the spot dimensions it follows that the beam divergence is responsible for the spot broadening, whereas contribution from the edge-scattering is negligible. Note, however, that because we used maximal allowed beam divergence, the calculated beam-spot spreading on targets presents an upper limit. Realistic beam spot spreading is anticipated to be smaller since accelerator beams are significantly paraxial.

CONCLUSIONS

Ray-tracing simulations using GEANT4 toolkit were performed to calculate the PPAL system's resolution performance. The calculations indicate that the slit edge-scattering will not

degrade the pattern edge sharpness. The beam spot spreading is mainly associated with the beam divergence. Since maximal possible beam divergence, set by the geometry of the system, was used in this paper, the calculated beam spreading represents an upper limit. The resolution performance of the PPAL system is expected to be better due to a significant paraxial component of typical accelerator beams.

ACKNOWLEDGMENTS

SG is grateful for travel support from Vilho, Yrjö ja Kalle Väisälän rahasto foundation. The work was carried out under the auspices of the Academy of Finland Centre of Excellence in nuclear and accelerator-based physics (Ref 213503).

REFERENCES

1. F. Watt, A.A. Bettiol, J.A. van Kan, E.J. Teo, M.B.H. Breese, International Journal of Nanoscience **4**, 269 (2005).
2. J.A. van Kan, A.A. Bettiol, F. Watt, Nano Letters **6**, 579 (2006).
3. J.A. van Kan, P.G. Shao, K. Ansari, A.A. Bettiol, F. Watt, Microsystem Technologies **13**, 431 (2006).
4. J.F. Ziegler, SRIM-2006, from http://www.SRIM.org
5. J.V. Erps et. al., IEEE Photonics Technologiy Letters **18**, 1165 (2006).
6. M.L. Taylor, A. Alves, P. Reichart, R.D. Franich, S. Rubanov, P. Johnston, D.N. Jamieson, Nucl. Instr. and Meth. B (2007), doi:10.1016/j.nimb.2007.02.057.
7. S. Gorelick, T. Ylimäki, T. Sajavaara, M. Laitinen, A. Sagari A.R., H.J. Whitlow, Nucl. Instr. and Meth. B (2007), doi:10.1016/j.nimb.2007.01.260.
8. S. Gorelick, P. Rahkila, A. Sagari A.R., T. Sajavaara, S. Cheng, L.B. Karlsson, J.A. van Kan, H.J. Whitlow, Nucl. Instr. and Meth. B (2007), doi:10.1016/j.nimb.2007.02.008.
9. S. Agostinelli et. al., Nucl. Instr. and Meth. A 506, **250** (2003); from http://geant4.web.cern.ch/geant4/
10. S. Incerti, C. Habchi, Ph. Moretto, J. Olivier, H. Seznec, Nucl. Instr. and Meth B **249**, 738 (2006).
11. S. Incerti, Ph. Barbaret, B. Courtois, C. Michelet-Habchi, Ph. Moretto, Nucl. Instr. and Meth. B **210**, 92 (2003).
12. GEANT4 Physics Reference Manual, available at http://geant4.web.cern.ch/geant4/UserDocumentation/UsersGuides/PhysicsReferenceManual/html/index.html
13. ROOT – an object-oriented data analysis framework, from http://root.cern.ch

Paper III

This article was published in THAI JOURNAL OF PHYSICS, SERIES 5,
Nitipon Puttaraksa, Michael W. Rhodes, Teerasak Kamwanna, Udomrat Tippawan, Chome Thongleurm, Witoon Ginamoon, Harry J. Whitlow, and Somsorn Singkarat
IN-SITU ION BEAM FLUENCE MONITORING SYSTEM FOR MeV ION BEAM LITHOGRAPHY AT CMU,
Copyright THAI PHYSICS SOCIETY (2010).

Reproduced with the permission of the publisher.

THAI JOURNAL OF PHYSICS, SERIES 5, 163 (2010)

IN-SITU ION BEAM FLUENCE MONITORING SYSTEM FOR MeV ION BEAM LITHOGRAPHY AT CMU

N. Puttaraksa[1,2*], M. W. Rhodes[3], T. Kamwanna[4], U. Tippawan[1,4], C. Thongleurm[3], W. Ginamoon[1], H. J. Whitlow[2], and S. Singkarat[1,4]

[1] *Plasma and Beam Physics Research Facility (PBP), Department of Physics, Faculty of Science, Chiang Mai University, Chiang Mai 50200, Thailand* [2] *Department of Physics, P.O. Box 35 (YFL), University of Jyväskylä FIN-40014, Finland* [3] *Science and Technology Research Institute, Chiang Mai University, Chiang Mai 50200, Thailand* [4] *Research Center in Particle Beam and Plasma Physics (PBPP), Thailand Center of Excellence in Physics, P.O. Box 70, Chiang Mai University, Chiang Mai 50202, Thailand*

Abstract

An in-situ ion beam fluence monitoring system has been attached to the 1.7 MV Tandetron accelerator beamline of the Plasma and Beam Physics Research Facility (PBP) at Chiang Mai University. The system facilitates a high precision determination of ion fluence on the samples in the MeV ion beam lithography equipment. In our system, a computerized dual-vane rotator is installed in front of the sample holder to periodically examine the beam intensity by correlating it with the yield of backscattered ions from the gold coated vanes. The gold peak is measured and evaluated in the same fashion as for a standard RBS experiment. The 83.3% of ions that are not intercepted by the vane are used for the lithographic exposure of the polymer samples. The beam size of the order of a millimeter, is precisely shaped to a micrometer rectangular shape by a pair of computerized L-shaped apertures. The sample holder has a built-in Faraday cup, directly connected to synchronous pulsed current integrator, which is used to calibrate the monitoring system. Here, we present the development of the system and some preliminary results.

1. INTRODUCTION

In the past decade, a new type of lithography, namely MeV ion beam lithography (MeV-IBL), has been emerged as a tool for patterning 3D micro- and nano-structures in resist polymers, such as poly- (methylmethacrylate) (PMMA) and SU-8 [1-3]. One of the most crucial parameters in MeV-IBL is determination with high accuracy the ion fluence which is equivalent to the number of incident ions per unit area on the sample.

There are several approaches to measurement of the ion fluence [4,5]. We choose to develop an in-situ ion beam fluence monitoring system that is able to take into account unpredictable beam fluctuations. The approach we used is based on Rutherford Backscattering Spectrometry (RBS) using a precision gold-coated dual vane rotator which has been described in detail elsewhere [6] in conjunction with synchronous current measurement. The development of the system for the MeV-IBL and some preliminary results will be discussed in this paper.

2. PRINCIPLE AND EXPERIMENTAL

2.1. Set-up for the MeV-IBL

A schematic diagram of the in-situ ion beam fluence monitoring system, attached to the 1.7 MV Tandetron accelerator of the Plasma and Beam Physics Research Facility (PBP) at Chiang Mai University, is illustrated in Fig. 1. A 3 MeV $^4He^{2+}$ beam was used for this study because these ions were successfully used in MeV ion beam lithography [1,7]. An aluminium dual vane rotator, of 30° for each vane in 5 cm length with total mass of 3.82 gm, was coated with a 180 nm gold film by using a thermal evaporator. The vane is rotated, by a unipolar stepper motor, with a constant angular speed of 6.15 rad/s implying the ion beam is intercepted by the dual vane at a frequency equal to $2f$, where f is the frequency of the dual vane.

A Silicon Surface Barrier (SSB) detector is located at 78.5 mm and 150° from the beam line with a solid angle (Ω) of 8.11 msr for collecting the backscattered ions every time the rotating dual vane intercepts the beam. In this set-up, each vane is hit approximately at 4 cm from the rotation axis. The geometry corresponds to 83.3% unblocked ions. Subsequently the millimetre-sized beam is collimated to a micrometer rectangular shape by a pair of computer-controlled L-shaped aperture blades. Each of the L-shaped blades is mounted on a MM-3M-F-1 Motorized MicroMini™ stage with 0.49609 μm/count resolution and 25.4 mm travel range [8], so one blade can be positioned in the X' direction and the other in Y' direction (see Fig. 1).

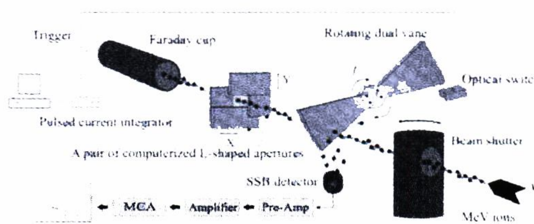

FIGURE 1. Schematic diagram of the in-situ ion beam fluence monitoring system for the calibration state. For lithographic exposures, the sample will be moved in place of the Faraday cup opening. Here f is 0.98 Hz.

* Corresponding author. E-mail: nipon@fnrf.science .cmu.ac.th

© 2010 Thai Physics Society

The shaped ion beam of micron size and rectangular is used to either expose the sample or it is stopped in the Faraday cup to allow calibration of the number of backscattered counts in terms of ion fluence.

For this set-up, any measuring period of time Δt can be divided into two parts as:

$$\Delta t = \Delta t_{block} + \Delta t_{pass} \quad (1)$$

where Δt_{block} is the duration of time where the ion beam hits the rotating dual vane, and Δt_{pass} is the duration of time when the ion beam passes through the rotating dual vane and hits the L-shaped apertures (see Fig. 1). For a period of time $\Delta t > 1/f$, the number of turns of the rotating dual vane (N_{vane}) is given by:

$$N_{vane} = f(\Delta t) \quad (2)$$

Accordingly, the number of ions (n_{vane}) that hit the dual vane is defined as:

$$n_{vane} = A_{beam}\rho v_{ion}\Delta t_{block} \quad (3)$$

where A_{beam}, ρ and v_{ion} are the cross-sectional area, ion density and ion velocity of the incident ion beam, respectively. The number of the ions ($n_{aperture}$) that is transmitted through the rotating dual vane to the precision aperture system can be expressed in a similar fashion as:

$$n_{aperture} = A_{beam}\rho v_{ion}\Delta t_{pass}\,. \quad (4)$$

For the RBS technique, which is a well established technique for ion beam analysis of thin films, the number of backscattered ions detected by the SSB detector (Y_g) is determined by [9]:

$$Y_g = n_{vane}G \quad (5)$$

where $G = (Nt)\Omega\sigma_r(E,\theta)$, in which Nt is the number of atoms per unit volume × thickness of the gold film, Ω is the small solid angle subtended by the SSB detector, and σ_r is the average differential scattering cross section of the incident ion beam.

Consequently, the correlation between $n_{aperture}$ and Y_g can be found as:

$$n_{aperture} = \left[\frac{N_{vane}}{f(\Delta t_{block})} - 1\right]\frac{Y_g}{G}\,. \quad (6)$$

For a model approximation, we assume that the ion beam profile is a cylindrically symmetric Gaussian distribution as shown in Fig.2. We represent the ion beam profile density $D(x,y)$ by [10]:

$$D(x,y) = \frac{K}{2\pi\sigma^2}e^{-\frac{x^2+y^2}{2\sigma^2}} \quad (7)$$

where K is the normalization factor and σ is the standard deviation of the Gaussian distribution.

The normalization factor is calculated from the expression:

$$n_{aperture} = \int_{-\infty}^{\infty}\int_{-\infty}^{\infty}\frac{K}{2\pi\sigma^2}e^{-\frac{x^2+y^2}{2\sigma^2}}dxdy\,. \quad (8)$$

This gives $K = \frac{n_{aperture}}{\left(1-e^{-R^2/2\sigma^2}\right)}$, where R is the radius of the beam. Thus, the number of ions after passing through the opening aperture area and impinge on the sample, n_{sample}, becomes:

$$n_{sample} = \left[\int_{y_1}^{y_2}\int_{x_1}^{x_2}\frac{e^{-\frac{x^2+y^2}{2\sigma^2}}}{2\pi\sigma^2\left(1-e^{-R^2/2\sigma^2}\right)}dxdy\right]n_{aperture}\,. \quad (9)$$

By substitution Eq. (6) into Eq. (9), we find the correlation between n_{sample} and Y_g as:

$$n_{sample} = \left[\frac{N_{vane}}{f(\Delta t_{block})} - 1\right]\frac{Y_g}{2\pi\sigma^2 G}\int_{y_1}^{y_2}\int_{x_1}^{x_2}\frac{e^{-\frac{x^2+y^2}{2\sigma^2}}}{\left(1-e^{-R^2/2\sigma^2}\right)}dxdy\,. \quad (10)$$

Finally, we get:

$$Y_g = \gamma\,\Phi \quad (11)$$

where

$$\gamma = \frac{2\pi\sigma^2 Gf(\Delta t_{block})\left(1-e^{-R^2/2\sigma^2}\right)A_{aperture}}{[N_{vane} - f(\Delta t_{block})]\int_{y_1}^{y_2}\int_{x_1}^{x_2}e^{-\frac{x^2+y^2}{2\sigma^2}}dxdy}\,,$$

which gives

$$\gamma = \frac{4Gf(\Delta t_{block})\left(1-e^{-R^2/2\sigma^2}\right)A_{aperture}}{\left[N_{vane} - f(\Delta t_{block})\right]F_1(x_1,x_2)F_2(y_1,y_2)} \quad (12)$$

where, $F_1(x_1,x_2) = erf\left(\frac{x_2}{\sigma\sqrt{2}}\right) - erf\left(\frac{x_1}{\sigma\sqrt{2}}\right)$ and

$F_2(y_1,y_2) = erf\left(\frac{y_2}{\sigma\sqrt{2}}\right) - erf\left(\frac{y_1}{\sigma\sqrt{2}}\right)$,

and $erf(x)$ is the error function of x, and

$$\Phi = n_{sample}/A_{aperture} \quad (13)$$

is the ion fluence on the sample during the duration Δt_{pass} and $A_{aperture}$ is the opening area of the rectangular aperture which is always smaller than the A_{beam}. Notice that γ (Eq. 12) depends on $A_{aperture}$ through x_1, x_2, y_1, y_2 (Fig. 2).

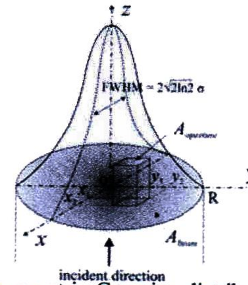

FIGURE 2. A symmetric Gaussian distribution of the ion beam profile at the aperture plane which is the x-y plane in this schematic. Here we represent a general case where the aperture opening is displaced from the centre of the ion beam.

2.2 Pulsed current integrator

To find a calibration curve according to Eq. (11), a cylindrical copper Faraday cup with 8 mm inner diameter and 65 mm depth is used to measure the Φ. It is directly connected to the purpose-built synchronous pulsed current integrator for measuring the number of ions after transmitting through the L-shaped apertures.

Conventional DC current integrators can not accurately determine the charge and fluence of a pulsed (chopped) beam. As such, a different technique is employed for this project to handle that situation. This is done by the

purpose-built pulsed current integrator. The system can be broken down into three primary elements, a low offset current transimpedance amplifier to directly convert the current to a voltage, a sample and hold analog to digital converter (ADC) and a PIC microcontroller to handle the data conversion and communication to a personal computer (PC).

A transimpedance amplifier is configured for a voltage to current conversion ratio of one millivolt per nanoamp and an offset bias current of a few femtoamps. The amplifier is followed by a buffer amplifier configured with a gain of 10 times giving an overall voltage to current ratio of 10 millivolts per one nanoamp. A serial mode 12 bit ADC with built in sample and hold is interfaced to a PIC microcontroller. The sample and hold timing is approximately two microseconds and the ADC conversion 14 microseconds allowing more than sufficient time to capture the beam current before being blocked again. The moving vane has an optical switch which generates a pulse to the PIC generating an interrupt at which time the microcontroller takes a snapshot of the beam current and converts it to 12 bits of digital and transfers it to the PC via an RS 232 serial port. The microcontroller software is written in PICBasic Pro version 2.5 and Melabs assembly language.

The PC control and communication software is written in Microsoft Visual Basic 6.0 with an additional commercial chart recorder control library. To simplify the calculation of current to charge, the PC reads the sampled current at precisely defined regular intervals giving the charge as the sum of the currents over the total measurement time period. Because the dual vane interrupts the beam, a correction factor of 0.833 or (83.3%) is applied to the current to obtain the true charge and fluence exposure of the sample.

3. RESULTS AND DISCUSSION

Fig. 3 reveals the number of backscattered ions within the gold peak, Y_g (counts), and the fluence, Φ (10^{12} ions/cm^2), of 3 MeV $^4He^{2+}$ ions with different opening aperture areas ($A_{aperture}$) defined by the pair of L-shaped aperture. It has been illustrated that the relation between Y_g and Φ of each $A_{aperture}$ is linear as shown in Eq. (11), the slope (γ) of each lines is depicted in Table 1. Correlation between the corresponding slope, γ, and the $A_{aperture}$ is illustrated in Fig. 4. It corresponds to the quadratic polynomial fitting curve as:

$$\gamma = 0.0362 A_{aperture}^2 - 4.5577 A_{aperture} + 188.0556 . \quad (14)$$

The reason for using the quadratic polynomial fitting curve is still under investigation and it is probably originates from the spatial distribution of the incident ion beam profile discussed above.

Consequently, Φ (in units of 10^{12} ion/cm^2) may therefore be expressed in term of Y_g as:

$$\Phi = \frac{Y_g}{(0.0362 A_{aperture}^2 - 4.5577 A_{aperture} + 188.0556)} . \quad (15)$$

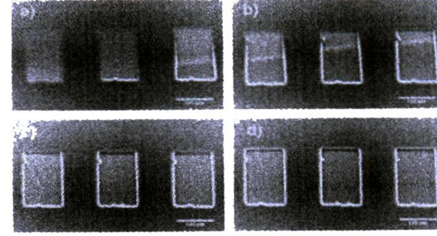

FIGURE 3. The number of counts (Y_g) from the gold peak of the RBS spectra vs Fluence (Φ) (10^{12} ions/cm^2) of 3 MeV $^4He^{2+}$ beam with various aperture areas ($A_{aperture}$)

TABLE 1: The slope (γ) of each lines in Fig. 2 with corresponding to the aperture area $A_{aperture}$.

Slope (γ)	$A_{aperture}$ (10^4 μm^2)
70.511	36.00
61.392	42.25
50.228	49.00
46.970	56.25
44.568	64.00

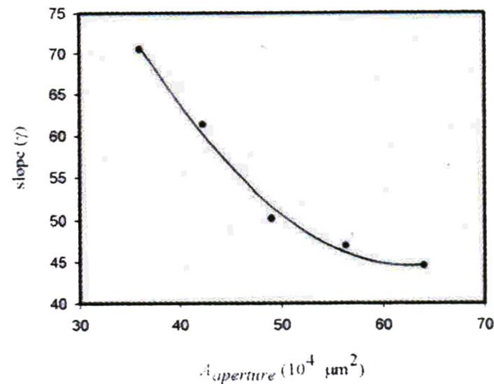

FIGURE 4. The number of counts (Y_g) from the gold peak of the RBS spectra vs Fluence (Φ) (10^{12} ions/cm^2) of 3 MeV $^4He^{2+}$ beam with various aperture areas ($A_{aperture}$).

The slope (γ) vs $A_{aperture}$ (10^4 μm^2). The smooth line represents Eq. (14) with 1.4743 standard error

Fig. 5(a)-(d) are SEM images of patterns fabricated by 3 MeV $^4He^{2+}$ ions in 6 μm of PMMA film after developed in an isopropanol + deionised water 7:3 mixture. Details of this fabricating technique can be found elsewhere [1]. By using the calibration in Eq. (15), we estimate that the patterns in Fig. 5(a), from the left to the right, are irradiated to the fluences of 0.71×10^{12}, 1.10×10^{12} and 1.41×10^{12} ions/cm^2, respectively. In Fig. 5(b), they are irradiated with 1.74×10^{12}, 2.15×10^{12} and 2.42×10^{12} ions/cm^2, from the left to the right, respectively, and also 2.78×10^{12}, 3.07×10^{12} and 3.23×10^{12} ions/cm^2 in Fig. 5(c). Finally, 5.20×10^{12}, 6.97×10^{12} and 8.60×10^{12} ions/cm^2, from the left to the right of Fig. 5(d), respectively, are the fluences irradiated in PMMA. It is clearly seen that the full exposure starts from the ion beam fluence of 3.07×10^{12} ions/cm^2 and extend to 8.6×10^{12} ions/cm^2 with out any sign of cross-linking [7].

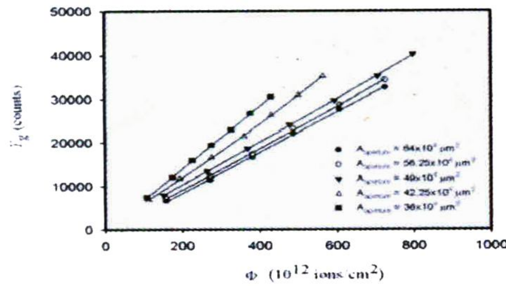

FIGURE 5. SEM micrographs of rectangular patterns of 100×150 μm^2 area fabricated in 6 μm thickness of PMMA film with various fluences of the 3 MeV $^4He^{++}$ ions: (a) 0.71, 1.10, and 1.41 ($\times 10^{12}$ ions/cm^2), (b) 1.74, 2.15, and 2.42 ($\times 10^{12}$ ion/cm^2), (c) 2.78, 3.07, and 3.23 ($\times 10^{12}$ ion/cm^2), (d) 5.20, 6.97, and 8.60 ($\times 10^{12}$ ion/cm^2), from left to right, respectively.

ACKNOWLEDGEMENTS

This work has been supported by the CoE Programme of Chiang Mai University and the Academy of Finland (Centre of Excellence in Nuclear and Accelerator Based Physics, Ref. 213503). N.P. is also gratefully acknowledges the financial support from the Royal Golden Jubilee Scholarship of the Thailand Research Fund. It is a pleasure to thank R. Pinchaiphat for his assistance on setting up the dual vane rotator.

REFERENCES

[1] N. Puttaraksa et. al. J. Vac. Sci. Tech. B 26 (2008) 1732.
[2] F. Watt et. al. Mater. Today 20 (2007) 30.
[3] F. Munnik et. al. Microelectron. Eng. 67-68 (2003) 96.
[4] F. Paszti et. al. Nucl. Instrum. Methods Phys. Res. B 47 (1990) 187-192.
[5] L. M. Redondo et. al. Nucl. Instrum. Methods Phys. Res. B 265 (2007) 576-580.
[6] T. Kamwanna et. al. Thai J. Phys., SERIES 4 (2009), in press.
[7] S. Gorelick, et. al. Nucl. Instrum. Methods. Phys. Res. B 266 (2008) 2461.
[8] Motorized MicroMini^{TM} stage, http:// www.nationalaperture.com.
[9] W.K.Chu, J.W. Mayer and M.A. Nicolet, Backscattering Spectrometry, (Academic Press, New York, 1978).
[10] F. Yongqi, et. al. J. Mater. Process. Technol. 104 (2000) 44-47.

Paper IV

This article was published in Nuclear Instrument and Methods, Section B,
doi:10.1016/j.nimb.2011.01.056,
Nitipon Puttaraksa, Rattanaporn Norarat, Mikko Laitinen, Timo Sajavaara,
Somsorn Singkarat, Harry J. Whitlow,
*Lithography exposure characteristics of poly(methyl methacrylate)
(PMMA) for carbon, helium and hydrogen ions*,
Copyright Elsevier (2011).

Reproduced with the permission of the publisher.

Nuclear Instruments and Methods in Physics Research B xxx (2011) xxx–xxx

Contents lists available at ScienceDirect

Nuclear Instruments and Methods in Physics Research B

journal homepage: www.elsevier.com/locate/nimb

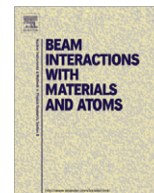

Lithography exposure characteristics of poly(methyl methacrylate) (PMMA) for carbon, helium and hydrogen ions

Nitipon Puttaraksa [a,b], Rattanaporn Norarat [a,*], Mikko Laitinen [a], Timo Sajavaara [a], Somsorn Singkarat [b,c], Harry J. Whitlow [a]

[a] Department of Physics, University of Jyväskylä, P.O. Box 35 (YFL), FIN-40014 Jyväskylä, Finland
[b] Plasma and Beam Physics Research Facility, Department of Physics and Materials Science, Faculty of Science, Chiang Mai University, Chiang Mai 50200, Thailand
[c] Thailand Center of Excellence in Physics, CHE, 328 Si Ayutthaya Road, Bangkok 10400, Thailand

A R T I C L E I N F O

Article history:
Available online xxxx

Keywords:
MeV ion beam lithography
PMMA
PPAL
Proton beam writing

A B S T R A C T

Poly(methyl methacrylate) is a common polymer used as a lithographic resist for all forms of particle (photon, ion and electron) beam writing. Faithful lithographic reproduction requires that the exposure dose, Θ, lies in the window $\Theta_0 \leqslant \Theta < \Theta_{\times_0}$, where Θ_0 and $\Theta_{\times_0}$ represent the clearing and cross-linking onset doses, respectively. In this work we have used the programmable proximity aperture ion beam lithography systems in Chiang Mai and Jyväskylä to determine the exposure characteristics in terms of fluence for 2 MeV protons, 3 MeV $^4He^{2+}$ and 6 MeV $^{12}C^{3+}$ ions, respectively. After exposure the samples were developed in 7:3 by volume propan-2-ol:de-ionised water mixture.

At low fluences, where the fluence is below the clearing fluence, the exposed regions were characterised by rough regions, particularly for He with holes around the ion tracks. As the fluence (dose) increases so that the dose exceeds the clearing dose, the PMMA is uniformly removed with sharp vertical walls. When Θ exceeds the cross-linking onset fluence, the bottom of the exposed regions show undissolved PMMA.

© 2011 Elsevier B.V. All rights reserved.

1. Introduction

MeV ion beam lithography methods such as proton beam writing (PBW) [1] and programable proximity aperture lithography (PPAL) are gaining interest as a powerful tool for direct-writing high aspect ratio structures. The direct-writing capability makes these techniques particularly well-suited for prototyping and master stamps for mass fabrication because no expensive mask is needed. This is driven by applications such as rapid prototyping of waveguides, optotronic metamaterials [2], bioscience applications [3] and microfluidics [4,5]. Poly(methyl methacrylate) (PMMA) is a widely used positive resist in MeV ion beam lithography. This resist is commonly used for electron beam lithography and is commercially available in a range of compositions for deposition by spinning and spray coating. The ions expose the resist by creating a cascade of low-energy electrons [6–9] around the ion track that induce main-chain scission in the PMMA [10]. This reduces the mean molecular weight of the polymer in the exposed regions rendering it more susceptible to dissolution by a suitable solvent (developer). After development, the exposed regions are dissolved away while the unexposed regions remain, creating a 3D structure with sharp vertical sidewalls. For very high doses, pendant side-chains are also removed in the PMMA, creating short chains with broken bonds that cross-link to form a 3D network that resists dissolution by solvent and creates a negative resist [10].

Patterns can be written by either intensity modulating a focused ion beam that is rastered over the resist-coated substrate or by writing complex patterns made up of a number of simple pattern elements, (circles, rectangles etc.). The former is widely used to write irregular structures, e.g. logos, while the latter is faster and generally used for microfluidics and optics patterns. Stitching by overlapping different pattern elements is used when writing complex pattern to avoid gaps associated with electrical and mechanical tolerances. The dose in the overlapped regions can be two, (or more) times that for the non-overlapped irradiated regions. An important question is then the choice of the optimal ion fluence for exposure of the pattern so that the pattern is fully exposed without over-exposure in the stitched regions. Generally, literature reports only give the fluence used for pattern writing without indication of how this relates to the clearing and cross-linking fluences.

In this work we have investigated the exposure characteristics of PMMA for different ion beams to determine the fluence (Θ), needed to completely remove the resist (clearing fluence, Θ_0) and the onset of cross-linking (cross-linking fluence, $\Theta_{\times_0}$).

* Corresponding author.
E-mail address: rattanaporn.norarat@phys.jyu.fi (R. Norarat).

0168-583X/$ - see front matter © 2011 Elsevier B.V. All rights reserved.
doi:10.1016/j.nimb.2011.01.056

Please cite this article in press as: N. Puttaraksa et al., Lithography exposure characteristics of poly(methyl methacrylate) (PMMA) for carbon, helium and hydrogen ions, Nucl. Instr. and Meth. B (2011), doi:10.1016/j.nimb.2011.01.056

2. Method

The samples for irradiation were prepared by spinning at 2500 rpm followed by a soft-bake at 160 °C of 950 kDa PMMA (A11 from MicroChem [11]) onto silicon substrates. This was repeated two or three times to give PMMA films of 6 μm or 9 μm thickness. Initial cleaning of the Si by a HF dip, O_2 plasma exposure and cleaning in acetone and propan-2-ol were tested. It was found that the best adhesion after ion exposure, development of unsupported walls of ~3 μm thickness and lowest level of particulate defects were obtained by using the HF dip and this was therefore used subsequently.

The ion exposures were carried out using the PPAL systems at the 1.7 MV Tandetron accelerator in Chiang Mai [12,13] and 1.7 MeV Pelletron in Jyväskylä [14,15]. The ion fluences were determined by integrating the current from the proximity apertures [13]. These currents were calibrated against the straight-through current measured in a Faraday cup without the sample in place. A correction factor to account for aperture size was applied. SNICS ion sources were used to obtain proton and ^{12}C ion beams while an Alphatross source was used for He ions.

After exposure the samples were developed in a freshly prepared 7:3 by volume mixture of propan-2-ol and de-ionised water at 25 °C for 5 min [16,17]. This developer was adopted because it is capable of nanometre resolution, poses no severe hazards and has a low viscosity allowing it to penetrate easily in narrow channels. Subsequently, the samples were rinsed in two changes of de-ionized water and allowed to dry under filtered air. The removal of the resist was characterized by optical and scanning electron microscopy (SEM).

3. Results and discussion

Fig. 1 shows a sequence of square shaped pattern elements that been exposed to different fluences with 2 MeV protons. The corresponding fluences are specified in Table 1. It is clearly seen from Fig. 1 and Table 1, that for fluences less than 2.6×10^{13} ions cm^{-2} the patterns are not fully exposed. While cross linking starts at $\sim 3.5 \times 10^{14}$ ions cm^{-2}. Fig. 2 presents the pattern file and the associated image for 6 MeV $^{12}C^{3+}$ ions in a 6 μm PMMA/Si sample. In this case a PMMA thickness of 6 μm was used to ensure the ion range (Table 2) exceeded the film thickness to minimise the effects of end of range spreading. This is an example of correct exposure where the pattern elements are stitched. The PMMA is completely removed down to the underlying Si in both the large (single expo-

Table 1
The ion fluence parameters for rectangular pattern elements exposed with 2 MeV protons.

Pattern no.	Fluence (ions cm^{-2})	Pattern no.	Fluence (ions cm^{-2})
A1	4.3×10^{12}	C1	2.0×10^{14}
A2	9.6×10^{12}	C2	2.2×10^{14}
A3	1.4×10^{13}	C3	2.4×10^{14}
A4	1.8×10^{13}	C4	2.7×10^{14}
A5	2.2×10^{13}	C5	3.0×10^{14}
A6	2.6×10^{13}	C6	3.2×10^{14}
B1	4.0×10^{13}	D1	3.5×10^{14}
B2	5.4×10^{13}	D2	3.8×10^{14}
B3	7.9×10^{13}	D3	4.2×10^{14}
B4	1.1×10^{14}	D4	5.2×10^{14}
B5	1.3×10^{14}	D5	6.2×10^{14}
B6	1.6×10^{14}	D6	7.8×10^{14}

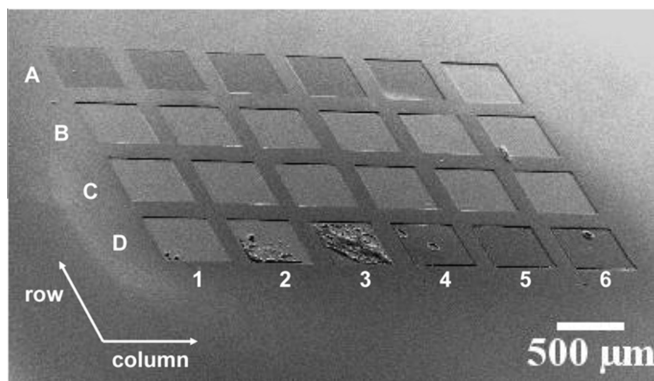

Fig. 1. SEM image of pattern elements on a PMMA/Si sample after development (see text.) that has been exposed with sequentially larger proton fluences. The fluences increased in small steps along each column and larger steps along each row from 4.3×10^{12} to 7.8×10^{14} ions cm^{-2}.

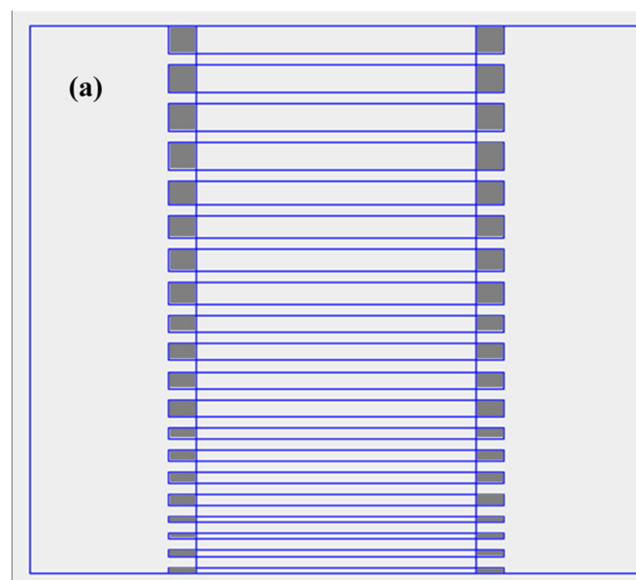

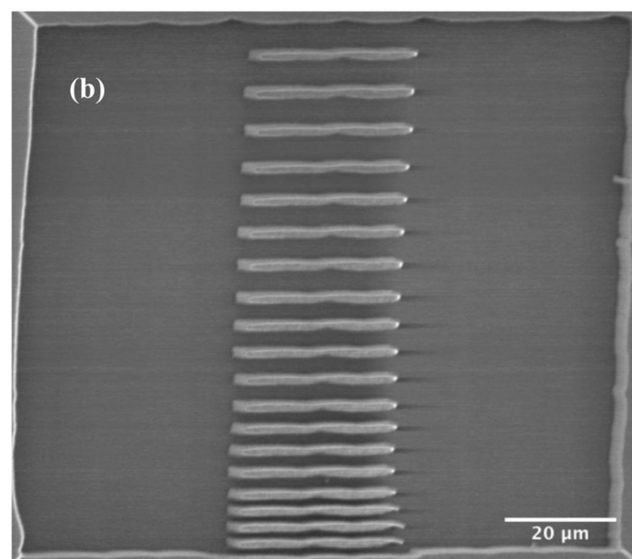

Fig. 2. (a) Exposure pattern made up of two large vertical rectangle exposed regions and 20 horizontal rectangular exposed rectangles. The "stitching" where the horizontal and vertical exposed regions overlap are shown in grey. (b) Corresponding SEM image of a 6 μm PMMA/Si sample after exposure with 2×10^{12} ions cm^{-2} of 6 MeV $^{12}C^{3+}$ ions.

Please cite this article in press as: N. Puttaraksa et al., Lithography exposure characteristics of poly(methyl methacrylate) (PMMA) for carbon, helium and hydrogen ions, Nucl. Instr. and Meth. B (2011), doi:10.1016/j.nimb.2011.01.056

Table 2
Clearing (Θ_0), onset of cross-linking ($\Theta_{\times_0}$) and fully cross-linking ($\Theta_{\times_\infty}$) fluences in PMMA.

Ion	Range (μm)	Θ_0 (ions cm^{-2})	$\Theta_{\times_0}$ (ions cm^{-2})	$\Theta_{\times_\infty}$ (ions cm^{-2})
2 MeV $^1H^+$	80.4	3.3×10^{13}	3.5×10^{14}	7.0×10^{14}
3 MeV $^4He^{2+}$	18.8	2.4×10^{13}	5.4×10^{13}	1.5×10^{14}
6 MeV $^{12}C^{3+}$	9.44	1.8×10^{12}	3.4×10^{12}	8.1×10^{12}

sure) regions and the stitched regions at the ends of the open channels (See Fig. 2(a)).

In these experiments we varied the fluence of the ions directed perpendicular to the surface. We can define a clearing fluence, Θ_0 that is the fluence required to completely remove the resist down to the resist/substrate interface. The condition for this is that the dose averaged over both depth and the many neighboring ion tracks, is able to deposit sufficient energy to create enough chain scissions to allow the polymer to be dissolved during development. Likewise, we can define a cross-linking fluence, $\Theta_{\times_0}$ which represents the onset of cross-linking. In order to write a positive tone pattern with straight vertical sidewalls that delineates regions where the resist has been completely removed the fluence must satisfy the conditions :

$$\Theta_0 \leqslant \Theta, \quad (1)$$

$$n\Theta < \Theta_{\times_0}, \quad (2)$$

where, n is the number of pattern elements that are overlapped by stitching. Similarly for negative tone, we have

$$\Theta_{\times_\infty} < n\Theta \quad (3)$$

Table 2 presents the measured fluences for clearance and cross-linking. Comparison of the ion stopping forces [18] (15.2, 121 and 816 eV/nm for protons, He and C ions, respectively) showed that as the stopping force increase, Θ_0, $\Theta_{\times_0}$ and $\Theta_{\times_\infty}$ decreased. The corresponding mean distance between ions at Θ_0 of 1.7, 2.0 and 7.4 nm for H, He and C ions respectively gives an effective ion track radius of $\sqrt{2}$ times these values. The effective track radius is an important parameter because in conjunction with the stoichiometrics of ion impingement [7], it determines the ultimate writing resolution [6] and edge roughness that can be achieved. The ratio, $\Theta_{\times_0}/\Theta_0$ gives a measure of the exposure tolerance analogous to the latitude of a photographic film. The values are $\sim$10 for protons and somewhat smaller $\sim$2 for He and C. This limits the number of areas, n that can be superposed by stitching about ten in PBW and two for He and C.

For fluences $\Theta \leqslant \Theta_0$, close inspection of the SEM images revealed that the PMMA was incompletely removed with a surface that has a roughness on a scale of tens of nanometres [4,19]. Close inspection also revealed that for $\Theta \gtrsim \Theta_0$ the edges of the irradiated areas were also rough with the features of individual ion tracks. Even for $\Theta < \Theta_0$, individual ion tracks could be discerned for $^4He^{2+}$ ions outside of the irradiated area that are presumably associated with edge scattering for the PPAL defining aperture [20–22]. The voltage build-up on the PMMA surface is unlikely to be the origin. This is because the energies of the ions are vastly greater than the product of the breakdown voltage of the PMMA film and ion charge.

4. Conclusions

The clearing and cross-linking threshold fluences for 2 MeV protons, 3 MeV $^4He^{2+}$ and 6 MeV $^{12}C^{3+}$ ions in PMMA resist have been investigated. The results show the threshold for both clearing and the onset of cross-linking decreases with increasing electronic stopping force. The exposure latitude is somewhat greater for protons than for heavy ions. At fluences less than the clearing dose the PMMA is incompletely removed, leaving a surface that is rough on a nanometre scale which reflects the spatial dose non-uniformity associated with individual ion impingement.

Acknowledgements

This work was supported the Academy of Finland, The OSKE organisation, Centre of Excellence in Nuclear and Accelerator Based Physics, ref. 213503 and grant 129999. RN was supported by a CIMO Fellowship. HJW is grateful for travel support from the Magnus Erhnrooth Foundation, which made this work possible.

References

[1] J.A. van Kan, A.A. Bettiol, Proton beam writing: a new 3D nanolithographic technique, in: R. Hellborg, H.J. Whitlow, Y. Zhang (Eds.), Ion Beams in Nanoscience and Technology, Springer, Heidelberg, 2010, p. 297.
[2] A.A. Bettiol, Proton beam writing of optical structures, in: R. Hellborg, H.J. Whitlow, Y. Zhang (Eds.), Ion Beams in Nanoscience and Technology, Springer, Heidelberg, 2010, p. 311.
[3] J.A. van Kan, A.A. Bettiol, Tissue engineering and bioscience methods using proton beam writing, in: R. Hellborg, H.J. Whitlow, Y. Zhang (Eds.), Ion Beams in Nanoscience and Technology, Springer, Heidelberg, 2010, p. 297.
[4] S. Gorelick, N. Puttaraksa, T. Sajavaara, H.J. Whitlow, Nucl. Instrum. Methods B 266 (2008) 2461.
[5] H.J. Whitlow, L.P. Wang, L. Gilbert, Adv. Mater. Res. 74 (2009) 129.
[6] H.J. Whitlow, M.L. Ng, V. Auzelyte, I. Maximov, L. Montelius, J.A. van Kan, A.A. Bettiol, F. Watt, Nanotechnology 15 (2004) 223.
[7] C.N.B. Udalagama, A.A. Bettiol, F. Watt, Nucl. Instrum. Methods B 260 (2007) 384.
[8] R. Spohr, in: K. Bethge (Ed.), Ion Tracks and Microtechnology: Principles and Applications, Vieweg, Braun chweig, 1990, pp. 112–116.
[9] Y. Zhang, H.J. Whitlow, Modification of materials by MeV ion beams, in: R. Hellborg (Ed.), Electrostatic Accelerators, Springer, Berlin Heidelberg New York, 2005, p. 506.
[10] A. Chapiro, Nucl. Instrum. Methods B 32 (1988) 111.
[11] NANO^{TM} PMMA and Copolymer, Microchem, 1254 Chestnut St. Newton, MA 02464, USA, 2001.
[12] H.J. Whitlow, S. Sangyuenyongpipat, L.P. Wang, S. Gorelick, T. Sajavaara, V. Marjomäki, L. Gilbert, N. Puttaraksa, S. Singkarat, Thai Phys. J. 5 (2010) XV.
[13] N. Puttaraksa, S. Unai, M.W. Rhodes, K. Singkarat, H.J. Whitlow, S. Singkarat, Nucl. Instrum. Methods B, doi:10.1016/j.nimb.2011.01.053.
[14] S. Gorelick, T. Ylimäki, T. Sajavaara, M. Laitinen, A. Sagari A.R., H.J. Whitlow, Nucl. Instrum. Methods B 260 (2007) 77.
[15] N. Puttaraksa, S. Gorelick, T. Sajavaara, M. Laitinen, S. Singkarat, H.J. Whitlow, J. Vac. Sci. Tech. B 26 (2008) 1732.
[16] Shazia Yasin, D.G. Hasko, H. Ahmed, Appl. Phys. Lett. 78 (2001) 2760.
[17] J.-S. Wi, H.-S. Lee, K.-B. Kim, Electr. Mater. Lett. 3 (2007) 1.
[18] J.F. Ziegler SRIM-2010.01, from <www.SRIM.org>.
[19] M. Skupinski, J. Jensen, A. Johansson, G. Possnert, M. Boman, K. Hjort, A. Razpet, J. Vac. Sci. Technol. B 25 (2007) 862.
[20] S. Gorelick, T. Sajavaara, H.J. Whitlow, Nucl. Instrum. Methods B 267 (2009) 2050.
[21] S. Gorelick, T. Sajavaara, H.J. Whitlow, J. Vac. Sci. Tech. B 27 (2009) 1102.
[22] S. Gorelick, T. Sajavaara, H.J. Whitlow, J. Vac. Sci. Tech. B 27 (2009) 1109.

Paper V

This article was published in THAI JOURNAL OF PHYSICS,
SERIES 4,
Nitipon Puttaraksa, Sergey Gorelick, Timo Sajavaara, Somsorn Singkarat,
Harry J. Whitlow
3D Micro-channel fabrication in PMMA based on MeV ion beam lithography,
Copyright THAI PHYSICS SOCIETY (2009).

Reproduced with the permission of the publisher.

THAI JOURNAL OF PHYSICS, SERIES 4, 89 (2009)

3D Micro-channel fabrication in PMMA based on MeV ion beam lithography

N. Puttaraksa[1,2,*], S. Gorelick[1], T. Sajavaara[1], S. Singkarat[2,3], H. J. Whitlow[1]

[1]*Sel Department of Physics, PO Box 35 (YFL), FIN-40014 University of Jyväskylä, Finland*
[2]*Plasma and Beam Physics Research Facility, Department of Physics, Faculty of Science, Chiang Mai University, Chiang Mai, 50200, Thailand*
[3]*Thailand Center of Excellent in Physics, P.O. Box 70 Chiang Mai University, Chiang Mai, 50200, Thailand*

A novel system for 3D micro-channel fabrication based on a MeV ion beam programmable proximity aperture lithography (PPAL) technique has been developed at the Accelerator Laboratory of the University of Jyväskylä (JYFL), Finland. In this technique, instead of focusing the ion beam by using lenses, the size and shape of the beam spot is defined by a computerized aperture in close proximity to the sample. By combining different aperture openings, with sample movement, in a plane perpendicular to the ion beam, entire rectangular or square elements with sizes 0-500 μm can be exposed in one exposure. The system has the capability for a rapid production of complex patterns made of large reservoirs connected by 3D micro-channels. A prototype lithographic structure was fabricated in a 7.5 μm thick polymethylmethacrylate (PMMA) resist using 3 MeV $^4He^{2+}$ ion beam from 1.7 MV Pelletron accelerator.

1. INTRODUCTION

In recent years, there is an increasing demand for high-aspect-ratio 3D micro-and nano-structures in many areas of application e.g. micro- and nanofluidics, photonics and nanoimprinting. MeV ion beam lithography is an alternative technique to deep lithography using synchrotron light that can be used to fabricate 3D micro- and nano-patterns in thick polymer resists (up to 100 μm) such as polymethylmethacrylate (PMMA) [1,2] and SU-8 [3]. Proton beam writing (PBW), which is the most predominant form of MeV ion beam lithography, is a direct writing technique that uses a focused MeV protons which is scanned across the resist material. This technique is capable of writing patterns of lines with 22 nm half-pitch [4].

An alternative approach which requires a much lower investment than the complex system of focusing and scanning MeV ion beams, is a programmable proximity aperture lithography (PPAL) system. This is a novel technique for MeV ion beam lithography that has been developed at the Accelerator Laboratory of the University of Jyväskylä, Finland. In this technique, MeV ion beams from a 1.7 MV Pelletron accelerator are collimated by a rectangular aperture made of a pair of computer controlled L-shaped Ta blades. A sample which is mounted on a computer controlled X-Y-Z stage, is placed in closed proximity behind the aperture (see Fig.1). An entire rectangular pattern element up to 500×500 μm can be written over a 20×20 mm field on the sample. This technique has a considerably faster speed than the conventional focused beams methods (e.g. PBW and electron beam lithography (EBL)) because the entire rectangular pattern element is being exposed at the same time [1,5]. In this article, some results will be presented and discussed.

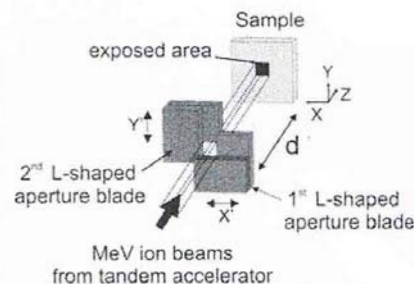

FIGURE 1. The programmable proximity aperture lithography (PPAL) configuration utilizing remotely adjustable aperture for control of the beam size and shape. In this method, d is small in the order of 1.5 mm.

2. PRINCIPLE

The advantage of using MeV ions for lithography is that their trajectories have a well-projected range depending on their trajectories have a well-projected range depending on the incident energy and the target material. For example, 3 MeV He ions have projected range of about 20 μm in PMMA, with a ~70 nm lateral broadening at the depth of 7.5 μm (see Fig. 2(a)). This information was obtained from SRIM simulations [6]. For this reason, it is possible to use MeV ion beam lithography to fabricate structures with straight and high wall channels in thick polymer resists. On the contrary, the trajectories for 40 keV electrons, as shown in Fig. 2(b) which were simulated by CASINO code [7], exhibit considerable spreading except close to the surface because of multiple scattering.

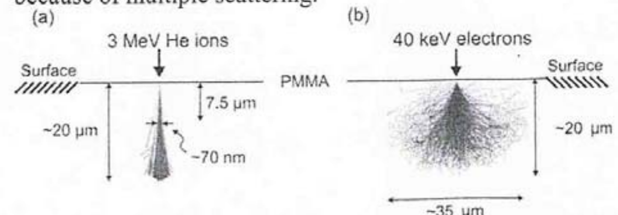

FIGURE 2. The simulated trajectories of (a) 3 MeV He ions and (b) 40 keV electrons in thick PMMA [6,7].

*Corresponding author. Tel.: + 668 3879 8485; fax: + 66 5322 2776
E-mail: nitipon@fnrf.science.cmu.ac.th

© 2009 Thai Physics Society

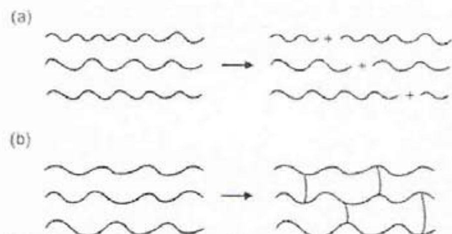

FIGURE 3. Schematic of two main effects inside a polymer induced by energetic ion beam which are (a) random chain scission and (b) cross-linking [8].

For this reason, electron beam lithography most suited for writing pattern in thin (10-200 nm) polymer resists. When high energetic ions penetrate a polymeric medium, the energy of the incident ions are transferred to polymeric chains by momentum transfer to the nucleus of the target atoms (i.e. nuclear stopping), and by exciting the electrons of the target, termed electronic stopping, until coming to rest if the medium is thick enough. Typically, the energetic ions cause scission and cross-linking of the polymeric chains. Atomic displacement by nuclear collisions can cause a random main chain scission. The resulting effect of chain scissions is to decrease the molecular weight of the polymeric materials (shown schematically in Fig. 3(a)). Another process is that the electronic energy deposition of the ion can create some free radicals that may recombine causing cross-linking, which results in molecular weight increase, as shown in Fig. 3(b).

Conventionally, it is considered that both nuclear and electronic stopping can induce the scission and cross-linking but there is a report [9] which suggests that nuclear stopping causes more scission while electronic stopping causes more cross-linking.

Figure 4 illustrates the basic principle of lithography in polymer resists by irradiating with MeV ions. Generally, polymer resists are divided into two types (i.e. positive and negative resists). Polymer resists in which chain scission predominates is called positive resist e.g. PMMA. In positive resist, the exposed area is preferentially soluble in the developer as its molecular weight is decreased. On the contrary, the exposed area with the energetic ions of negative resist, e.g. SU-8, in which cross-linking predominates, is less soluble in the developer. Consequently, in this case the solvent preferentially dissolves the unexposed area.

3. EXPERIMENT

The In this experiment, an adjustable rectangular beam spot is defined by a pair of L-shaped Ta aperture blades. The first blade is made from two pieces of 8×13 mm that are 100 μm thick. The second L-shaped Ta aperture blade is made from two 9×13 mm pieces. The edge of each Ta piece was sequentially polished with 600, 800, 1500 and 2000 grade SiC paper and finished with diamond paste of 6 μm and 0.5 μm grain size. Between each polishing step the aperture blades were carefully cleaned as described below. The roughness of the edge was characterized by a profilometer; the result showed that it was better than 100 nm [5]. After final polishing, the surface of Ta sheets were cleaned in acetone for 10 minutes and then rinsed in ethanol and de-ionized water for 2 minutes, respectively, in an ultrasonic bath. Finally, each pair was glued together using a vacuum-compatible two-component epoxy adhesive. The edges were arranged perpendicular using a 90° angle reference under an optical microscope.

PMMA A11 solution with molecular weight of 950 kDa was spin-coated onto a clean Si substrate at 2500 rpm for 45 s duration. After spinning, the excess solvent was removed by a soft-bake at 160 °C for 5 minutes. The process was repeated 3 times to obtain a 7.5 μm thick PMMA resist film.

For irradiation, 3 MeV $^{4}He^{2+}$ ion beam from the Pelletron accelerator was firstly defined by setting the aperture opening to 1×1 mm. The beam current after this slit was measured by a secondary electron supressed Faraday cup of about 3 cm^2 opening area behind the sample holder. For a beam intensity equivalent to a 1 nA beam current passing through the 1×1 mm aperture, the exposure time was 10-20 s per pattern element. The corresponding ion fluence of 6.25×10^{12} ions/cm^2 is required to completely expose a pattern element in PMMA. After exposure, the sample was developed in a 7 : 3 solution of isopropanol + de-ionized water mixture for 4 minutes and rinsed in de-ionized water.

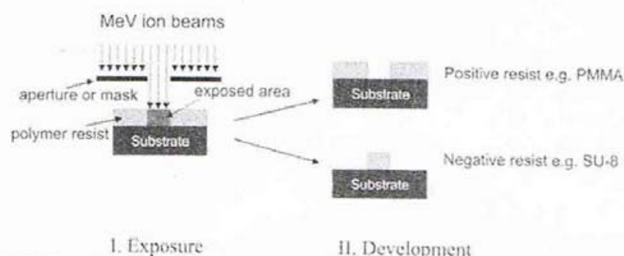

FIGURE 4. Schematic illustration of basic principle of MeV ion beam lithography.

4. RESULTS AND DISCUSSIONS

In our PPAL technique, the quality of the L-shaped Ta aperture blades defines the quality of the patterns produced. Fig. 5 illustrates a Scanning Electron Microscope (SEM) image of one of L-shaped Ta aperture blades. An unwanted piece of debris seems to be firmly attached to the edge of a Ta sheet (see Fig. 5) and from the experimental evidence it can be seen that it stops the ion beam in the same way as the mask edge.

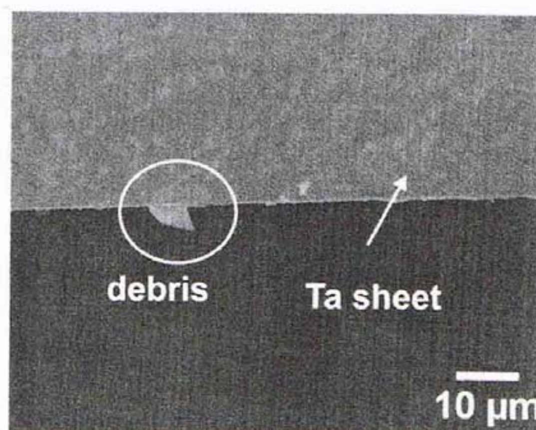

FIGURE 5. SEM image of part of the L-shaped Ta aperture blade that has a debris.

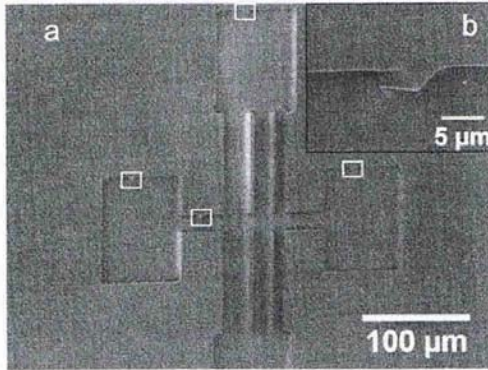

FIGURE 6. (a) SEM image of test pattern produced by using 3 MeV 4He2+ ions in 7.5 µm thick PMMA. (b) Higher resolution image of an edge protrusion in one of the white rectangles. These features were systematically created by the piece of debris shown in Fig.5.

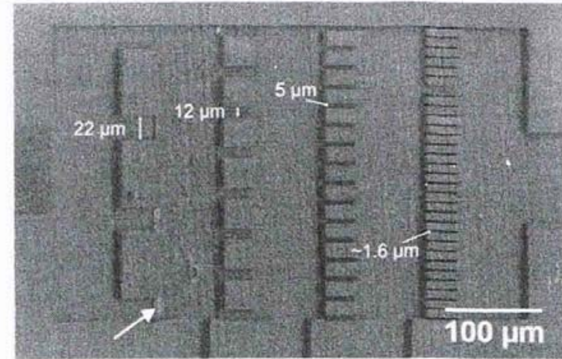

FIGURE 7. SEM micrograph of a prototype 3D micro-channel pattern fabricated by using 3 MeV $^4He^{2+}$ ions in 7.5 µm thick PMMA.

Figure 6 (a) depicts a SEM micrograph of a test pattern fabricated using 3 MeV $^4He^{2+}$ ions in 7.5 µm thick PMMA. The pattern consists of four reservoirs (75×100 µm) by which two of them are connected through 15 µm flow channel while others are connected through ~22, ~14 and ~8 µm wide channels. Fig. 6 (b) illustrates a magnified edge deflect region for one of the position marked with white squares in Fig. 6 (a). The defect was associated with the debris on the aperture blade shown in Fig. 5. It is clearly seen that the shape of the debris is faithfully reproduced in the pattern after development by the solvent. The origin of the debris is under investigation.

Figure 7 illustrates the capacity of our technique. From several size channels (i.e. 22, 12, 5 and ~1.6 µm) we have been realized that it can be developed for use as sorting devices for cellular and sub-cellular studies [2]. This figure also shows, as pointed by an arrow, the existence of undeveloped resist due to an over exposure. More discussion of this effect can be found elsewhere [2]. We found that the smallest pattern feature that produced by our technique was a 7.5 µm high PMMA wall of only 700 nm thick. The aspect ratio between height and width of this pattern element is approximately 10 [1].

5. CONCLUSIONS

MeV ion beam programmable proximity aperture lithography (PPAL) technique has been developed at the Accelerator Laboratory of the University of Jyväskylä, Finland. This technique has the capability to fabricate 3D micro-structures in thick polymethylmethacrylate (PMMA). In this work we have shown that quality of the pattern features is sensitive to the quality of the L-shaped aperture blade. The special capabilities of the method make it particularly useful for producing microfluidics circuits and devices for fundamental cellular or sub-cellular biomedical research.

ACKNOWLEDGMENTS

This work has been supported by the Academy of Finland Centre of Excellence in Nuclear and Accelerator-based Physics (Ref.213503) and the BOGOTAS consortium. NP is very grateful for the financial support from the Royal Golden Jubilee (RGJ) Scholarship of the Thailand Research Fund (TRF).

1. N. Puttaraksa, S. Gorelick, T. Sajavaara, M. Laitinen, S. Singkarat, and H.J. Whitlow, J. Vac. Sci. and Technol. B 26(5), Sep/Oct 2008 1732-1739.
2. S. Gorelick, N. Puttaraksa, T. Sajavaara, S. Singkarat, H.J. Whitlow, Nucl. Instr. and Meth. B 266 (2008) 2461.
3. C.N.B. Udalagama, A.A. Bettiol, J.A. van Kan, F. Watt, Nucl. Instr. and Meth. B 210 (2003) 256-259.
4. F. Watt, M.B.H. Breese, A.A. Bettiol, and J.A. van Kan, Proton beam writing, Materials Today 30 (2007) 20.
5. S. Gorelick, T. Ylimäki, T. Sajavaara, M. Laitinen, A. Sagari A. R., H.J. Whitlow, Nucl. Instr. and Meth. B 206 (2007) 77.
6. J.F. Ziegler, SRIM-2006, http://www.SRIM.org.
7. P. Hovington, D. Drouin, R. Gauvin, D. C. Joy and N. Evans, Scanning19, 29 (1997), http://www.gel.usherb.ca/casino/index.html.
8. I. Adesida, Nucl. Instr. and Meth. B 209/210 (1983) 79-86.
9. E.H. Lee, G.R. Rao, M.B. Lewis, and L.K. Mansur, J. Mater. Res. 9 (1994) 1043.

Paper VI

This article was published in Nuclear Instrument and Methods, Section B, volume 266,
Sergey Gorelick, Nitipon Puttaraksa, Timo Sajavaara, Mikko Laitinen, Somsorn Singkarat, Harry J. Whitlow,
Fabrication of microfluidic devices using MeV ion beam Programmable Proximity Aperture Lithography (PPAL),
pp. 2461-2465
Copyright Elsevier (2008).

Reproduced with the permission of the publisher.

Available online at www.sciencedirect.com
ScienceDirect
Nuclear Instruments and Methods in Physics Research B 266 (2008) 2461–2465
NIM B Beam Interactions with Materials & Atoms
www.elsevier.com/locate/nimb

Fabrication of microfluidic devices using MeV ion beam Programmable Proximity Aperture Lithography (PPAL)

S. Gorelick [a,*], N. Puttaraksa [a,b], T. Sajavaara [a], M. Laitinen [a], S. Singkarat [b], H.J. Whitlow [a]

[a] Department of Physics, University of Jyväskylä, P.O. Box 35 (FL), FIN 40014 Jyväskylä, Finland
[b] Fast Neutron Research Facility, Department of Physics, Chiang Mai University, Chiang Mai 50200, Thailand

Available online 7 March 2008

Abstract

MeV ion beam lithography is a direct writing technique capable of producing microfluidic patterns and lab-on-chip devices with straight walls in thick resist films. In this technique a small beam spot of MeV ions is scanned over the resist surface to generate a latent image of the pattern. The microstructures in resist polymer can be then revealed using a chemical developer that removes exposed resist, while leaving unexposed resist unaffected. In our system the size of the rectangular beam spot is programmably defined by two L-shaped tantalum blades with well-polished edges. This allows rapid exposure of entire rectangular pattern elements up to 500 × 500 μm in one step. By combining different dimensions of the defining aperture with the sample movements relative to the beam spot, entire fluidic patterns with large reservoirs and narrow flow channels can be written over large areas in short time. Fluidic patterns were written in PMMA using 56 MeV $^{14}N^{3+}$ and a 3 MeV $^{4}He^{2+}$ beams from K130 cyclotron and a 1.7 MV Pelletron accelerators, respectively, at the University of Jyväskylä Accelerator Laboratory. The patterns were characterized using SEM, and the factors affecting patterns quality are discussed.
© 2008 Elsevier B.V. All rights reserved.

PACS: 29.20.Ba; 29.20.dg; 41.85.Si; 87.85.Lf; 87.85.Ox; 61.80.Jh

Keywords: MeV ion beam lithography; Heavy ion beam lithography; Single ion-tracks; Proximity aperture; Microfluidic device; Cell-growth substrate; PMMA

1. Introduction

Microfluidic devices become increasingly relevant in biomedical applications and research. Such devices can be effectively used to manipulate and navigate selected cells to a desired location on a patterned substrate [1], to sort different types of cells [2], to evaluate membrane electrical properties of single cells to determine their viability [3], to detect, sequence and size DNA molecules [4–6], and for other numerous applications [7,8]. For our bone–tissue research at cellular and sub-cellular levels [9] we are interested in rapid production of cell-growth substrates and microfluidic devices in thick polymer films with a large number of pattern elements covering large areas. For this purpose we have constructed a lithography facility for writing patterns with MeV ion beams in polymer resist films, e.g. PMMA [10].

The MeV ion beam writing is a rapidly evolving lithography technique which has proven its capability to produce 3D structures in thick resists with extraordinarily high linewidth to resist-thickness aspect ratio (>100), nanometre feature sizes (∼20 nm), and a high degree of smoothness [12–14].

MeV ion beam writing, such as Proton Beam Writing (PBW) [12–14], is similar to electron beam lithography (EBL). An ion beam (typically protons or alpha particles) from an accelerator is focused into a small beam spot which is magnetically scanned over the resist surface to

* Corresponding author. Tel.: +358 14 260 2399; fax: +358 14 260 2351.
E-mail address: gorliks@jyu.fi (S. Gorelick).

0168-583X/$ - see front matter © 2008 Elsevier B.V. All rights reserved.
doi:10.1016/j.nimb.2008.03.035

generate a latent image of the desired pattern. The advantage of MeV ions, as opposed to electrons, is that MeV ions can penetrate deep into the resist along a straight path and with minimal scattering. In an alternative approach, rather than focusing the MeV ion beam and scanning it across the resist, the target is moved relative to a small beam spot defined by collimators [15,16]. In Programmable Proximity Aperture Lithography (PPAL) used in our system, the size of the rectangular beam spot of MeV ions is programmably defined by two L-shaped tantalum blades (each blade is made of two 100 μm Ta sheets with well-polished edges that are glued together). To control the size of the penumbra the aperture blades are in close proximity to the resist. Precise movement of each L-shaped blade in the X' and Y' directions defines the size of the beam spot (Fig. 1). This allows rapid exposure of entire rectangular pattern elements with sizes up to 500 × 500 μm in one step. By combining different dimensions of the defining aperture with the x and y sample movements relative to the beam spot, entire fluidic patterns with large reservoirs and narrow flow channels can be written on large areas in short time (Fig. 1). In addition, the PPAL approach eliminates the need of time consuming beam focusing and beam optimization routines. As the PPAL approach is purely based on shadowcasting, it can be used with accelerators where beam focusing is not straightforward, e.g. for high rigidity MeV heavy ion beams or with cyclotron beams having large divergence. A more detailed technical description of the PPAL system can be found elsewhere [10,11].

To examine the feasibility of the PPAL approach several test patterns were written in PMMA using 56 MeV $^{14}N^{3+}$ beam from the Jyväskylä cyclotron and a 3 MeV $^{4}He^{2+}$ beam from a Pelletron accelerator.

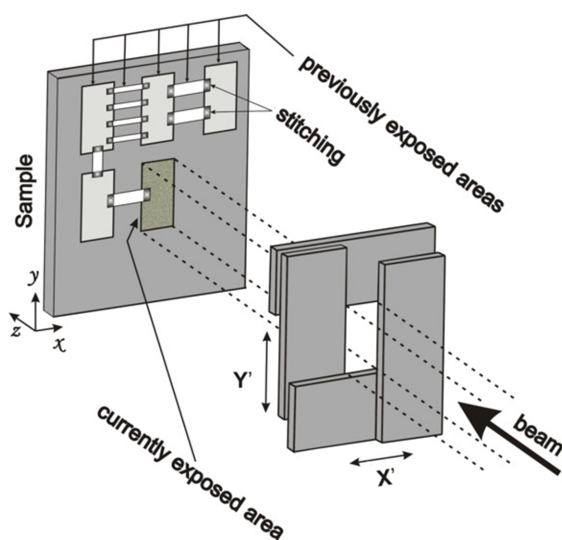

Fig. 1. Schematic illustration of the PPAL system. Two L-shaped aperture blades, each made up of two 100 μm thick Ta sheets glued together, define the beam spot shape and size on the sample. By combining X' and Y' of the blades with the x and y movement of the sample, entire patterns made up of rectangular structures can be rapidly exposed.

2. Experimental procedures

PMMA A11 resist solution was spin-coated on Si substrates at 2500 rpm followed by a soft-bake at 160 °C for 5 min. The procedure was repeated three times to yield a final 7.5 μm resist thickness. The ion beam irradiations were carried out at the Accelerator Laboratory of the Jyväskylä University using the K-130 cyclotron [17] for $^{14}N^{3+}$ and the recently commisioned NEC 1.7 MV Tandem Pelletron accelerator for $^{4}He^{2+}$. Typically 100 nC mm^{-2} of 2 MeV protons are required to expose PMMA [18]. Taking into account that the stopping force of 56 MeV ^{14}N and 3 MeV ^{4}He in PMMA is 30 and 8 times larger than that of 2 MeV protons [19], respectively, we estimated that the required fluence is 3.3 particle-nC mm^{-2} for ^{14}N and 12.5 particle-nC mm^{-2} for ^{4}He. To verify the estimated exposure parameters, a series of lines were written in PMMA with gradually increasing delivered fluences spanning two orders of magnitude. The required exposure fluences appeared to be in good agreement with the previously reported proton fluences [18] taking into account differences in the stopping forces for different ions.

The exposure times were determined by means of a Faraday cup positioned behind the sample holder measuring the current of the beam collimated by 1 × 1 mm^{2} or 0.5 × 0.5 mm^{2} variable aperture openings. To prevent the excessive heating of the computer-controlled aperture by energetic ^{14}N ions, the ~9 W cyclotron beam was first collimated by a water-cooled 1 mm diameter Ta aperture located 1.76 m upstream close to the exit of the switching magnet. With close to 500 nA of $^{14}N^{3+}$ available at the water-cooled aperture, only ~100 pA was transported through a 1 × 1 mm^{2} opening of the computer-controlled aperture. With such current densities, approximately 100 s exposure per rectangular pattern element was required. Between the pattern elements exposure the beam was blanked by a TTL signal that gated the cyclotron injection system.

The heating power of 3 MeV ^{4}He is much reduced compared to 56 MeV ^{14}N, therefore the water-cooled aperture was not used when the He irradiations were performed. As one might expect, removing this aperture also increased the available beam current on target. With approximately 20 nA of $^{4}He^{2+}$ measured by a Faraday cup near the exit from the switching magnet of the Pelletron, ~1–2 nA are transported through the 1 × 1 mm^{2} opening of the computer-controlled aperture. With such current densities, 15–30 s irradiations per pattern element are sufficient to fully expose PMMA. The beam control between the exposures was realized using an electrostatic two-plate beam blanker positioned downstream from the Faraday cup immediately after the switching magnet. The beam blanking was controlled by a TTL signal fed to a high voltage relay connected to a high voltage supply that applies 1–3 kV to the plates to deflect the beam away from the sample. The apertures and samples stage as well as the the beam blanking were controlled by purpose-built LabView™ software.

Normally, a safety-factor of 50% was added to the exposure times in order to compensate for the beam current and position instabilities. During the exposures the samples were positioned at ~1–1.5 mm behind the blade.

After the exposures the samples were developed in IPA:de-ionized water (7:3) solution [20] for 4–6 min followed by rinsing in de-ionized water and dried under helium flow.

3. Results and discussion

Fig. 2 shows a test pattern written using the PPAL system with a 56 MeV nitrogen beam. The pattern is made of three large (100 × 100 μm) reservoirs connected by two flow channels (12 μm and 30 μm wide). This image reveals the limitations of the system. Firstly, the pattern edge quality is clearly sensitive to dust particles adhering to the aperture edges and also the straightness of the aperture blades. In general, the patterns were written with only limited success with nitrogen ions. One problem is that PMMA is sensitive to the nitrogen fluence fluctuations and easily crosslinks in the stitching areas that receive double the fluence (not shown). At low fluences (Fig. 3(a)) the PPAL system can be used to write regions of non-overlapping ion tracks. These could be used as capillary pumps and as filters and permeable membranes in 3D microfluidics circuits. At increasing fluences the ion tracks overlap (Fig. 3(b) and (c)). At still higher fluences, but not so high that the crosslinking occurs, the exposed PMMA is completely removed after development (Fig. 3(b)). It was observed that the pattern-edges were relatively rough (e.g. as compared to He irradiation, below). This may be attributed to the stochastic dose variations close to the edge of the irradiated area as the individual ion tracks have relatively large diameter. The case where the ion tracks overlap is a particularly interesting situation where a "carpet" of fiber-like polymer columns with nanometre dimensions is formed (Fig. 3(c)). These structures have potential application as a substrate for biomimetic studies as they can be coated with signal substances to probe the influence of chemical signalling

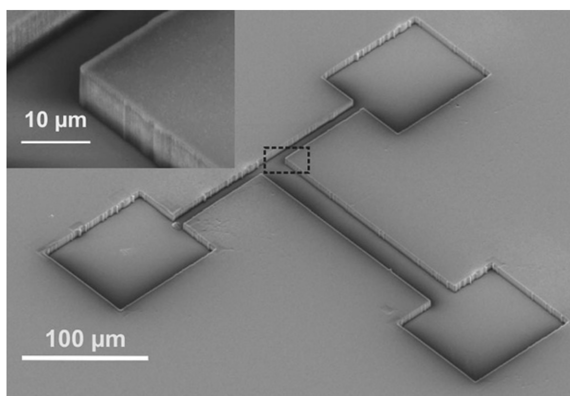

Fig. 2. SEM micrograph of a test pattern produced in a 7.5 μm thick PMMA layer using PPAL system with 56 MeV $^{14}N^{3+}$ beam from the Jyväskylä cyclotron (tilt angle 45°).

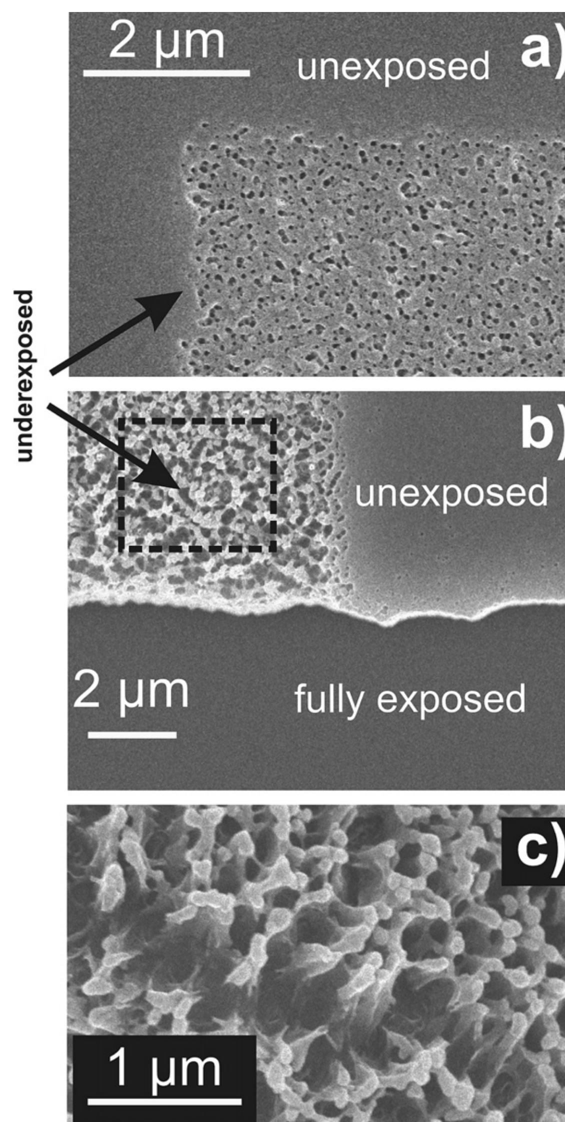

Fig. 3. Illustration of structures formed in PMMA resist by exposure with different fluences of 56 MeV $^{14}N^{3+}$ ions. (a) Lithographically defined region of single ion-tracks, (b) higher fluences giving partial overlap of the ion tracks and a fully exposed region and (c) magnified region of the underexposed region in (b).

combined with nanometre-scale topography on cell proliferation.

Fig. 4 illustrates a prototype pattern written using 3 MeV $^{4}He^{2+}$ beam. The pattern consists of five large (200 × 200 μm) reservoirs (not shown) connected through 30 μm wide flow channels to a sorting device illustrated in Fig. 4(a). The sorting device consists of a series of flow channels with decreasing dimensions. Fig. 4(b) shows magnified image of 22 μm and 12 μm wide channels, while Fig. 4(c) and (d) shows 5 μm and ~1.6 μm wide channels, respectively. These ~1.6 μm wide channels are the smallest feature written systematically so far with the PPAL system. One may expect that ions scattered from the aperture edges degrade the sharpness of the pattern in a stochastic way. Aperture edge roughness on the other hand is not stochastic

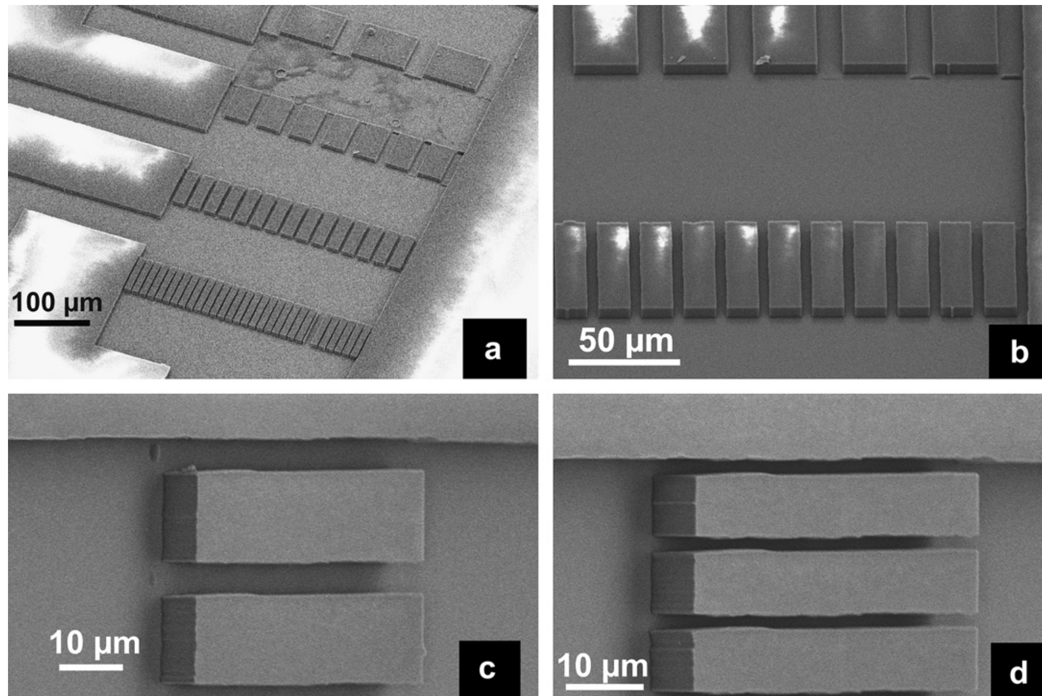

Fig. 4. SEM micrographs of patterns written in 7.5 µm thick PMMA layer using PPAL system with 3 MeV He beam from a Pelletron accelerator, (a) closeup of the sorting device, in the central area of a microfluidic device. The device consists of large 200 × 200 µm reservoirs (not shown) connected via flow channels to the sorting device that has a series of flow channels with decreasing dimensions, (b) magnified image of the 20 µm and 10 µm wide channels, (c) magnified image of the 5 µm wide channels and (d) magnified image of the 1.5 µm wide channels.

but will follow the departures from perfectly straight aperture edges. Close inspection of Fig. 4(c) and (d) show that the detailed shape of the upper and lower edges of the channels is reproduced for each channel. The major contribution to pattern-edge roughness (the smallest channel mean-width $d_{mean} = 1.6$ µm, minimal width $d_{min} = 1.3$ µm, and maximal width $d_{max} = 1.9$ µm) can be associated with aperture edge roughness. This is in agreement with the preliminary theoretical study of the ion-scattering by the aperture edges [21] performed using the GEANT4 toolkit [22]. It is then clear that the pattern quality can be further improved by improved polishing of the Ta blade edges, e.g. using sputtering or cluster-ion bombardment [23]. Positioning accuracy of the linear-motion drives [24] is important for obtaining the correct dimensions of the desired structures. To estimate the positioning accuracy, corresponding channel-edge-to-channel-edge distances were measured for the smallest channels. In this case, the standard deviation of the measured distances distribution (0.14 µm), or the FWHM of the distribution (0.34 µm), are measures of the positioners accuracy. The measured positioning accuracy is then comparable with the edge-to-edge measurement error (~0.3 µm) resulting from an uncertainty in the pattern edge thickness of a few pixels and an uncertainty of the pixel size in the SEM images of the channels.

Sometimes, cross-linked PMMA can be observed in some of the stitching areas, (regions where two rectangular pattern areas are overlapped to prevent unwanted gaps). These can be associated with variations in the beam current and were particularly prominent in the case of the 56 MeV $^{14}N^{3+}$ exposures. This can be corrected by normalising the exposure time for each pattern element according to the beam current (e.g. using a Rutherford backscattering signal, secondary electron signals [25] or ionoluminescence [26]). Likewise, we have observed a tendency for some large pattern elements areas (>200 µm) to be exposed non-uniformly. This could be attributed to beam spot inhomogeneity. A simple correction for this is by de-focussing the beam albeit at the expense of increasing the exposure times.

4. Conclusions

Test microfluidic patterns were fabricated in thick PMMA using a novel approach of MeV ion beam Programmable Proximity Aperture Lithography (PPAL). The patterns exhibit sharp edges, straight and relatively smooth walls thus proving the feasibility of the PPAL approach with MeV ions. The minimal size structure systematically written with the system is 1.5 µm at the moment, which can be further improved. The system can also be used to lithographically define regions of ion tracks having features with nanometre dimensions, which may be useful in biomedical and cellular studies.

Acknowledgements

This work has been carried out under the auspices of the Academy of Finland Centre of Excellence in Nuclear and

Accelerator Based Physics (Ref. 213503) and the BOGOTAS consortium. SG is grateful for travel support from the Graduate School of Particle and Nuclear Physics. Professors Matti Vuento and Frank Watt, as well as Andrew Bettiol and Jeroen van Kan are warmly thanked for helpful discussions and advise.

References

[1] M. Yoshida, K. Tohda, M. Gratzl, Anal. Chem. 75 (2003) 4686.
[2] P.S. Dittrich, P. Schwille, Anal. Chem. 75 (2003) 5767.
[3] Y. Huang, N.S. Sekhlon, J. Borninski, N. Chen, B. Rubinsky, Sensors Actuat. A 105 (2003) 31.
[4] M. Foquet, J. Korlach, W. Zipfel, W.W. Webb, H.G. Craighead, Anal. Chem. 74 (2002) 1415.
[5] H.-P. Chou, C. Spence, A. Scherer, S. Quake, Proc. Natl. Acad. Sci. USA 96 (1999) 11.
[6] A. van Orden, H. Cai, P.M. Goodwin, R.A. Keller, Anal. Chem. 71 (1999) 2108.
[7] T. Vilkner, D. Janasek, A. Manz, Anal. Chem. 76 (2004) 3373.
[8] E. Delamarche, D. Juncker, H. Schmidt, Adv. Mater. 17 (2005) 2911.
[9] S. Gorelick, P. Rahkila, A. Sagari A.R., T. Sajavaara, S. Cheng, L.B. Karlsson, J.A. van Kan, H.J. Whitlow, Nucl. Instr. and Meth. B 260 (2007) 130.
[10] S. Gorelick, T. Ylimäki, T. Sajavaara, M. Laitinen, A. Sagari A.R., H.J. Whitlow, Nucl. Instr. and Meth. B 206 (2007) 77.
[11] N. Puttaraksa, S. Gorelick, T. Sajavaara, M. Laitinen, S. Singkarat, H.J. Whitlow, Programmable proximity aperture lithography with MeV ion, J. Vac. Sci. Technol. B (2008), submitted for publication.
[12] F. Watt, M.B.H. Breese, A.A. Bettiol, J.A. van Kan, Mater. Today 30 (2007) 20.
[13] J.A. van Kan, A.A. Bettiol, F. Watt, Nucl. Instr. and Meth. B 260 (2007) 396.
[14] S.Y. Chiam, J.A. van Kan, T. Osipowicz, C.N.B. Udalagama, F. Watt, Nucl. Instr. and Meth. B 260 (2007) 455.
[15] J. van Erps, B. Volckaerts, H. van Amerongen, P. Vynck, R. Krajewski, C. Debaes, J. Watte, A. Hermanne, H. Thienpont, IEEE Photon. Technol. Lett. 18 (2006) 1164.
[16] M.L. Taylor, A. Alves, P. Reichart, R.D. Franich, S. Rubanov, P. Johnston, D.N. Jamieson, Nucl. Instr. and Meth. B 260 (2007) 426.
[17] E. Liukkonen, et al., in: Proceedings of the 13th International Conference on Cyclotrons and their Applications, Vancouver, 1992, p. 22.
[18] J.A. van Kan, J.L. Sanchez, B. Xu, T. Osipowitz, F. Watt, Nucl. Instr. and Meth. B 158 (1999) 179.
[19] J.F. Ziegler, SRIM–2006. Available from: <http://www.SRIM.org>.
[20] S. Yasin, D.G. Hasko, H. Ahmed, Microelectr. Eng. 61–62 (2002) 745.
[21] S. Gorelick, T. Sajavaara, M. Laitinen, N. Puttaraksa, H.J. Whitlow, Mater. Res. Soc. Symp. Proc. 1020 (2007) 67.
[22] S. Agostinelli et al., Nucl. Instr. and Meth. A 506 (2003) 250. Available from: <http://geant4.web.cern.ch/geant4> .
[23] I. Yamada, Nucl. Instr. and Meth. B 257 (2007) 632.
[24] Newport ESP300 1–3 Axis Motion Controller/Driver, MFA-CCV6 Miniature Linear Stages. <http://www.newport.com>.
[25] A.A. Bettiol, I. Rajta, E.J. Teo, J.A. van Kan, F. Watt, Nucl. Instr. and Meth. B 190 (2002) 154.
[26] C.N.B. Udalagama, A.A. Bettiol, J.A. van Kan, F. Watt, Nucl. Instr. and Meth. B 210 (2003) 256.

Paper VII

This article was published in Nuclear Instrument and Methods, Section B, doi:10.1016/j.nimb.2011.01.053,
Nitipon Puttaraksa, Somrit Unai, Michael W. Rhodes, Kanda Singkarat, Harry J. Whitlow, Somsorn Singkarat,
Fabrication of a negative PMMA master mold for soft-lithography by MeV ion beam lithography,
Copyright Elsevier (2011).

Reproduced with the permission of the publisher.

Nuclear Instruments and Methods in Physics Research B xxx (2011) xxx–xxx

Contents lists available at ScienceDirect

Nuclear Instruments and Methods in Physics Research B

journal homepage: www.elsevier.com/locate/nimb

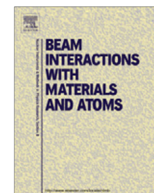

Fabrication of a negative PMMA master mold for soft-lithography by MeV ion beam lithography

Nitipon Puttaraksa [a,b,*], Somrit Unai [a], Michael W. Rhodes [c], Kanda Singkarat [a], Harry J. Whitlow [b], Somsorn Singkarat [a,d]

[a] *Plasma and Beam Physics Research Facility, Department of Physics and Materials Science, Faculty of Science, Chiang Mai University, Chiang Mai 50200, Thailand*
[b] *Department of Physics, P.O. Box 35 (YFL), FIN-40014 University of Jyväskylä, Finland*
[c] *Science and Technology Research Institute, Chiang Mai University, Chiang Mai 50200, Thailand*
[d] *Thailand Center of Excellence in Physics, CHE, 328 Si Ayutthaya Road, Bangkok 10400, Thailand*

A R T I C L E I N F O

Article history:
Available online xxxx

Keywords:
MeV ion beam lithography
PDMS
Soft-lithography

A B S T R A C T

In this study, poly(methyl methacrylate) (PMMA) was investigated as a negative resist by irradiation with a high-fluence 2 MeV proton beam. The beam from a 1.7 MV Tandetron accelerator at the Plasma and Beam Physics Research Facility (PBP) of Chiang Mai University is shaped by a pair of computer-controlled L-shaped apertures which are used to expose rectangular pattern elements with 1–1000 μm side length. Repeated exposure of rectangular pattern elements allows a complex pattern to be built up. After subsequent development, the negative PMMA microstructure was used as a master mold for casting poly(dimethylsiloxane) (PDMS) following a standard soft-lithography process. The PDMS chip fabricated by this technique was demonstrated to be a microfluidic device.

© 2011 Elsevier B.V. All rights reserved.

1. Introduction

Poly(methyl methacrylate), or PMMA, is well-known as a lithographic "positive" resist due to the predominant main-chain scission reactions upon exposure to ionizing radiation [1]. As a resist material, it has many useful features such as high insulation, good resolution, good etch resistance, and acceptable sensitivity and adhesion. Because of this, PMMA is one of the most commonly used polymers as a mask in the semiconductor fabrication process and in LIGA applications [2,3]. However, because of this positive behavior, PMMA has not been considered to be a practical resist for particle beam writing of master molds for casting poly(dimethylsiloxane) (PDMS) microfluidic structures. For this application, a SU-8 "negative" resist is favored; but its shorter shelf life, high sensitivity to UV/ambient room light, and very hard-to-remove contamination from equipment makes it difficult to handle in some workplaces. Recently it was found that a PMMA resist has a two-in-one characteristic. At a sufficiently intense fluence of radiation, PMMA can also undergo cross-linking which allows it to be used as negative resist [4,5]. This condition makes possible the fabrication of molds with ridges that can be used for casting channels using an ion beam. In this work, utilization of the negative tone of PMMA was investigated for making a micropatterning mold by using 2 MeV H^+ beam programmable proximity aperture lithography (PPAL) [6,7] for microfluidic application. The results obtained for protons constitute useful basic information for using beams of heavier ions. There is evidence that higher linear energy transfer (LET) ions induces higher cross-linking in polymers [8,9] so that lower fluence is expected for the same level of chemical modification.

2. Experimental

2.1. Ion beam irradiation

The experimental arrangement for ion beam irradiation when using the PPAL technique is shown in Fig. 1. A PMMA film was prepared by spinning PMMA A11 solution of 950 kDa (MicroChem, Newton, MA) [10] onto a silicon substrate at 2500 rpm for 45 s; this was followed by soft-baking on a hot plate at 160 °C for 2 min. The procedure was repeated three times to reach a PMMA total thickness of 8.8 ± 0.1 μm as measured by an ellipsometer [11]. For ion irradiation, a 1.7 MV Tandetron accelerator at the Plasma and Beam Physics Research Facility (PBP) of Chiang Mai University was used to produce a 2 MeV proton beam. Two L-shaped aperture blades, each independently mounted on computerized MM-3M-F-1 Motorized MicroMini™ stages (National Aperture, Salem, NH) [12], were used to shape the proton beam into a rectangle of variable width and height between 1 μm and 1 mm. In combination with *X–Y* micro-step translation of the

* Corresponding author at: Plasma and Beam Physics Research Facility, Department of Physics and Materials Science, Faculty of Science, Chiang Mai University, Chiang Mai 50200, Thailand. Tel.: +66 53 222973; fax: +66 53 222776.
E-mail address: nitipon@fnrf.science.cmu.ac.th (N. Puttaraksa).

0168-583X/$ - see front matter © 2011 Elsevier B.V. All rights reserved.
doi:10.1016/j.nimb.2011.01.053

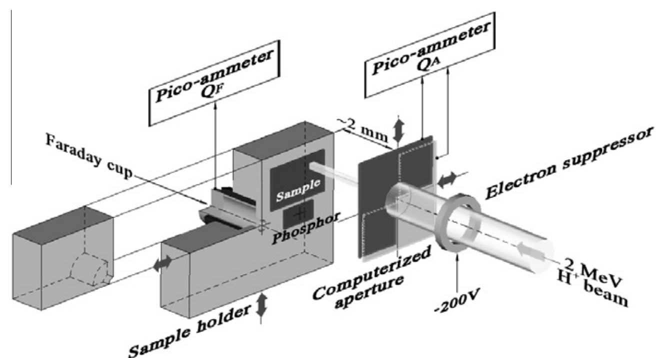

Fig. 1. Simplified schematic diagram of the experimental system (not to scale).

sample holder, a large-area complex pattern can be drawn on the sample by stitching together the rectangular subpatterns. For observation of the transformation mechanism and to determine the cross-linking fluence threshold (in ions cm^{-2}), the sample was separately irradiated with several single-square areas of different ion fluences, followed by developing in a 7:3 mixture (by volume) of isopropyl alcohol (IPA) and deionized (DI) water to remove PMMA that had undergone scission. Part of the result is shown in Fig. 2. To make the master mold, the designed pattern must be drawn at the cross-linking fluence on the PMMA layer through a serial writing method, as mentioned above. Final development with acetone revealed the master mold, as shown in Fig. 3(a).

2.2. Fluence monitoring

For the reproducibility of the process mentioned above, a sensitive and reliable ion fluence monitoring system is very important. Here, the accumulated charges were measured by a purpose designed current integrator with a resolution of 4.8 pC.

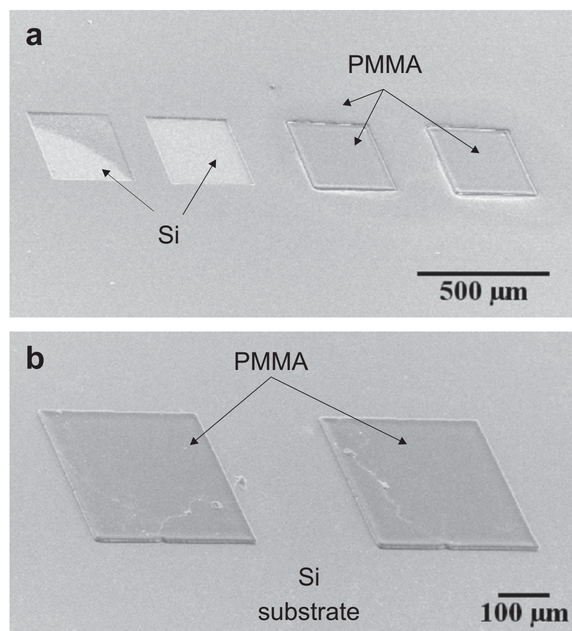

Fig. 2. (a) SEM image of patterns exposed to 2 MeV H^+ beams at four ion fluences of, from left to right, 2.67×10^{13}, 1.08×10^{14}, 1×10^{15} and 1.14×10^{15} ions cm^{-2} after developing in a mixture of IPA + DI water in 7:3 by volume at 25 °C for 4 min. (b) SEM image of the sample after developing in acetone at 25 °C for 5 min.

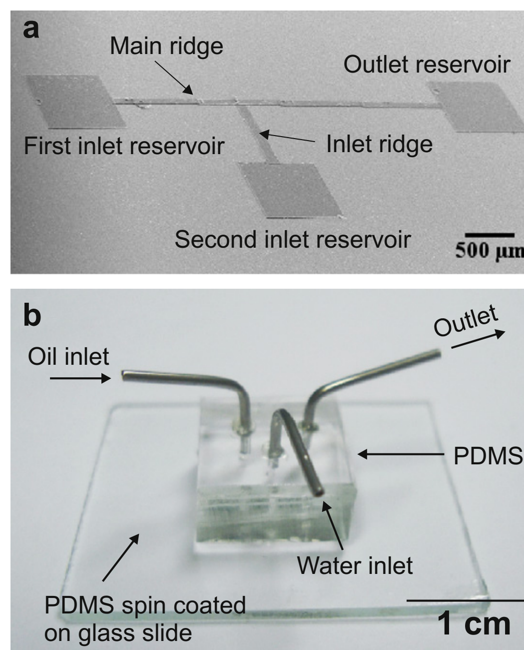

Fig. 3. (a) SEM micrograph of the T-junction pattern of the negative master mold made by the method of this work and (b) its microfluidic chip fabricated via soft-lithography.

The front end is battery operated, with an isolated grounding system to reduce sensitivity to noise and ground loop issues. The calibration curve for the setup shown in Fig. 1, is the relationship between the total charges of the incident beam on the aperture blades (Q_A) and of the beam passing through the aperture (Q_F). This must be determined first, which was done by integrating the currents measured on the aperture blades and a faraday cup behind the aperture for a fixed aperture size and different times and assuming the beam current density is constant over the area of the aperture. The measurement was performed by moving the faraday cup (65 mm long, 8 mm inner diameter, made of copper) to the irradiation position so that its opening was centered on the beam passing through the aperture. The ion fluence at the PMMA was calculated from Q_F. This was estimated (by using the calibration curve) from the measured Q_A, which was also an in situ ion beam monitor, and the known area of the rectangular aperture. In this system; to prevent secondary electrons, from escaping, an electron suppressor made of a copper ring with a 5 mm diameter hole biased at -200 V, was mounted in front of the aperture.

2.3. Device fabrication

Soft-lithography is commonly used for fabricating microfluidic devices from PDMS because the process is simple, fast and inexpensive [13]. Typically, a microfluidic channel in the PDMS is transferred from a micro-ridge of a master mold. Here, a 10:1 ratio (by volume) of base to curing agent of PDMS from a Sylgard 184 silicone elastomer kit (Dow Corning, Midland, MI) was mixed together. The mixture was degassed under coarse vacuum to remove air bubbles, poured over the negative PMMA master mold, and then placed on a hot plate for curing at 70 °C for 1 h. Subsequently, the embossed PDMS layer was peeled off. After that the PDMS replica was sealed with a PDMS film prepared by spin coating the PDMS mixture onto a clean glass slide pre-cured at 70 °C for 6 min. To achieve full hardening of the PDMS film, the microfluidic chip was cured again at 70 °C for 45 min. The device is shown in Fig. 3(b).

Please cite this article in press as: N. Puttaraksa et al., Fabrication of a negative PMMA master mold for soft-lithography by MeV ion beam lithography, Nucl. Instr. and Meth. B (2011), doi:10.1016/j.nimb.2011.01.053

2.4. Microfluidic experiments

In this experiment, oil and dyed deionized water were used as the working fluids for formation of water in oil (W/O) droplets using the PDMS microfluidic chip, as shown in Fig. 3(b). Positive pressure was applied to both of the streams by means of two independent computerized microliter syringe pumps. This allowed the volumetric flow rates to be easily adjusted. A Zeiss optical microscope (100× maximum) in connection with a Sony CCD camera (30 fps) were employed to observe the motion of fluids and to collect images, either as still photos or as movies on a personal computer, for further detailed analysis. The video images were analyzed using the ImageJ program [14].

3. Results and discussion

Fig. 2(a) shows a scanning electron microscope (SEM) micrograph of patterns exposed to 2 MeV protons at four levels of ion fluences, after first being developed in a solution of IPA and DI water (7:3 by volume), then rinsed twice with DI water, and dried by a flow of nitrogen gas. At low ion fluences, the irradiated PMMA patterns are dissolved by the developer solution due to the effect of the chain scission mechanism in accordance with its well-known characteristic as a "positive" resist. When increasing the ion fluence, as shown on the right-hand side of Fig. 2(a), the two irradiated areas are inert to the developer (similar to the pristine PMMA) due to the transformation from a dominant chain scission mechanism to a dominant cross-linking mechanism. More investigation of this phenomenon can be found elsewhere. Here we only conclude that cross-linking fully occurs at a fluence above $\Theta_x = 3.5 \times 10^{14}$ ions cm^{-2}. This value is based on several repeat measurements. After 5 min in the second developer (an acetone) at 25 °C rinsing in DI water and then drying with nitrogen gas, the two cross-linked square patterns still existed while all other PMMA was removed, as is clearly seen in Fig. 2(b). This is strong evidence that this method can be used to fabricate a negative PMMA master for standard soft-lithography. It was found that the master mold could be used repeatedly without deterioration.

Fig. 3(a) illustrates a SEM micrograph of a T-junction microfluidic pattern in a 7.5 μm thick PMMA resist irradiated by 2 MeV proton beams at an ion fluence of 1.9×10^{15} ions cm^{-2}. The mold is for a PDMS replica, consisting of a main straight ridge with inlet and outlet reservoirs at the ends and perpendicularly connected with the second inlet reservoir. A magnified image of the master mold reveals the effects of the doubled fluence in the stitching regions where the exposed pattern elements overlap, as has been discussed elsewhere [6,7]. This results in an increased microchannel depth in these regions, which is caused by swelling of the PMMA when irradiated by higher fluence. The stitching error can be decreased by careful alignment of both of the aperture blades so that their edges are closely parallel to the X–Y translation axes of the sample holder. We also found that a constant proton beam is important to the success of the process, since only one imperfect pattern element (due to temporary beam variation) is enough to ruin the entire pattern-drawing process. The PDMS microfluidic device is shown in Fig. 3(b). It was tested by injecting oil into the first inlet, and red-dyed DI water into the second inlet.

Fig. 4 shows microphotographs of the formation of water droplets in an oil phase using the T-junction microfluidic chip. The length of the droplet, L, can be calculated from the following equation [15]:

$$L = [1 + (d/w)(V_{\text{water}}/V_{\text{oil}})]w, \quad (1)$$

where w is the main channel width (95 μm), d is the width of the second inlet channel (150 μm), and V_{water} and V_{oil} are the flow rates

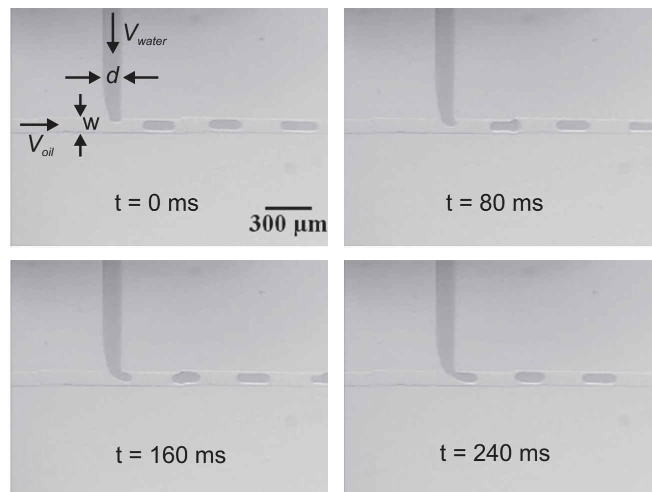

Fig. 4. Optical micrographs of water droplets (darker color from the red dyed) generated in a main stream of oil using T-junction PDMS microfluidic device.

of the dyed water and oil streams, respectively. Here, equal volumetric flow rates of 0.16 μL/min were used. The experiment indicates that the droplet has a length of $L_{\text{exp}} = 237.5$ μm, which is in good agreement with the calculation from Eq. (1), within 3% of the error ($L_{\text{cal}} = 245$ μm). A small perturbation was observed at some connecting spot, but was not strong enough to break the droplets.

4. Conclusions

We have demonstrated an alternative method for making a master mold that uses PMMA as a negative rather than a positive resist. We observed that the PMMA transforms from positive to negative resist at the threshold fluence of 3.5×10^{14} ions cm^{-2} for 2 MeV protons. This value was confirmed by repeating several times. This also indicates that the current integrator together with the experimental system, enables precise determination of the beam fluence. The results also suggest that dozens of PDMS devices can be generated from a common PMMA master, since our PMMA mold has been used many times without any deterioration. This demonstrates the suitability of the method for fabricating a PDMS microfluidic device.

Acknowledgements

This work was supported in part by the CoE Program of Chiang Mai University (CMU) and the International Atomic Energy Agency (IAEA, Vienna). NP gratefully acknowledges financial support from the Royal Golden Jubilee Scholarship of the Thailand Research Fund and also would like to thank the Thailand Center of Excellence in Physics (ThEP Center), the Department of Physics and Materials Science, and the Graduate School of CMU for his traveling expenses. The Academy of Finland, Centre of Excellence in Nuclear and Accelerator Based Physics, ref. 213503 and grant 129999 supported the work of NP and HJW's travel was supported by the Magnus Erhnrooth Foundation. SU is supported by the ThEP Center scholarship. Mr. Chome Thongleurm and Mr. Witoon Ginamoon are also acknowledged for their technical support.

References

[1] T.M. Hall, A. Wagner, L.F. Thompson, J. Appl. Phys. 53 (6) (1982) 3997.
[2] S.A. Rizvi, S. Pas, in: R. Doering, Y. Nishi (Eds.), Handbook of Semiconductor Manufacturing Technology, second ed., CRC Press, Florida, 2008. p. 20.

[3] D. Fink (Ed.), Fundamentals of Ion-Irradiated Polymers, Springer-Verlag, Germany, 2004. p. 14, 21.
[4] L. Ressier, J. Grisolia, C. Martin, J.P. Peyrade, B. Viallet, C. Vieu, Ultramicroscopy 107 (2007) 985.
[5] J.C. Choi, B.M. Lee, C.H. Jung, I.T. Hwang, M.Y. An, J.S. Lee, S.K. Hong, K.M. Huh, Y.C. Nho, Appl. Chem. 12 (2) (2008) 253.
[6] N. Puttaraksa, S. Gorelick, T. Sajavaara, M. Laitinen, S. Singkarat, H.J. Whitlow, J. Vac. Sci. Technol. B 26 (5) (2008) 1732.
[7] S. Gorelick, N. Puttaraksa, T. Sajavaara, S. Singkarat, H.J. Whitlow, Nucl. Instr. Meth. B 266 (2008) 2461.
[8] S. Seki, K. Maeda, Y. Kunimi, S. Tagawa, Y. Yoshida, H. Kudoh, M. Sugimoto, Y. Morita, T. Iwai, H. Shibata, K. Asai, K. Ishigure, J. Phys. Chem. B 103 (15) (1999) 3043.
[9] E.H. Lee, Nucl. Instr. Meth. B 151 (1999) 29.
[10] http://www.microchem.com/products/pdf/PMMA_Data_Sheet.pdf
[11] http://www.jawoollam.com/
[12] http://www.nationalaperture.com
[13] J.C. Mcdonald, G.M. Whitesides, Acc. Chem. Res. 35 (2002) 491.
[14] M.D. Abramoff, P.J. Magelhaes, S.J. Ram, Biophoton. Int. 11 (2004) 36.
[15] P. Garstecki, M.J. Fuerstman, H.A. Stone, G.M. Whitsides, Lab Chip 6 (2006) 437.

Please cite this article in press as: N. Puttaraksa et al., Fabrication of a negative PMMA master mold for soft-lithography by MeV ion beam lithography, Nucl. Instr. and Meth. B (2011), doi:10.1016/j.nimb.2011.01.053

Paper VIII

Nitipon Puttaraksa, Mari Napari, Orapin Chienthavorn, Rattanaporn Norarat, Timo Sajavaara, Mikko Laitinen, Somsorn Singkarat, and Harry J. Whitlow,
Direct writing of channels for microfluidics in silica by MeV ion beam lithography,

Submitted to Advanced Materials Research.

Direct writing of channels for microfluidics in silica by MeV ion beam lithography

Nitipon Puttaraksa[1,2,a], Mari Napari[1,b], Orapin Chienthavorn[3,c], Rattanaporn Norarat[1,d], Timo Sajavaara[1,e], Mikko Laitinen[1,f], Somsorn Singkarat[2,4,g], Harry J Whitlow[1,h]

[1]*Department of Physics, P.O. Box 35 (YFL), FIN-40014 University of Jyväskylä, Finland*
[2]*Plasma and Beam Physics Research Facility, Department of Physics and Materials Science, Faculty of Science, Chiang Mai University, Chiang Mai 50200, Thailand*
[3]*Department of Chemistry, Kasetsart University, Bangkok 10900, Thailand*
[4]*Thailand Center of Excellence in Physics, CHE, 328 Si Ayutthaya Road, Bangkok 10400, Thailand*

[a]nitipon.n.puttaraksa@jyu.fi, [b]mari.napari@jyu.fi, [c]fsciopc@ku.ac.th, [d]rattanaporn.norarat@jyu.fi, [e]timo.sajavaara@jyu.fi, [f]mikko.i.laitinen@jyu.fi, [g]scphi005@chiangmai.ac.th, [h]harry.j.whitlow@jyu.fi

Keywords: MeV ion beam lithography, direct writing, silica, etching, microfluidic channels

Abstract. The lithographic exposure characteristic of amorphous silica (SiO_2) was investigated for 6.8 MeV $^{16}O^{3+}$ ions. A programmable proximity aperture lithography (PPAL) technique was used for the ion beam exposure. After exposure, the exposed pattern was developed by selective etching in 4% v/v HF. Here, we report on the development of SiO_2 in term of the etch depth dependence on the ion fluence. This showed an exponential approach towards a constant asymptotic etch depth with increasing ion fluence. An example of microfluidic channels produced by this technique is demonstrated.

Introduction

Amorphous silica (SiO_2) is used in microfabrication because it is commercially available with extremely high purity (e.g. synthetic fused silica) and it has a high chemical inertness, mechanical rigidity, high-temperature resistance and optical transparency extending deep into the ultraviolet [1-4]. These make it suitable for demanding applications such as the stationary phase in chromatography. Microfabrication in silica is also used for components such as waveguides and microfluidic channels. Pattern transfers to silicon dioxide have been made by several techniques, namely ion track lithography [5-6], X-ray exposure [7], and electron beam lithography (EBL) [8].

Recently, MeV ion beam lithography (MeV-IBL) has emerged as a technique for fabricating three-dimensional (3D) micro- and nanostructures not only in polymer resists e.g. PMMA, SU-8 and HSQ [9-13], but also in inorganic materials, such as Si and GaAs [14]. Here, we used the MeV ion beam programmable proximity aperture lithographic (PPAL) technique [9] for studying the exposure characteristics of silica using 6.8 MeV $^{16}O^{3+}$ ion beams. This technique is considered to be a fast writing method since large area rectangular pattern elements (500 × 500 μm) can be written in one exposure. This makes the PPAL technique suitable for making microfluidic structures. The irradiation introduces network damage into the silica, which is subsequently more susceptible to removal in selective etching in an aqueous hydrofluoric acid (HF) solution.

In this paper, we report on an investigation of the ion fluence (ions/cm^2) dependence of the effective etch depth and demonstrate the use of the technique for direct writing of microfluidic channels in silica.

Experimental details

Natural fused silica samples were cleaned in an aqueous solution of 2% v/v HF for 30 s, followed by rinsing with deionised water for 3 minutes, and dried at room temperature. The samples were then exposed to 6.8 MeV $^{16}O^{3+}$ ions in the PPAL system [9]. A 1.7 MV Pelletron accelerator in the Accelerator Laboratory of the University of Jyväskylä, Finland, was used to produce the oxygen ion beam. The beam was shaped to a rectangular area of 0.2-500 μm side length by two L-

shaped aperture blades in close proximity to the sample. The two L-shaped aperture blades and the sample holder were mounted on five vacuum-compatible Newport MFA-CCV6 DC servo motor driver linear motion drives. The size and shape of the rectangular apertures, the X-Y sample position, and the beam blanking were controlled by a LabVIEW™ program. More details of the principle of the PPAL technique are given elsewhere [9].

In order to precisely determine the ion fluence (Φ, ions/cm^2), a current integrator was developed. A Keithley Instruments model 6485 picoammeter was used to measure the beam current. Then, the accumulated charge was determined by integrating the measured current every second. Details of the ion fluence determination procedure were reported previously [11].

Aqueous hydrofluoric acid (HF) solution etches irradiated and unirradiated silica at different rates [5,6]. The *effective etch depth, z* is the difference between the etch depths of the irradiated and unirradiated silica. A part of the unexposed area was masked by PMMA film prior to development. Subsequently, the sample was etched (developed) in a 4% v/v HF solution for 60 minutes and rinsed in deionised water for 5 minutes. Finally, the PMMA film was removed in hot acetone and rinsed with iso-propanol (IPA). The experimental procedure is shown schematically in Fig. 1.

The etched depths of the exposed and unexposed regions were measured by a stylus profilometer (KLA-Tencor P-15 Profiler).

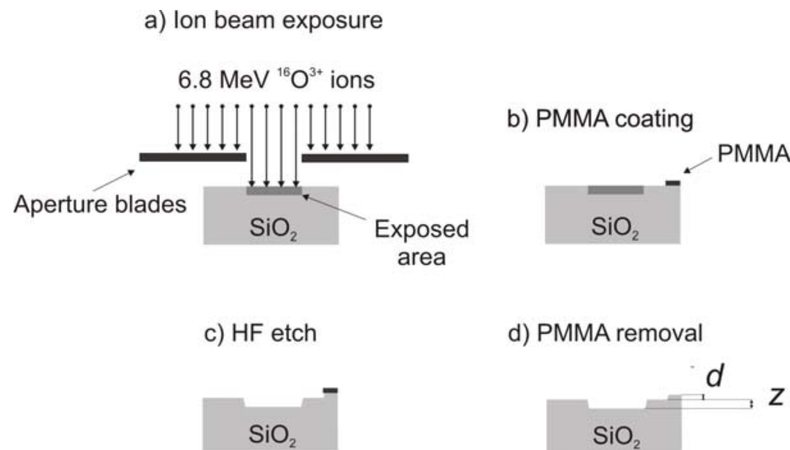

Figure1. Schematic diagram of the experimental procedure.

Results and discussion

Fig. 2a shows an optical microscope image after development of 200 × 200 µm square irradiated patterns in silica, which were exposed to different fluences of 6.8 MeV $^{16}O^{3+}$ ions.

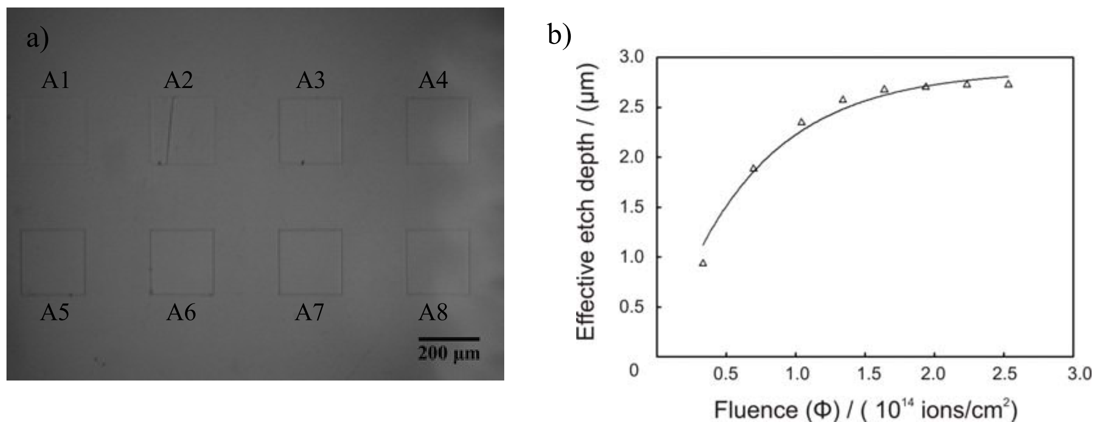

Figure 2. a) Optical micrograph of square patterns after development, that were irradiated with different ion fluences of 6.8 MeV $^{16}O^{3+}$ ions. b) The effective etch depth vs fluence (60 minutes development).

Table 1. The ion fluence parameters and effective etch depth of each pattern element (60 minutes development).

Pattern no.	Fluence (ions/cm^2)	Effective etch depth (μm)	Pattern no.	Fluence (ions/cm^2)	Effective etch depth (μm)
A1	3.3×10^{13}	0.93	A5	1.6×10^{14}	2.67
A2	7.0×10^{13}	1.98	A6	1.9×10^{14}	2.72
A3	1.0×10^{14}	2.34	A7	2.2×10^{14}	2.72
A4	1.3×10^{14}	2.57	A8	2.5×10^{14}	2.72

Table 1 presents the fluence and the effective etch depth for each pattern element in Fig. 2a for an etching time of 60 minutes. The experimental results (Fig. 2b) show that the effective etch depth asymptotically approaches a constant value with increasing ion fluence according to: $z = A[1- \exp(-k\Phi)]$, where z is the effective etch depth, A is the amplitude, and k is the exponential etch constant. The fitted values of A and k are 2.9 μm and 1.5×10^{-14} cm^2/ions, respectively. The respective uncertainties in Φ and R are estimated to be ± 5% and ± 3%. z reaches ~90% of its asymptotic value at an ion fluence level of $\Phi_t = 1.6\times10^{14}$ ions/cm^2. At this fluence the mean spacing between ion impingements in the irradiated areas is ~1.3 nm. Similar behaviour was observed for different development times. The etch depth of the unexposed region, d (Fig. 1) was 0.49 μm.

Swift ion irradiation of solid materials causes atomic target displacements from their original atomic sites in the network by two main processes, nuclear and electronic stopping. In silica this presumably leads to network disruption by breaking the Si–O bonds. This network damage enhances the etch rate of exposed areas in 4% v/v HF [6].

Fig. 3 presents a scanning electron microscope (SEM) image of a test prototype pattern. This structure was fabricated using 6.8 MeV oxygen ions at a fluence of 3×10^{14} ions/cm^2, and 60 minutes development time was used. The ion fluence was chosen to be above the level for asymptotic etch depth, to maintain a nearly constant etch depth, as discussed above. The effective depth of the pattern was ~2.5 μm measured with the profilometer. The pattern can be used as the basis of microfluidic devices for hydrodynamic focusing or droplet generation [11]. In order to change the open channel structure into a closed channel system, conventional SiO_2-SiO_2 fusion bonding can be used [15].

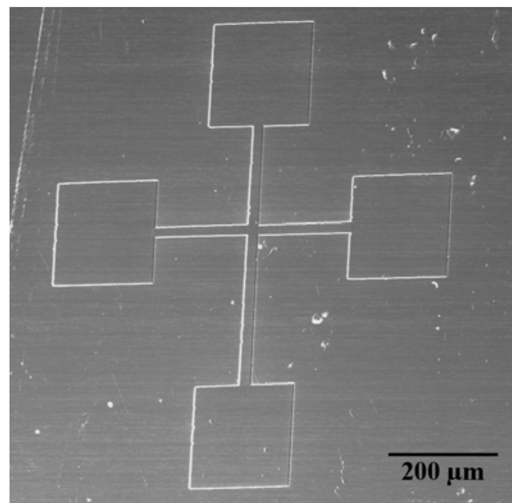

Figure 3. SEM micrograph of a test pattern fabricated using 6.8 MeV $^{16}O^{3+}$ at a fluence of 3×10^{14} ions/cm^2, and after development in an aqueous 4% v/v HF for 60 minutes.

Conclusions

We have demonstrated Programmable Proximity Aperture Lithography (PPAL) using 6.8 MeV $^{16}O^{3+}$ ions for direct writing of lithographic patterns in silica. The dependence on the ion fluence of the effective etch depth of silica in 4% v/v HF was measured. We found that for a 60 minute development the effective etch depth, z (μm) follows a $z = 2.9[1 - \exp(-1.5\Phi)]$ law, where Φ (10^{14} ions/cm^2) is the ion fluence. The etch depth approaches an asymptotic value above a fluence of about 1.6×10^{14} ions/cm^2. Channel structures suitable for fabricating practical microfluidic devices have been produced using this technique.

Acknowledgements

This work has been carried out under the auspices of the Academy of Finland Centre of Excellence in Nuclear and Accelerator Based Physics (Ref. 213503) and grant (Ref. 129999). NP gratefully acknowledges a financial support from the Royal Golden Jubilee Scholarship (RGJ) of the Thailand Research Fund (TRF). The work is supported by an OSKE grant and the Schwartz Foundation.

References

[1] H. Klauk, M. Halik, U. Zschieschang, G. Schmid, and W. Radlik, J. Appl. Phys. 92 (2002) 5259.
[2] J. Wibbeler, G. Pfeifer, and M. Hietschold, Sens and Actua. A 71 (1998) 74.
[3] J.H. Teng, J.R. Dong, S.J. Chua, B.S. Foo, M.Y. Lai, Y.J. Wang, S.S. Ang, and R. Yin, Appl. Phys. Lett. 90 (2007) 171107.
[4] J.T. Martin, J.D. Barchas, and K.F. Faull, Anal. Chem. 54 (1982) 1806.
[5] M. Skupiński, J. Jensen, A. Johansson, G. Possnet, M. Boman, K. Hjort, and A. Razpet, J. Vac. Sci. Technol. B 25(3) (2007) 862.
[6] J. Jensen, A. Razpet, M. Skupiński, and G. Possnet, Nucl. Instr. Meth. B 243 (2006) 119.
[7] H. Mekaru, M. Fujimaki, K. Awazu, and M. Takahashi, Microsyst. Technol. 16 (2010) 1339.
[8] A. Beaumont, C. Dubuc, J. Beauvais, and D. Drouin, J. Vac. Sci. Technol. B 28(5) (2010) 940.
[9] N. Puttaraksa, S. Gorelick, T. Sajavaara, M. Laitinen, S. Singkarat, and H.J. Whitlow, J. Vac. Sci. Technol. 26(5) (2008) 1732.
[10] S. Gorelick, N. Puttaraksa, T. Sajavaara, M. Laitinen, S. Singkarat, and H.J. Whitlow, Nucl. Instr. Meth. B 266 (2008) 2461.
[11] N. Puttaraksa, S. Unai, M.W. Rhodes, K. Singkarat, H.J. Whitlow, and S. Singkarat, Nucl. Instr. Meth. B (2011), doi:10.1061/j.nimb.2011.01.053.
[12] J.A. van Kan, J.L. Sanchez, T. Osipowicz, and F. Watt, Microsyst. Technol. 6 (2000) 82.
[13] S. Gorelick, F. Zhang, P.G. Shao, J.A. van Kan, H.J. Whitlow, and F. Watt, Nucl. Instr. Meth. B 267 (2009) 2309.
[14] P. Mistry, I. Gomez-Morilla, G.W. Grime, R.P. Webb, R. Gwilliam, A. Cansell, M. Merchant, K.J. Kirkby, E.J. Teo, M.B.H. Breese, A.A. Bettiol, D.J. Blackwood, and F. Watt, Nucl. Instr. Meth. B 237 (2005) 188.
[15] M.J. Madou, Fundamentals of Microfabrication: The Science of Miniaturization, 2nd ed., CRC Press, Boca Raton, 2002, pp. 487-490.